Universidade de São Paulo
Instituto de Física

Observational Constraints on Models with an Interaction between Dark Energy and Dark Matter

André Alencar da Costa

Advisor: Prof. Dr. Elcio Abdalla

Thesis presented to the Institute of Physics of the University of São Paulo in partial fulfillment of the requirements for the degree of Doctor in Science

Examining Commission:

Prof. Dr. Elcio Abdalla (IF-USP)

Prof. Dr. Luis Raul Weber Abramo (IF-USP)

Prof. Dr. Marcos Vinicius Borges Teixeira Lima (IF-USP)

Prof. Dr. Ioav Waga (IF-UFRJ)

Prof. Dr. Luís Carlos Bassalo Crispino (FACFIS-UFPA)

São Paulo

2014

-
-
-

FICHA CATALOGRÁFICA
Preparada pelo Serviço de Biblioteca e Informação
do Instituto de Física da Universidade de São Paulo

Costa, André Alencar da

Observational constraints on models with an interaction between dark energy and dark matter / Vínculos observacionais em modelos com interação entre energia escura e matéria escura. São Paulo, 2014.

Tese (Doutorado) – Universidade de São Paulo. Instituto de Física. Depto. de Física Matemática

Orientador: Prof. Dr. Elcio Abdalla

Área de Concentração: Física

Unitermos: 1. Cosmologia; 2. Matéria escura; 3. Energia escura.

USP/IF/SBI-097/2014

Universidade de São Paulo
Instituto de Física

Vínculos Observacionais em Modelos com Interação entre Energia Escura e Matéria Escura

André Alencar da Costa

Orientador: Prof. Dr. Elcio Abdalla

Tese de doutorado apresentada ao Instituto de Física para a obtenção do título de Doutor em Ciências

Banca Examinadora:

Prof. Dr. Elcio Abdalla (IF-USP)

Prof. Dr. Luis Raul Weber Abramo (IF-USP)

Prof. Dr. Marcos Vinicius Borges Teixeira Lima (IF-USP)

Prof. Dr. Ioav Waga (IF-UFRJ)

Prof. Dr. Luís Carlos Bassalo Crispino (FACFIS-UFPA)

São Paulo

2014

Acknowledgments

First of all I would like to thank my advisor Elcio Abdalla for his guidance and patience. I also acknowledge him for the incentive to scientific independence and for the high quality research environment he provided me.

Many thanks to the several collaborators during the years of the doctorate, especially professor Bin Wang for helpful discussions about phenomenological models on interacting dark energy, and the colleagues Elisa Ferreira, Leila Graef, Lucas Olivari, Riis Rhavia and Xiao-Dong Xu.

I am also very grateful to the colleagues of the department of mathematical physics for the friendship, especially my office mates Eduardo Matsushita, Ricardo Pereira, Lucas Secco, Arthur Loureiro and Carolina Queiroz.

I could not forget the couple Jacinto and Bernadete for their hospitality and generosity, opening the doors of their home to me and my wife for the first month we arrived in São Paulo. I also thank their children and grandchildren for all the moments we passed together.

During these years in São Paulo I was benefited by the friendship of many people, especially I would like to thank the people of the Presbyterian Church in Jardim Bonfiglioli who have been a second family to me, my wife and now my daughter.

Certainly I would not have arrived here without the encouragement and support of my family and friends. I am especially grateful for my wife Lidiane, for her love, standing on my side all these years even with the cost of being apart from her family, and my daughter Ana Beatriz, who made these last months full of happiness and pleasure.

I gratefully acknowledge the partial financial support from CAPES, Coordenação de Aperfeiçoamento de Pessoal de Nível Superior, and the financial support from CNPq, Conselho Nacional de Desenvolvimento Científico e Tecnológico - Brasil. This work would not be possible without the funding from these agencies.

This work has made use of the computing facilities of the Laboratory of Astroinformatics (IAG/USP, NAT/Unicsul), whose purchase was made possible by the Brazilian agency FAPESP (grant 2009/54006-4) and the INCT-A.

Abstract

In this thesis we go beyond the standard cosmological ΛCDM model and study the effect of an interaction between dark matter and dark energy. Although the ΛCDM model provides good agreement with observations, it faces severe challenges from a theoretical point of view. In order to solve such problems, we first consider an alternative model where both dark matter and dark energy are described by fluids with a phenomenological interaction given by a combination of their energy densities. In addition to this model, we propose a more realistic one based on a Lagrangian density with a Yukawa-type interaction. To constrain the cosmological parameters we use recent cosmological data, the CMB measurements made by the Planck satellite, as well as BAO, SNIa, H_0 and Lookback time measurements.

Keywords: Cosmology. Dark Matter. Dark Energy.

Resumo

Nesta tese vamos além do modelo cosmológico padrão, o ΛCDM, e estudamos o efeito de uma interação entre a matéria e a energia escuras. Embora o modelo ΛCDM esteja de acordo com as observações, ele sofre sérios problemas teóricos. Com o objetivo de resolver tais problemas, nós primeiro consideramos um modelo alternativo, onde ambas, a matéria e a energia escuras, são descritas por fluidos com uma interação fenomenológica dada como uma combinação das densidades de energia. Além desse modelo, propomos um modelo mais realista baseado em uma densidade Lagrangiana com uma interação tipo Yukawa. Para vincular os parâmetros cosmológicos usamos dados cosmológicos recentes como as medidas da CMB feitas pelo satélite Planck, bem como medidas de BAO, SNIa, H_0 e Lookback time.

Palavras-Chave: Cosmologia. Matéria Escura. Energia Escura.

Contents

Introduction

The large amount of precise astronomical data released in the past few years provided opportunities to answer questions in cosmology and astrophysics. Such a precision allows us to test cosmological models and determine cosmological parameters with high accuracy.

The simplest cosmological model one can build that reasonably explains the current data is the ΛCDM model. This model consists in a cosmological constant Λ to account for the observed acceleration of the Universe, plus cold dark matter (CDM) necessary to produce the gravitational potential wells inferred on galactic to cosmological scales.

However, theoretically the ΛCDM model itself faces challenges, the cosmological constant problem[1] and the coincidence problem[2]. The first one refers to the small observed value of the cosmological constant, incompatible with the vacuum energy description in field theory. The second one refers to the fact that we have no natural explanation for why the energy densities of dark matter and vacuum energy are of the same order today. These problems open the avenue for alternative models of dark energy to substitute the cosmological constant description.

One way to alleviate the coincidence problem, which embarrasses the standard ΛCDM cosmology, is to consider an interaction between dark energy and dark matter. Considering that dark energy and dark matter contribute with significant fractions of the contents of the Universe, it is natural, in the framework of field theory, to consider an interaction between them. The interaction between dark energy and dark matter will affect significantly the expansion history of the Universe and the evolution of density perturbations, changing their growth. The possibility of the interaction between dark sectors has been widely discussed in the literature [3–36]. Determining the existence of dark matter and dark energy interactions is an observational endeavor that could provide an interesting insight into the nature of the dark sectors.

Since the physical properties of dark matter and dark energy at the present moment

are unknown, we cannot derive the precise form of the interaction from first principles. For simplicity, most considerations of the interaction in the literature are from phenomenology. Attempts to describe the interaction from field theory have been proposed in [37–39]. One possibility is a phenomenological model of the interaction, Q, between dark matter and dark energy, which is in a linear combination of energy densities of the dark sectors $Q = 3H(\xi_1\rho_c + \xi_2\rho_d)$ [13, 29, 40]. In this interaction, H is the Hubble parameter, ξ_1 and ξ_2 are dimensionless parameters, assumed to be time independent, for simplicity, and ρ_c and ρ_d are the energy densities of dark matter and dark energy, respectively. Such a model was widely studied in [13, 18, 34, 41–44]. It was disclosed by the late integrated Sachs-Wolf (ISW) effect [25, 27] that the interaction between dark matter and dark energy influences the cosmic microwave background (CMB) at low multipoles and at high multipoles through gravitational lensing [44, 45]. With the WMAP data [25, 27] together with galaxy cluster observations [34, 35] and also recent kinetic Sunyaev-Zel'dovich effect observations [46], it was found that this phenomenological interaction between dark energy and dark matter is viable and the coupling constant is positive, indicating that there is energy flow from dark energy to dark matter, which is required to alleviate the coincidence problem and to satisfy the second law of thermodynamics [16].

It is of great interest to build alternative models of the Universe and employ the latest high-precision data to further constrain them. This is the main motivation of the present work. We will combine the CMB data from Planck [47–49] with other cosmological probes such as the baryonic acoustic oscillations (BAO) [50–52], supernovas [53], the latest constraint on the Hubble constant [54] and lookback time [55, 56]. We want to see how these different probes will influence the cosmological parameters and put tight constraints on the interaction between dark sectors.

This thesis is organized as follows: in the first chapter we introduce some fundamental aspects of cosmology and present the contents of the Universe. Chapter two goes beyond the homogeneous and isotropic universe and describe the linear perturbations. Our models of interactions between dark energy and dark matter are presented in chapter three. The data analysis and our fitting results appear in chapter four. Finally, we conclude and discuss some perspectives for future works.

Chapter 1

Introduction to Cosmology: The Need of Dark Matter and Dark Energy

Cosmology is the study of the Universe as a whole. Despite the great complexity of this system, if we are interested in its dynamics on large scales, it is possible to construct a relatively simple model to describe it. On large scales, the interactions between the constituents of the Universe are governed by the laws of gravitation which, nowadays, are best explained by the theory of general relativity published by Einstein in 1915 [57].

1.1 Homogeneous and Isotropic Universe

General relativity establishes that the geometry of the spacetime is determined by the energy content of the Universe and this geometry governs the motion of free particles. In general, the geometry of the spacetime is described by the line element

$$ds^2 = g_{\mu\nu} dx^\mu dx^\nu, \tag{1.1}$$

where $g_{\mu\nu}$ are the components of the metric tensor. The indices μ, ν are defined such that x^0 represents the time coordinate and x^i, with $i = 1, 2, 3$, represent the spatial coordinates. We are using the Einstein's convention where repeated indices are summed.

To determine the form of the line element of a given cosmological model we use the

underlying symmetries. The simplest cosmological model can be built assuming that the constituents of the Universe present the properties of statistical homogeneity and isotropy, known as *the cosmological principle*. In fact, observations of the cosmic microwave background have shown isotropy of one part in 100.000 [58]. Also, evidences of galaxy surveys suggest that the Universe is homogeneous on large scales [59].

Using the cosmological principle, the metric of the spacetime must be the Friedmann-Lemaitre-Robertson-Walker (FLRW) metric [57], which is given by

$$ds^2 = -dt^2 + a(t)^2 \left[\frac{dr^2}{1 - Kr^2} + r^2 \left(d\theta^2 + \sin^2 \theta d\phi^2 \right) \right]. \tag{1.2}$$

Here $a(t)$ is a scale factor accounting for the expansion or contraction of the Universe and K is a constant that establishes the geometry of the spatial section. If $K > 0$ the spatial section is closed, while for $K = 0$ it is flat and $K < 0$ means that the spatial section is open. Throughout this work we are using natural units such that $\hbar = c = k_B = 1$.

The motions of free particles follow the geodesic equations

$$\frac{d^2 x^\mu}{d\lambda^2} + \Gamma^\mu_{\alpha\beta} \frac{dx^\alpha}{d\lambda} \frac{dx^\beta}{d\lambda} = 0, \tag{1.3}$$

where λ is a monotonically increasing parameter that parameterizes the particle's path and $\Gamma^\mu_{\alpha\beta}$ are the Christoffel symbols. The Christoffel symbols are related to the metric tensor by the expression

$$\Gamma^\mu_{\alpha\beta} = \frac{g^{\mu\nu}}{2} \left(\frac{\partial g_{\alpha\nu}}{\partial x^\beta} + \frac{\partial g_{\beta\nu}}{\partial x^\alpha} - \frac{\partial g_{\alpha\beta}}{\partial x^\nu} \right), \tag{1.4}$$

where $g^{\mu\nu}$ is the inverse of the metric tensor such that $g^{\mu\alpha} g_{\alpha\nu} = \delta^\mu_\nu$ with δ^μ_ν, the Kronecker delta, defined as zero unless $\mu = \nu$ in which case it is equal to one.

To obtain $a(t)$ and K we need the dynamical equations governing the Universe. In the context of general relativity it is determined by the Einstein equations [60]

$$R_{\mu\nu} - \frac{1}{2} g_{\mu\nu} R = 8\pi G T_{\mu\nu}, \tag{1.5}$$

where $R_{\mu\nu}$ is the Ricci tensor, which can be written in terms of the Christoffel symbol as

$$R_{\mu\nu} = \frac{\partial \Gamma^\alpha_{\mu\nu}}{\partial x^\alpha} - \frac{\partial \Gamma^\alpha_{\mu\alpha}}{\partial x^\nu} + \Gamma^\alpha_{\beta\alpha} \Gamma^\beta_{\mu\nu} - \Gamma^\alpha_{\beta\nu} \Gamma^\beta_{\mu\alpha}. \tag{1.6}$$

$R = g^{\mu\nu}R_{\mu\nu}$ is the Ricci scalar, or curvature scalar, G is the Newton gravitational constant and $T_{\mu\nu}$ is the energy-momentum tensor of the content in the Universe. All the quantities in the left hand side of (1.5) are geometrical quantities, while the right hand side presents the energy content. Thus, the Einstein equations relate the geometry of the Universe to the energy content.

On large scales the constituents of the Universe can be treated as a fluid. The most general energy-momentum tensor for a fluid component "A", $T^A_{\mu\nu}$, is given by

$$T^A_{\mu\nu} = (\rho^A + P^A)u^A_\mu u^A_\nu + g_{\mu\nu}P^A + \pi^A_{\mu\nu} + q^A_\mu u^A_\nu + q^A_\nu u^A_\mu, \tag{1.7}$$

where ρ^A is the energy density, P^A is the pressure, u^A_μ is the four-velocity vector, $\pi^A_{\mu\nu}$ is the anisotropic stress and q^A_μ is the heat flux vector relative to u^A_μ, all these quantities with respect to the A-fluid. The total energy-momentum tensor is $T_{\mu\nu} = \sum_A T^A_{\mu\nu}$. However, if the fluid has at each point a velocity $\vec{v}$, such that an observer with this velocity sees the fluid around him as isotropic, this is known as a *perfect fluid* [57] and in this case the anisotropic stress and the heat flux are null.

Using the FLRW metric (1.2) and the energy-momentum tensor (1.7) for all components with the assumption of a perfect fluid, the Einstein equations (1.5) result in two independent equations. The time-time component gives the Friedmann equation

$$H^2(t) = \frac{8\pi G}{3}\rho(t) - \frac{K}{a^2(t)} \tag{1.8}$$

and the space-space components result in

$$\dot{H}(t) = -4\pi G\left[\rho(t) + P(t)\right] + \frac{K}{a^2(t)}, \tag{1.9}$$

where $H(t) \equiv \dot{a}(t)/a(t)$ is called *Hubble parameter*, ρ, P denote the total energy density and pressure and a dot means differentiation with respect to the cosmic time t.

We can define a *critical density* ρ_{crit} by

$$\rho_{crit} \equiv \frac{3H^2(t)}{8\pi G}, \tag{1.10}$$

such that the abundance of a substance in the Universe can be expressed with respect to

it. Constructing the *density parameter* Ω as

$$\Omega = \sum_A \Omega_A \equiv \sum_A \frac{\rho_A}{\rho_{crit}}, \tag{1.11}$$

the Friedmann equation (1.8) can be rewritten as

$$\Omega - 1 = \frac{K}{H^2(t)a^2(t)}. \tag{1.12}$$

From this equation we can see that the curvature of the spacial section K is determined by the energy content of the Universe. In fact,

$$\begin{cases} \rho < \rho_{crit} \Rightarrow \Omega < 1 \Rightarrow K < 0, \\ \rho = \rho_{crit} \Rightarrow \Omega = 1 \Rightarrow K = 0, \\ \rho > \rho_{crit} \Rightarrow \Omega > 1 \Rightarrow K > 0. \end{cases} \tag{1.13}$$

To solve the Friedmann equation (1.8) and find how the scale factor $a(t)$ evolves with time, we have to know what is the dependence of ρ with time, or equivalently with the scale factor. Combining (1.8) and (1.9), or using the conservation of the energy-momentum tensor, results

$$\dot{\rho} + 3H(\rho + P) = 0. \tag{1.14}$$

As (1.14) can be obtained from (1.8) and (1.9), it means that only two of equations (1.8), (1.9) and (1.14) are independent. Equation (1.14) is valid for the total energy density, but if the individual components are independent, they will obey similar equations. Thus, if we know what are the components of the Universe and the equation of state they satisfy, we can solve Eq. (1.14) for each individual component and find their dependence with the scale factor. Knowing this, we can solve the Friedman equation (1.8).

There is another relation that can be obtained from equations (1.8) and (1.9). Eliminating K/a^2 from those equations, we obtain

$$\frac{\ddot{a}}{a} = -\frac{4\pi G}{3}(\rho + 3P). \tag{1.15}$$

This equation tells us that an accelerated expansion only occurs if $\rho + 3P < 0$. As the energy density must be a positive quantity, this means that in order to realize an accel-

erated expansion, the Universe must contain some component with a negative pressure. Considering a fluid with a linear barotropic equation of state[1], $P = \omega\rho$, the accelerated expansion can occur if $w < -1/3$.

1.2 Cosmic Distances

In the previous section we established a theoretical model for a homogeneous and isotropic universe. Solving the system of equations (1.8) and (1.14) allows us to determine the evolution of the scale factor $a(t)$ and consequently the history of the Universe. However, to solve that system of equations we need to determine the values of some parameters as K, the initial value of $H(t)$, the initial energy densities of all the constituents of the Universe and their equation of state, usually assumed to be of the form $\omega = P/\rho$. To describe the real Universe these parameters must be in agreement with observations, which means we need observables that allow us to compare theory with observations.

A fundamental step to compare theory with observations is the measurement of distances on cosmological scales. These measurements enable us to relate physical observables with the parameters in our model such that we can constrain it and make predictions. Actually, there are several ways to define distances in cosmology as we show below.

From the FLRW line element (1.2), a light ray traveling along the radial direction satisfies the geodesic equation

$$ds^2 = -dt^2 + a^2(t)d\chi^2 = 0, \tag{1.16}$$

where we defined $d\chi \equiv dr/(1 - Kr^2)^{1/2}$. Therefore, considering that a light ray have traveled from the time $t = 0$, we can find the total comoving distance that it could travel until the time t as

$$\eta \equiv \int_0^t \frac{dt'}{a(t')}. \tag{1.17}$$

This distance establishes a limit beyond which no information can further propagate in the comoving frame. Thus, η can be thought as a *comoving horizon*. Because η is monotonically increasing, it can also be defined as a time variable, which is called *conformal time*. Using equation (1.16), we can obtain the comoving distance from a

[1] A barotropic fluid is a fluid whose pressure depends on the density alone [61].

distant object at scale factor a to us:

$$\chi(a) = \int_{t(a)}^{t_0} \frac{dt'}{a(t')} = \int_a^{a_0} \frac{da'}{a'^2 H(a')}, \tag{1.18}$$

where the subscript "0" represents quantities at the present time.

The comoving coordinates are constant over the expansion history of the Universe. Thus, using Eq. (1.18), a light ray emitted at time $t + \delta t$ and observed at time $t_0 + \delta t_0$ satisfies

$$\int_t^{t_0} \frac{dt'}{a(t')} = \int_{t+\delta t}^{t_0+\delta t_0} \frac{dt'}{a(t')}. \tag{1.19}$$

Manipulating the limits of integration, we can write

$$\int_t^{t+\delta t} \frac{dt'}{a(t')} = \int_{t_0}^{t_0+\delta t_0} \frac{dt'}{a(t')}. \tag{1.20}$$

At first order in δt we have

$$\frac{\delta t}{a(t)} = \frac{\delta t_0}{a(t_0)}. \tag{1.21}$$

If δt is the period of emission of the light ray and δt_0 the period of detection, as the wave frequency ν is the inverse of the period and the wave length is defined as $\lambda = c/\nu$, we obtain

$$1 + z \equiv \frac{\nu_{emit}}{\nu_{obs}} = \frac{\lambda_{obs}}{\lambda_{emit}} = \frac{a_0}{a}. \tag{1.22}$$

This expression defines a cosmological Doppler effect associated with the expansion or contraction of the Universe. To account with this effect we defined the redshift z. The above equation allows us to relate the redshift of a distant object to the scale factor when the light ray was emitted.

Basically, there are two ways of inferring distances in astronomy: using a *standard ruler* or a *standard candle*. With the knowledge of trigonometry astronomers have inferred lengths for a long time. Measuring the angle θ subtended by an object of known physical size l (a standard ruler), the distance to that object is

$$d_A = \frac{l}{2\tan(\frac{\theta}{2})} \approx \frac{l}{\theta}, \tag{1.23}$$

assuming the angle subtended is small. On the other hand, using the line element (1.2),

we can see that the physical length l of an object described by an angle θ is given by

$$l = a(t) r \theta. \tag{1.24}$$

Therefore, comparing Eqs. (1.23) and (1.24), we observe that the *angular diameter distance* is

$$d_A = a(t) r = a(t) \begin{cases} \frac{1}{H_0\sqrt{\Omega_{k0}}} \sinh(H_0\sqrt{\Omega_{k0}}\chi) & \Omega_k > 0, \\ \chi & \Omega_k = 0, \\ \frac{1}{H_0\sqrt{-\Omega_{k0}}} \sin(H_0\sqrt{-\Omega_{k0}}\chi) & \Omega_k < 0, \end{cases} \tag{1.25}$$

where we used the definitions of χ and $\Omega_k \equiv -K/H^2(t)a^2(t)$, and we are using a normalization such that $a_0 = 1$.

Another important technique to determine distances is to find an object of known intrinsic brightness, a *standard candle*, such that any difference between the apparent brightness of two of these objects is a result of their different distances from us. Given an object of known luminosity L, the observed flux F a distance d_L from the source is

$$F = \frac{L}{4\pi d_L^2}. \tag{1.26}$$

On an expanding universe we can write a similar equation considering a comoving grid as

$$F = \frac{L(\chi)}{4\pi r^2(\chi)}, \tag{1.27}$$

where $L(\chi)$ is the luminosity of the source through a comoving spherical shell with radius $r(\chi)$. Assuming that the photons are emitted with the same energy, the luminosity $L(\chi)$ is the energy multiplied by the number of photons crossing the shell per unit time. As the Universe expands, the number of photons passing through the spherical shell per unit time becomes smaller by a factor of a. On the other hand, Eq. (1.22) tells us that the wave lengths of the photons are stretched by a factor of $1/a$. Thus, as the energies of the photons are inversely proportional to the wave length, they will decrease accordingly. Therefore, the energy per unit time on the spherical shell at $r(\chi)$ will be a factor of a^2 smaller than the luminosity at the source

$$F = \frac{La^2}{4\pi r^2(\chi)}. \tag{1.28}$$

If we define the *luminosity distance* d_L as

$$d_L \equiv \frac{r(\chi)}{a} = \frac{1}{a(t)} \begin{cases} \frac{1}{H_0\sqrt{\Omega_{k0}}} \sinh(H_0\sqrt{\Omega_{k0}}\chi) & \Omega_k > 0, \\ \chi & \Omega_k = 0, \\ \frac{1}{H_0\sqrt{-\Omega_{k0}}} \sin(H_0\sqrt{-\Omega_{k0}}\chi) & \Omega_k < 0, \end{cases} \tag{1.29}$$

we can keep the form of the flux given by Eq. (1.26). Comparing Eq. (1.25) with Eq. (1.29) we observe that

$$d_A = a^2(t) d_L = \frac{d_L}{(1+z)^2}, \tag{1.30}$$

which is valid in general since the flux is conserved [61].

From equations (1.18), (1.25) and (1.29) we see that in the limit $z \ll 1$ all distances recover the Euclidean distance in Minkowski spacetime.

1.3 Components of the Universe

To calculate the equation (1.14) we need to know what are the constituents of the Universe and what are the equations of state they obey. Thus, we sketch below the standard model of particle physics (SM) and describe some properties of the fundamental ingredients that build the Universe.

1.3.1 The Standard Model of Particle Physics

The standard model of particle physics contains our present knowledge of the fundamental particles that compose all the material content in the Universe and the interactions between them. The standard model consists in a gauge group

$$G_{SM} \equiv SU(3)_c \times SU(2)_L \times U(1)_Y, \tag{1.31}$$

where $U(N)$ is defined by its fundamental representation as the group of unitary matrices $N \times N$ and $SU(N)$ is the group of special unitary matrices, i.e. unitary matrices $N \times N$ with determinant equal to 1. Thus, $SU(3)_c$ describes the internal symmetry for hadrons, which are particles that can interact via the strong interaction because they have a color charge c. This theory is described by Quantum Chromodynamics (QCD). On the other hand, $SU(2)_L \times U(1)_Y$ represents the symmetry of electroweak interaction. The indices

L, Y mean that the symmetries $SU(2)$, $U(1)$ correspond to left-handed doublets and hypercharge, respectively.

The fundamental constituents of matter are fermions with spin 1/2 which are classified as quarks or leptons. Quarks appear together forming hadrons such as: protons, neutrons, pions, kaons, etc. They have color and interact strongly as explained by QCD. Leptons, such as the electron and neutrino, have no color degree of freedom and cannot interact via strong interaction. Besides this, neutrinos do not carry electric charge either, their motion is influenced only by weak interaction.

In the standard model, interactions among quarks and leptons are mediated by gauge bosons with spin 1. There are five types of gauge bosons: photons, which are responsible for the electromagnetic interaction; $W^{\pm}$ and Z^0, that mediate the weak interaction; finally, the gluons in the strong interaction. Below is a sketch of the standard model:

$$\begin{array}{lccc} & \text{1st Generation} & \text{2nd Generation} & \text{3rd Generation} \\ \text{Quarks} & \begin{pmatrix} u^c \\ d^c \end{pmatrix}_L, u_R^c, d_R^c, & \begin{pmatrix} c^c \\ s^c \end{pmatrix}_L, c_R^c, s_R^c, & \begin{pmatrix} t^c \\ b^c \end{pmatrix}_L, t_R^c, b_R^c, \end{array} \tag{1.32}$$

$$\text{Leptons} \quad \begin{pmatrix} \nu_e \\ e^- \end{pmatrix}_L, e_R^-, \qquad \begin{pmatrix} \nu_\mu \\ \mu^- \end{pmatrix}_L, \mu_R^-, \qquad \begin{pmatrix} \nu_\tau \\ \tau^- \end{pmatrix}_L, \tau_R^-, \tag{1.33}$$

$$\text{Gauge bosons} \quad \begin{cases} \text{photon} \quad \gamma, \\ \text{weak bosons} \quad W^{\pm}, Z^0, \\ \text{gluons} \quad g, \end{cases} \tag{1.34}$$

$$\text{Higgs bosons} \quad H. \tag{1.35}$$

We can see that quarks and leptons come in three generations. The corresponding particles in each generation have the same quantum numbers except for its mass. The first family is the less massive and the third is the most massive. The $SU(3)$ triplets are represented by the color index c and the $SU(2)$ doublets are arranged in columns. Also, the upper quarks have electric charge equal to 2/3 and the lower ones have charge $-1/3$. On the other hand, neutrinos have no electric charge and their leptonic partners carry electric charge equal to -1. All of them have antiparticles with the same mass and opposite quantum numbers.

The last component of the standard model, the Higgs boson, is a scalar particle that is responsible for the Higgs mechanism. In the gauge group (1.31) the particles cannot be massive otherwise the symmetries are not preserved. Therefore, to obtain massive particles as observed in Nature we have to break the symmetry group (1.31) at some time. The Higgs mechanism accounts for that performing a spontaneous symmetry breaking (SSB), where the Lagrangian remains symmetric under (1.31) while the physical vacuum becomes non-invariant. In this way

$$SU(3)_c \times SU(2)_L \times U(1)_Y \to SU(3)_c \times U(1)_Q, \tag{1.36}$$

where Q denotes the electric charge generators.

The standard model of particle physics agrees pretty well with the observed particles and the corresponding interactions. However, from a theoretical point of view, there are some remarkable difficulties. Therefore, it is a consensus that a more fundamental theory must exist coinciding with the standard model in the low-energy limit. It should also be noted that the SM does not include gravitation.

As we said before, on large scales the behavior of the particles are governed by the gravitational interaction. In fact the strong and weak interactions act only in the nuclear range. On the other hand, the atoms that build the matter content are neutral and have spin oriented randomly so that on large scale matter do not interact with each other electromagnetically. Actually, these interactions are important in the early Universe when it was hotter and denser, but can be neglected at more recent epochs.

1.3.2 Photons

For a dilute weakly-interacting gas with g_* internal degrees of freedom, the number density n, energy density ρ and pressure P are given by [60, 62]

$$n = \frac{g_*}{(2\pi)^3}\int f(\vec{x},\vec{p})d^3p, \tag{1.37}$$

$$\rho = \frac{g_*}{(2\pi)^3}\int E(\vec{p})f(\vec{x},\vec{p})d^3p, \tag{1.38}$$

$$P = \frac{g_*}{(2\pi)^3}\int \frac{|\vec{p}|^2}{3E(\vec{p})}f(\vec{x},\vec{p})d^3p, \tag{1.39}$$

where $E^2 = |\vec{p}|^2 + m^2$ and $f(\vec{x}, \vec{p})$ is the phase space distribution function (or occupation number) which counts the number of particles around position $\vec{x}$ and momentum $\vec{p}$ in phase space. If some component is in kinetic equilibrium, i.e. is in equilibrium at temperature T, the distribution function is

$$f(\vec{x}, \vec{p}) = \frac{1}{e^{(E-\mu)/T} \pm 1}, \tag{1.40}$$

where μ is the chemical potential. Fermions obey Fermi-Dirac statistics which is represented by the above equation with the $+1$ sign and bosons obey Bose-Einstein statistics that is given by the -1 sign.

Basically, all information of the outside space comes from photons. They have a well known homogeneous and isotropic distribution at one part in 10^5. Presently, the temperature amounts to $T_0 = 2.725(2)\,\mathrm{K}$ as measured by the FIRAS instrument aboard the COBE satellite [63]. Combining equations (1.38) and (1.39) for a relativistic particle ($k_B T \gg m$) we have that

$$P = \frac{1}{3}\rho. \tag{1.41}$$

Thus, photons obey a linear barotropic equation of state with $\omega = 1/3$ and using (1.14) we can see that their energy density evolves as $\rho_\gamma \propto a^{-4}$.

Photons can be described as a gas with a temperature given by the COBE satellite and a chemical potential $\mu = 0$, since they can be freely created or destroyed. In fact, observationally, the limits on a chemical potential are $|\mu|/T < 9 \times 10^{-5}$ [64], thus μ can be safely neglected. With these assumptions, and knowing that photons have two degenerate states given by their polarizations, we obtain from (1.38)

$$\rho_\gamma = \frac{\pi^2}{15} T^4. \tag{1.42}$$

Since $\rho_\gamma \propto a^{-4}$ this tells us that the temperature of the CMB must vary as $T \propto a^{-1}$.

With respect to the critical density today, the photon energy density is

$$\frac{\rho_\gamma}{\rho_{crit}} = \frac{\pi^2}{15}\left(\frac{2.725K}{a}\right)^4 \frac{1}{8.098 \times 10^{-11}\, h^2\, \mathrm{eV}^4} = \frac{2.47 \times 10^{-5}}{h^2 a^4}, \tag{1.43}$$

where h parameterizes the Hubble constant $H_0 = 100h\ kmsec^{-1}Mpc^{-1}$ and we used that $1eV = 11605K$. Substituting the observational value of h above, $h = 0.72$ [65], and using

a normalization of a given by $a_0 = 1$, we have $\Omega_{\gamma 0} \approx 5 \times 10^{-5}$.

1.3.3 Baryons

Generally in cosmology, we call the protons, neutrons and electrons that together build the atoms, as baryons. Although electrons are not baryons, but leptons, because their masses are so small in comparison with that of the protons and neutrons, we can consider that atoms are made of baryons. In this way, the baryons form all the known matter content in the Universe.

Using equations (1.37), (1.38) and (1.39) for non-relativistic particles ($m \gg k_B T$), both fermionic and bosonic components result in the same equations for the number density, energy density and pressure

$$n = g_* \left(\frac{mT}{2\pi}\right)^{3/2} e^{-(m-\mu)/T}, \tag{1.44}$$

$$\rho = mn, \tag{1.45}$$

$$P = nT \ll \rho. \tag{1.46}$$

Combining these equations we can construct an equation of state $P(\rho) = \omega\rho \approx 0$ for non-relativistic particles. In an ideal case we consider that $\omega = const. = 0$. Thus, as baryons are non-relativistic particles, we consider that they obey an equation of state with $\omega = 0$. With this equation of state, the continuity equation (1.14) gives us that $\rho_b \propto a^{-3}$.

Now, we know how the energy density of baryons evolves with the scale factor. In this way, if we obtain the value of the energy density at some epoch, all the history will be established. However, unlike the CMB photons which can be described by a gas with a temperature T and zero chemical potential, the above equations show that the energy density for non-relativistic particles does not depend on the temperature T only. Therefore, the energy density for non-relativistic particles must be measured directly from observations.

There are four methods to measure the density of baryons and all of them are in good agreement [66]. The first method consists in observing baryons in galaxies today, the baryon density can be obtained estimating the mass of stars and mainly the mass of gas in the groups of galaxies. The second way is obtained by observing the spectra of distant quasars and the amount of light absorbed by the intervening hydrogen [67].

The anisotropies in the Universe also depend on the baryon density and studying them constitutes another form to infer the baryon density [68]. At last, the light element abundances are able to pin down the baryon density [69]. All of these observations restrict the baryon density in the Universe to $2-5\%$ of the critical density.

1.3.4 Neutrinos

Neutrinos were in equilibrium with the initial cosmic plasma, but lost contact with it slightly before the annihilation of electrons and positrons when the temperature was of the order of the electron mass. Therefore, neutrinos did not receive any energy contribution from this annihilation while the photons did. Then, photons are hotter than the neutrinos.

From the second law of thermodynamics

$$TdS = d(\rho V) + PdV - \mu d(nV), \tag{1.47}$$

we obtain that the entropy density is defined by

$$s \equiv \frac{\rho + P - \mu n}{T}. \tag{1.48}$$

Now, as all evidences indicate that $|\mu| \ll T$, we can assume that all chemical potentials are zero. Thus, using the energy conservation (1.14) it can be demonstrated that the entropy per comoving volume is conserved, $sa^3 = constant$.

Equations (1.38) and (1.48) tell us that massless bosons contribute with $2\pi^2 T^3/45$ to the entropy density for each degenerate state, massless fermions with $7/8$ of this value and from (1.44), (1.45) and (1.46) we see that massive particles have a negligible contribution to the entropy density. Before the annihilation of electrons and positrons, the particles in equilibrium in the cosmic plasma were electrons, positrons, neutrinos, anti-neutrinos and photons. Considering the degeneracies of these particles, the entropy density at this epoch a_1 was

$$s(a_1) = \frac{2\pi^2}{45} T_1^3 \left[2 + \frac{7}{8}(2+2+3+3)\right] = \frac{43\pi^2}{90} T_1^3. \tag{1.49}$$

After the annihilation, there are no electrons or positrons and the neutrinos are not in

equilibrium with the photons. Thus at an epoch a_2 after annihilation, we have

$$s(a_2) = \frac{2\pi^2}{45}\left(2T_\gamma^3 + \frac{7}{8}6T_\nu^3\right). \tag{1.50}$$

However, since $sa^3 = constant$, we obtain

$$s(a_1)a_1^3 = \frac{43\pi^2}{90}(a_1T_1)^3 = \frac{4\pi^2}{45}\left[\left(\frac{T_\gamma}{T_\nu}\right)^3 + \frac{21}{8}\right](a_2T_\nu)^3 = s(a_2)a_2^3. \tag{1.51}$$

The neutrino temperature varies proportionally to a^{-1}, i.e. $a_1T_1 = a_2T_\nu$, thus the above relation implies

$$\frac{T_\nu}{T_\gamma} = \left(\frac{4}{11}\right)^{1/3}. \tag{1.52}$$

Now that we can associate a temperature with the neutrinos, we can use (1.38) for a massless fermion to compute the energy density of neutrinos. Each neutrino has one degree of freedom and there are three generations of them with their corresponding anti-particles, thus taking into account all of these contributions the neutrinos possess a total of six degrees of freedom. In this way

$$\rho_\nu = \frac{7\pi^2}{40}\left(\frac{4}{11}\right)^{4/3}T_\gamma^4. \tag{1.53}$$

With respect to the critical density, results

$$\Omega_{\nu 0} = \frac{\rho_{\nu 0}}{\rho_{crit0}} = \frac{1.68\times 10^{-5}}{h^2}. \tag{1.54}$$

Actually, neutrinos seem to be massive as observed from oscillations of solar [70] and atmospheric neutrinos [71]. Nevertheless, at epochs where the temperature is much larger than the predicted mass of the neutrinos, we can consider them as massless. Just when $k_BT \sim m_\nu$ or less, we have to consider the mass of the neutrinos. For a massive neutrino, the relative energy density will be [60]

$$\Omega_{\nu 0} = \frac{m_\nu}{94h^2eV}. \tag{1.55}$$

Finally, we emphasize that, unlike baryons and photons, cosmic neutrinos have not been observed. Their contributions come from theoretical arguments.

1.3.5 Dark Matter

There is a large number of evidences in ranges from the galactic to cosmological scales indicating the presence of a new component in the Universe or some deviation from the known laws of gravitation. If it actually is a new component, it cannot interact electromagnetically, since its presence can only be detected via gravitational effects. Thus, it is dubbed *dark matter*.

On galactic scales, the most convincing and direct evidence of dark matter comes from observations of the rotation curves. The rotation curves of galaxies are a measure of circular velocities of stars and gas as a function of their distance from the galactic center. Theoretically, using Newtonian dynamics, we expect the circular velocities to be

$$v(r) = \sqrt{\frac{GM(r)}{r}}, \tag{1.56}$$

where $M(r) \equiv 4\pi \int \rho(r) r^2 dr$ is the mass interior to the radius r and $\rho(r)$ is the mass density profile. The above equation tells us that beyond the optical disc the circular velocity should scale as $v(r) \propto 1/\sqrt{r}$. However, observationally, rotation curves usually exhibit a flat behavior at large distances from the galactic center as can be seen in Fig. 1.1.

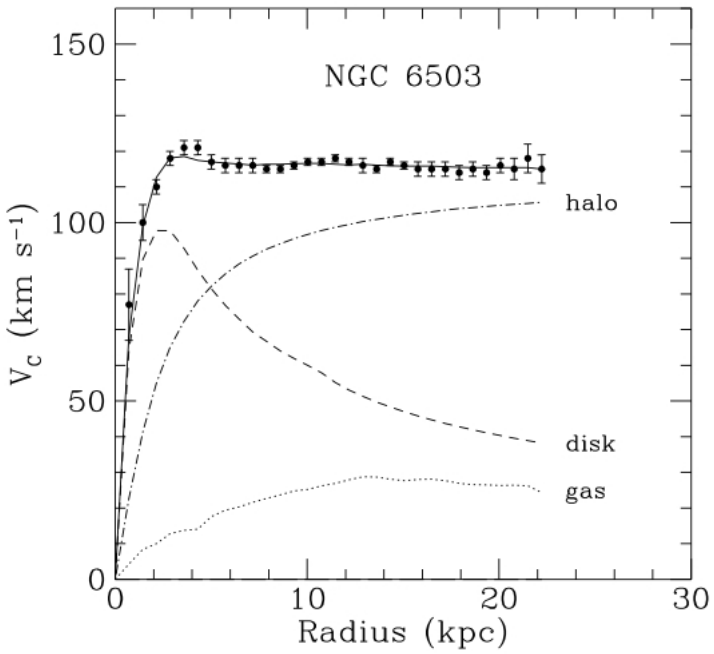

Figure 1.1: Rotation curve for the spiral galaxy NGC 6503. The dotted, dashed and dash-dotted lines are the contributions to the circular velocities of gas, disk and dark matter halo, respectively. Extracted from [72], itself based on [73].

Actually, the first indication of dark matter was obtained by Zwicky in 1933 [74]. Studying the Coma cluster he inferred a mass-to-light ratio of 400 solar masses per solar luminosity, two orders of magnitude greater than observed in the solar neighborhood. The mass of a galaxy cluster can be determined in several ways: applying the virial theorem to the observed distribution of radial velocities, by weak gravitational lensing, and from the X-ray emitted by the hot gas in the cluster. All of these measurements are consistent with $\Omega_m \sim 0.2 - 0.3$ [75–77].

Finally, on cosmological scales, the anisotropies of the cosmic microwave background (CMB) provide stringent constraints on the abundance of baryons and dark matter in the Universe as placed by the Wilkinson Microwave Anisotropy Probe (WMAP) data. Recent determinations give $\Omega_{dm0} = 0.228 \pm 0.013$ [68].

All of these evidences show that there must be in the Universe a component that contributes with around 25% of the critical energy density. Since baryons contribute with only 5%, this component must be nonbaryonic. Because it does not interact electromagnetically the first guess would be neutrinos. However, from (1.55) and the upper limit on the neutrino mass $m_\nu < 2.05eV$ [78], we have

$$\Omega_\nu h^2 \leq 0.07, \tag{1.57}$$

which means that there are not enough neutrinos to be the dominant component of dark matter. Thus, dark matter must really be a new component.

1.3.6 Dark Energy

Observations of anisotropies in the CMB have shown that the geometry of the spatial section is very close to a flat one [79–82]. Actually, we also expect this theoretically from inflationary scenarios in the early Universe [60]. This means that the total energy density should be equal to the critical density. However, summing the contributions of all the components described so far, we obtain that they contribute with around 30% of the critical density. Thus, there is a lack of 70% in the energy content of the Universe.

Using the luminosity distance (1.29) we can find the apparent magnitude m of an

object with intrinsic magnitude M. Conventionally we have

$$m - M = 5 \log \left(\frac{d_L}{10pc} \right) + \mathcal{K}, \tag{1.58}$$

where $\mathcal{K}$ is a shifting correction factor of the spectrum into the wavelength range measured. In 1998, two groups measured the apparent magnitude of various supernovae Type Ia and established that a universe dominated by a vacuum energy density, i.e. a cosmological constant, with equation of state $\omega = -1$ is favored by the data [83, 84], as shown in Figure 1.2.

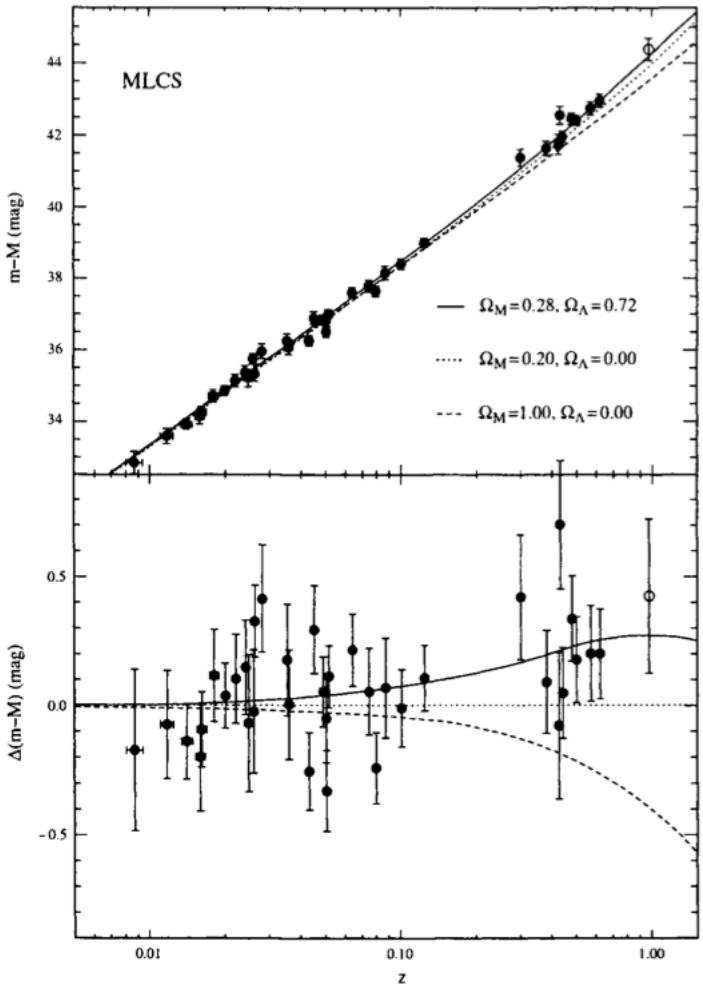

Figure 1.2: Hubble diagram from distant Type Ia supernovae. It is plotted three curves predicted by different energy contents in the Universe. Extracted from [60].

These two sets of observational evidences show that beyond dark matter there must be another unknown component in the Universe, which is called *dark energy*. Then, we conclude that our present Universe is composed of around 5% of baryons, 25% of dark matter and 70% of dark energy, with insignificant contributions of photons and neutrinos.

Nowadays, the best model explaining the data is the ΛCDM, with cold dark matter (CDM) and where dark energy is the cosmological constant Λ.

The ΛCDM model is the simplest one that fits the data. However, it suffers of two theoretical problems. The first occurs when we try to associate the cosmological constant with the vacuum energy density. In quantum field theory, we generally introduce a cut off on the energy beyond which our theory cannot describe the physics. If we introduce this cut off at the Planck reduced mass $M_{Pl} = (8\pi G)^{-1/2} = 2.436 \times 10^{18} GeV$ [85], the vacuum energy density will be given by $\rho_{vac} \sim M_{Pl}^4 \sim 10^{73}(GeV)^4$. On the other hand, the energy density of dark energy today is $\rho_\Lambda = 3M_{Pl}^2 H_0^2 \Omega_\Lambda \sim 10^{-47}(GeV)^4$. Thus, there is a difference of 120 orders of magnitude, which is known as *the cosmological constant problem.*

The second problem arises when we consider the evolution of the components in the Universe. As we already saw, the non-relativistic matter (baryons and dark matter) scales as $\rho_m \propto a^{-3}$, radiation scales as $\rho_r \propto a^{-4}$ and the cosmological constant has a density $\rho_\Lambda = constant$. Therefore, each component scales in a very different way. But, as mentioned above, matter and dark energy have the same order of magnitude today. Thus, the question arise: "why matter and dark energy have the same order of magnitude exactly now in the whole history of the Universe?". This is called *the coincidence problem.*

These difficulties in the ΛCDM model have motivated the search for new models of dark energy. In conclusion we observe that both dark matter and dark energy have no explanation in the standard model of particle physics.

Chapter 2

Cosmological Perturbations

The description of the Universe was, up to now, performed considering it as homogeneous and isotropic, as described by the cosmological principle. However, the structures around us imply that at some point we have to break these assumptions and introduce inhomogeneities and anisotropies in our model. Because on large scales the cosmological principle leads to correct results, we shall do that using perturbation theory.

2.1 Perturbed Metric

The metric of a flat FLRW universe with small perturbations can be written as

$$ds^2 = \left[{}^{(0)}g_{\mu\nu} + \delta g_{\mu\nu}(x^\gamma)\right] dx^\mu dx^\nu, \tag{2.1}$$

where ${}^{(0)}g_{\mu\nu}$ corresponds to the unperturbed part and $|\delta g_{\mu\nu}| \ll |{}^{(0)}g_{\mu\nu}|$. Using the conformal time (1.17), the most general components of the metric tensor are given by [86]

$$g_{00} = -a^2(1+2\psi), \tag{2.2}$$

$$g_{0i} = a^2(B_{,i} + S_i), \tag{2.3}$$

$$g_{ij} = a^2\left[(1+2\phi)\delta_{ij} + D_{ij}E + F_{i,j} + F_{j,i} + h_{ij}\right], \tag{2.4}$$

where the perturbations are introduced by the scalar functions ψ, B, ϕ and E; the divergence free vectors S_i and F_i; and a traceless and transverse tensor h_{ij}. Here the comma means differentiation with respect to the respective spatial index, e.g. $B_{,i} = \partial B/\partial x^i$. We

also define

$$D_{ij} = \left(\partial_i\partial_j - \frac{1}{3}\delta_{ij}\nabla^2\right). \tag{2.5}$$

From the three types of perturbations, the scalars are the most important in cosmology because they present gravitational instability and can lead to structure formation in the Universe. The vector perturbations are responsible for rotational motions of the fluid and decay very quickly. Finally, tensor perturbations describe gravitational waves, but in the linear approximation they do not induce perturbations in the perfect fluid. Moreover, the decomposition theorem [60, 86] states that these three types of perturbations evolve independently. Thus, in this work, we will only be interested in scalar perturbations. In this case the metric becomes

$$ds^2 = a^2\left[-(1+2\psi)d\eta^2 + 2\partial_i B d\eta dx^i + (1+2\phi)\delta_{ij}dx^i dx^j + D_{ij}E dx^i dx^j\right]. \tag{2.6}$$

Given a coordinate transformation

$$x^\mu \to \tilde{x}^\mu = x^\mu + \xi^\mu, \tag{2.7}$$

where $\xi^\mu \equiv (\xi^0,\ \xi^i_\perp + \zeta'^i)$ are infinitesimally small functions of space and time, the metric tensor has its components changed by

$$\tilde{g}_{\mu\nu}(\tilde{x}^\rho) = \frac{\partial x^\gamma}{\partial\tilde{x}^\mu}\frac{\partial x^\delta}{\partial\tilde{x}^\nu}g_{\gamma\delta}(x^\rho) \approx {}^{(0)}g_{\mu\nu}(x^\rho) + \delta g_{\mu\nu} - {}^{(0)}g_{\mu\delta}\xi^\delta{}_{,\nu} - {}^{(0)}g_{\gamma\nu}\xi^\gamma{}_{,\mu}\ , \tag{2.8}$$

at first order in δg and ξ. The new coordinate system also allows to split the metric into a background and a perturbed part

$$\tilde{g}_{\mu\nu}(\tilde{x}^\rho) = {}^{(0)}g_{\mu\nu}(\tilde{x}^\rho) + \delta\tilde{g}_{\mu\nu}, \tag{2.9}$$

where ${}^{(0)}g_{\mu\nu}(\tilde{x}^\rho)$ is the Friedmann metric in the new coordinates. On the other hand, expanding the background part of (2.1) in a Taylor series around the coordinates $\tilde{x}$, we have

$${}^{(0)}g_{\mu\nu}(x^\rho) \approx {}^{(0)}g_{\mu\nu}(\tilde{x}^\rho) - {}^{(0)}g_{\mu\nu,\gamma}\,\xi^\gamma\ . \tag{2.10}$$

Therefore, comparing Eqs. (2.8) and (2.9) and also using Eq. (2.10), we obtain the gauge

transformation law

$$\delta g_{\mu\nu} \to \delta\tilde{g}_{\mu\nu} = \delta g_{\mu\nu} - {}^{(0)}g_{\mu\nu,\gamma}\,\xi^{\gamma} - {}^{(0)}g_{\mu\delta}\xi^{\delta}{}_{,\nu} - {}^{(0)}g_{\gamma\nu}\xi^{\gamma}{}_{,\mu}\ . \tag{2.11}$$

Using the gauge transformation law (2.11), the metric (2.6) has its components changed as

$$\tilde{\psi} = \psi - \frac{1}{a}(a\xi^0)', \tag{2.12}$$

$$\tilde{B} = B - \zeta' + \xi^0, \tag{2.13}$$

$$\tilde{\phi} = \phi - \frac{1}{6}\nabla^2 E - \frac{a'}{a}\xi^0, \tag{2.14}$$

$$\tilde{E} = E - 2\zeta. \tag{2.15}$$

Here a prime means the derivative with respect to the conformal time. The coordinate transformation (2.7) is completely arbitrary, then we can choose ξ^0 and ζ freely. Thus, the above transformations of the metric components show we can choose ξ^0 and ζ appropriately in order to eliminate two of the four functions ψ, B, ϕ and E. Therefore, there are just two physical perturbations. Combining equations (2.12)-(2.15), we can construct two gauge-invariant functions which span the two-dimensional space of physical perturbations

$$\Psi = \psi - \frac{1}{a}\left[\left(-B + \frac{E'}{2}\right)a\right]', \tag{2.16}$$

$$\Phi = \phi - \frac{1}{6}\nabla^2 E + \frac{a'}{a}\left(B - \frac{E'}{2}\right). \tag{2.17}$$

Instead of working with gauge-invariant functions, we can impose two conditions on the coordinate transformation, which is equivalent to a gauge choice. In particular, the *conformal-Newtonian gauge* is obtained with coordinates ξ^0 and ζ such that $B = E = 0$. Another gauge, widely used in the literature, is the *synchronous gauge*. It corresponds to the gauge choice $\psi = B = 0$. However, unlike the conformal-Newtonian gauge, the synchronous gauge does not fix the coordinates uniquely. If the conditions $\psi = B = 0$ are satisfied in a coordinate system $x^\mu \equiv (\eta, \vec{x})$, they will also be satisfied in any coordinate system $\tilde{x}^\mu$ given by

$$\tilde{\eta} = \eta + \frac{C_1(x^j)}{a}, \qquad \tilde{x}^i = x^i + C_{1,i}\,(x^j)\int\frac{d\eta}{a} + C_{2,i}\,(x^j), \tag{2.18}$$

where $C_1(x^j)$ and $C_2(x^j)$ are arbitrary functions of the spatial coordinates.

Equations (2.16) and (2.17) allow to relate the gauge-invariant perturbations with the perturbations in a particular gauge. Thus, if we know a solution for perturbations with gauge-invariant variables, or using the conformal-Newtonian gauge, we can transform it into the synchronous gauge without needing to solve the Einstein equations again.

2.2 Einstein Equations

Now we know the components of the perturbed metric tensor. We can thus obtain their evolution using the Einstein equations (1.5). Assuming the perturbations are small we can expand them in a Taylor series. Thus, as we did to the metric tensor, it is possible to split the Einstein tensor G^μ_ν and the energy-momentum tensor T^μ_ν into background and perturbed parts: $G^\mu_\nu = {}^{(0)}G^\mu_\nu + \delta G^\mu_\nu$ and $T^\mu_\nu = {}^{(0)}T^\mu_\nu + \delta T^\mu_\nu$. The zeroth order terms correspond to the homogeneous and isotropic background and the others give us the perturbed Einstein equations

$$\delta G^\mu_\nu = 8\pi G \delta T^\mu_\nu. \tag{2.19}$$

The geometric part of the Einstein equations (2.19) can be solved following the same procedure adopted in the last chapter. Thus, using the perturbed metric (2.6) in the conformal-Newtonian gauge and keeping only first-order terms, we obtain

$$\begin{aligned}
\delta G^0_0 &= 2a^{-2}\left[3\mathcal{H}\left(\mathcal{H}\Psi - \Phi'\right) + \nabla^2\Phi\right], && (2.20)\\
\delta G^0_i &= 2a^{-2}\left(\Phi' - \mathcal{H}\Psi\right)_{,i}, && (2.21)\\
\delta G^i_j &= 2a^{-2}\left[\left(\mathcal{H}^2 + 2\mathcal{H}'\right)\Psi + \mathcal{H}\Psi' - \Phi'' - 2\mathcal{H}\Phi'\right]\delta^i_j + \\
&\quad a^{-2}\left[\nabla^2\left(\Psi + \Phi\right)\delta^i_j - \left(\Psi + \Phi\right)_{,j}^{,i}\right]. && (2.22)
\end{aligned}$$

Here we defined the conformal Hubble parameter $\mathcal{H} \equiv \frac{1}{a}\frac{da}{d\eta} = Ha$ and from Eqs. (2.16) and (2.17) we see that $\Psi = \psi$ and $\Phi = \phi$ in this gauge.

From equations (2.20)-(2.22), we observe that the Einstein equations (2.19) turn out to be a set of linear partial differential equations. If we Fourier expand all perturbation

quantities

$$\theta(\vec{x},\eta) = \int \frac{d^3k}{(2\pi)^3} e^{i\vec{k}\cdot\vec{x}} \tilde{\theta}_k(\eta), \tag{2.23}$$

where θ denotes a generic perturbation and the subscript k represents a Fourier mode for each wavenumber k, the resulting Fourier amplitudes obey ordinary differential equations. Thus, working in the Fourier space makes things easier. Furthermore, the Fourier modes θ_k evolve independently in the linear regime. Therefore, instead of solving an infinite number of coupled equations, we can solve for one k-mode at a time. In practice, each perturbation quantity θ and its derivatives can be substituted as

$$\theta(\vec{x},\eta) \rightarrow e^{i\vec{k}\cdot\vec{x}}\tilde{\theta}(\eta), \tag{2.24}$$

$$\vec{\nabla}\theta(\vec{x},\eta) \rightarrow ie^{i\vec{k}\cdot\vec{x}}\vec{k}\tilde{\theta}(\eta), \tag{2.25}$$

$$\nabla^2\theta(\vec{x},\eta) \equiv \nabla_i\nabla^i\theta(\vec{x},\eta) \rightarrow -e^{i\vec{k}\cdot\vec{x}}k^2\tilde{\theta}(\eta), \tag{2.26}$$

where we are omitting the subscript k to simplify the notation.

The Einstein equations are a set of 16 equations. However, the symmetries in the indices μ, ν reduce the number of independent equations to 10. Only two of the four scalar functions in the metric (2.6) represent physical states. Thus, choosing the conformal-Newtonian gauge, we just need two Einstein equations to obtain the evolution of the functions Ψ and Φ. We choose the time-time component of the Einstein equations (2.19)

$$\delta\tilde{G}^0_0 = \frac{2}{a^2}\left[3\mathcal{H}\left(\mathcal{H}\tilde{\Psi} - \tilde{\Phi}'\right) - k^2\tilde{\Phi}\right] = 8\pi G\delta\tilde{T}^0_0 \tag{2.27}$$

and the longitudinal traceless projection of the space-space components

$$\left(\hat{k}_i\hat{k}^j - \frac{1}{3}\delta^j_i\right)\delta\tilde{G}^i_j = \frac{2}{3a^2}k^2(\tilde{\Psi}+\tilde{\Phi}) = 8\pi G\left(\hat{k}_i\hat{k}^j - \frac{1}{3}\delta^j_i\right)\delta\tilde{T}^i_j. \tag{2.28}$$

These equations were written in the Fourier space and we defined the unit direction wavevector $\hat{k}^i = \hat{k}_i$, which satisfies $\delta_{ij}\hat{k}^i\hat{k}^j = 1$.

2.3 Boltzmann Equation

To solve the Einstein equations (2.27) and (2.28) we need the first-order components of the energy-momentum tensor. This could be obtained using the hydrodynamic equations

as in the homogeneous and isotropic case. However, those equations can be obtained by the first moments of the Boltzmann equation, which means that it is more general. Furthermore, the radiation description is made using fluctuations of the temperature, and the Boltzmann formalism is more natural in this case.

The Boltzmann equation formalizes the statement that the variation in the distribution of some species is equal to the difference between the rates of ingoing and outgoing particles of that species. In its differential form, the Boltzmann equation is

$$\frac{df}{dt} = C[f], \tag{2.29}$$

where f is the distribution function and $C[f]$ is a functional of the distribution function, which establishes all possible collision terms of the particle of interest. In general, f is a function of the spacetime point $x^\mu = (t, \vec{x})$ and also of the four-dimensional momentum vector in comoving frame

$$P^\mu \equiv \frac{dx^\mu}{d\lambda}, \tag{2.30}$$

where λ parametrizes the particle's path. The four-vector P^μ is related to the physical momentum four-vector p^μ by $P^\mu = \frac{\partial x^\mu}{\partial \tilde{x}^\nu} p^\nu$, with $\tilde{x}^\nu$ in the physical frame.

In order to calculate the perturbed energy-momentum tensor, we develop below the Boltzmann equation for each component in the Universe.

2.3.1 Photons

Photons satisfy the energy-momentum relation

$$P^2 \equiv g_{\mu\nu} P^\mu P^\nu = -(1+2\Psi)(P^0)^2 + g_{ij} P^i P^j = -(1+2\Psi)(P^0)^2 + p^2 = 0, \tag{2.31}$$

where we used the metric (2.6) in the conformal-Newtonian gauge passing to the cosmic time and p^2 is the generalized magnitude of the momentum. The above relation allows us to express P^0 in terms of p. Thus, there are only three independent components of the four-dimensional momentum vector. Then, we can expand the total time derivative of f in the Boltzmann equation (2.29) considering only the momentum magnitude p and

angular direction $\hat{p}^i = \hat{p}_i$:

$$\frac{df}{dt} = \frac{\partial f}{\partial t} + \frac{\partial f}{\partial x^i} \cdot \frac{dx^i}{dt} + \frac{\partial f}{\partial p} \cdot \frac{dp}{dt} + \frac{\partial f}{\partial \hat{p}^i} \cdot \frac{d\hat{p}^i}{dt}, \tag{2.32}$$

where $\delta_{ij}\hat{p}^i\hat{p}^j = 1$.

Let us begin to solve equation (2.32). The last term does not contribute at first order in perturbation theory. In fact, the zeroth order part of f depends only on p, which means $\partial f/\partial \hat{p}^i$ is nonzero only in a perturbed level. In the same way, a photon moves in a straight line in the absence of the potentials Ψ and Φ, therefore, $d\hat{p}^i/dt$ is also a perturbed quantity. Thus, the last term of (2.32) must be of second order.

Using the definition of the comoving energy-momentum vector (2.30), we obtain

$$\frac{dx^i}{dt} = \frac{dx^i}{d\lambda}\frac{d\lambda}{dt} = \frac{P^i}{P^0}. \tag{2.33}$$

From (2.31) the time-component of P^μ is given by

$$P^0 = \frac{p}{\sqrt{1+2\Psi}} = p(1-\Psi), \tag{2.34}$$

where the last equality is valid at first order. On the other hand, the spatial component is proportional to the unit direction vector $\hat{p}^i$

$$P^i \equiv |P|\hat{p}^i. \tag{2.35}$$

Plugging (2.35) in the definition of the spatial magnitude, we find

$$p^2 \equiv g_{ij}P^iP^j = a^2(1+2\Phi)(\delta_{ij}\hat{p}^i\hat{p}^j)P^2 = a^2(1+2\Phi)P^2, \tag{2.36}$$

which gives $|P| = p(1-\Phi)/a$ at first order. Therefore, combining equations (2.34) and (2.35), we have

$$\frac{dx^i}{dt} = \frac{1-\Phi+\Psi}{a}\hat{p}^i. \tag{2.37}$$

The next term we need to evaluate is dp/dt. This factor can be calculated from the time component of the geodesic equation $dP^0/d\lambda = -\Gamma^0_{\mu\nu}P^\mu P^\nu$ in a simple, although

tedious, way [60]. Here we just show the final result

$$\frac{dp}{dt} = -p\left(H + \frac{\partial\Phi}{\partial t} + \frac{\hat{p}^i}{a}\frac{\partial\Psi}{\partial x^i}\right). \tag{2.38}$$

Combining the terms obtained so far, the left hand side of the Boltzmann equation for photons yields

$$\frac{df}{dt} = \frac{\partial f}{\partial t} + \frac{\hat{p}^i}{a}\frac{\partial f}{\partial x^i} - p\frac{\partial f}{\partial p}\left(H + \frac{\partial\Phi}{\partial t} + \frac{\hat{p}^i}{a}\frac{\partial\Psi}{\partial x^i}\right), \tag{2.39}$$

where we neglected the product of $\partial f/\partial x^i$ and either Ψ or Φ because they are second-order terms.

Photons in a homogeneous and isotropic distribution with an equilibrium temperature T obey the Bose-Einstein statistics given by equation (1.40). There, T is a function of time only. To describe perturbations about this distribution, we have to introduce inhomogeneities, so that it must have an $\vec{x}$ dependence, and anisotropies, which means a dependence with the direction of propagation $\hat{p}$. Thus, for photons, the distribution function is given by

$$f(t,\vec{x},p,\hat{p},) = \left\{\exp\left[\frac{p}{T(t)[1+\Theta(t,\vec{x},\hat{p})]}\right] - 1\right\}^{-1}, \tag{2.40}$$

where $T(t)$ is the zero-order temperature and $\Theta \equiv \delta T/T$ characterizes the perturbation to the distribution function. Here we have assumed that Θ does not depend on the magnitude p, which is a valid assumption since in a Compton scattering p is approximately conserved. Expanding up to first order,

$$f = f^{(0)} + T\frac{\partial f^{(0)}}{\partial T}\Theta = f^{(0)} - p\frac{\partial f^{(0)}}{\partial p}\Theta. \tag{2.41}$$

Plugging Eq. (2.41) into Eq. (2.39) and collecting terms of similar order, at zeroth order we find the background equations for the number and energy conservation from the first moments of the Boltzmann equation. Finally, the first-order terms result in

$$\frac{df^{(1)}}{dt} = -p\frac{\partial f^{(0)}}{dp}\left[\frac{\partial\Theta}{\partial t} + \frac{\hat{p}^i}{a}\frac{\partial\Theta}{\partial x^i} + \frac{\partial\Phi}{\partial t} + \frac{\hat{p}^i}{a}\frac{\partial\Psi}{\partial x^i}\right]. \tag{2.42}$$

The last step necessary to calculate the Boltzmann equation for photons is the collision

term. Photons interact with electrons through the Compton scattering

$$e^-(\vec{q}) + \gamma(\vec{p}) \leftrightarrow e^-(\vec{q}') + \gamma(\vec{p}'), \tag{2.43}$$

where the momentum of each particle is indicated. To obtain the effect of the Compton scattering in the distribution function of photons with momentum $\vec{p}$, we must sum the contributions of all the other momenta to the collision term [60]

$$C[f(\vec{p})] = \frac{1}{p}\int \frac{d^3q}{(2\pi)^3 2E_e(q)} \int \frac{d^3q'}{(2\pi)^3 2E_e(q')} \int \frac{d^3p'}{(2\pi)^3 2E(p')} |\mathcal{M}|^2 (2\pi)^4 \\ \times \delta^3[\vec{p}+\vec{q}-\vec{p}'-\vec{q}']\delta[E(p)+E_e(q)-E(p')-E_e(q')] \times \{f_e(\vec{q}')f(\vec{p}') - f_e(\vec{q})f(\vec{p})\}\,. \tag{2.44}$$

Some explanation about the collision term is fruitful here. First we note that in the Boltzmann equation (2.29) we considered the total time derivative of the distribution f. However, general relativity requires derivatives with respect to the affine parameter λ, $\frac{df}{d\lambda} = \frac{dt}{d\lambda}\frac{df}{dt} = P^0\frac{df}{dt}$. At first order this introduces the factor $\frac{1}{p}$ in front of the integrals. Actually, the integrals are over the four-momentum vectors and the factors of $2E$ come from the integration over the time component. $\mathcal{M}$ is the scattering amplitude of the process in question, which can be found using the Feynman rules. The delta functions arise from conservation of energy and momentum. Finally, the last terms count the number of particles with the given momenta [1].

At the epochs of interest the energies are the relativistic limit for photons $E(p) = p$ and the non-relativistic limit for electrons $E_e(q) = m_e + q^2/(2m_e) \approx m_e$. Thus, we can use the three-dimensional delta function to eliminate the integral over $\vec{q}'$

$$C[f(\vec{p})] = \frac{\pi}{4m_e^2 p}\int \frac{d^3q}{(2\pi)^3} \int \frac{d^3p'}{(2\pi)^3 p'} |\mathcal{M}|^2 \times \delta[p + \frac{q^2}{2m_e} - p' - \frac{(\vec{q}+\vec{p}-\vec{p}')^2}{2m_e}] \\ \times \{f_e(\vec{q}+\vec{p}-\vec{p}')f(\vec{p}') - f_e(\vec{q})f(\vec{p})\}\,. \tag{2.45}$$

For non-relativistic Compton scattering very little energy is transferred $E_e(q) - E_e(\vec{q}+\vec{p}-\vec{p}') \approx \frac{(\vec{p}'-\vec{p})\cdot\vec{q}}{m_e}$, which holds since $\vec{q}$ is much larger than $\vec{p}$ and $\vec{p}'$. In this limit, the scattering is nearly elastic $p' \approx p$. As the change in the electron energy is small, it makes

[1] We should include additional factors of $1+f$ and $1-f_e$ for stimulated emission and Pauli blocking, respectively. However, at first order these terms can be neglected.

sense to expand the final electron kinetic energy $(\vec{q}+\vec{p}-\vec{p}\,')^2/(2m_e)$ around its zeroth order value $q^2/(2m_e)$. Therefore, we can make the formal expansion in the delta function

$$\begin{aligned}\delta[p+\frac{q^2}{2m_e}-p'-\frac{(\vec{q}+\vec{p}-\vec{p}\,')^2}{2m_e}] &\approx \delta(p-p') \\ &+ [E_e(q')-E_e(q)]\left.\frac{\partial\delta[p+E_e(q)-p'-E_e(q')]}{\partial E_e(q')}\right|_{E_e(q)=E_e(q')} \\ &= \delta(p-p')+\frac{(\vec{p}-\vec{p}\,')\cdot\vec{q}}{m_e}\frac{\partial\delta(p-p')}{\partial p'}. \end{aligned} \tag{2.46}$$

Using this expansion and $f_e(\vec{q}+\vec{p}-\vec{p}\,')\approx f_e(\vec{q})$, we obtain

$$\begin{aligned}C[f(\vec{p})] = \frac{\pi}{4m_e^2 p}\int\frac{d^3q}{(2\pi)^3}f_e(\vec{q})\int\frac{d^3p'}{(2\pi)^3p'}|\mathcal{M}|^2 \\ \times\left\{\delta(p-p')+\frac{(\vec{p}-\vec{p}\,')\cdot\vec{q}}{m_e}\frac{\partial\delta(p-p')}{\partial p'}\right\}\times\{f(\vec{p}\,')-f(\vec{p})\}\,. \end{aligned} \tag{2.47}$$

The amplitude for Compton scattering can be found using the Feynman rules [87]

$$|\mathcal{M}|^2 = 12\pi\sigma_T m_e^2(\hat{\epsilon}\cdot\hat{\epsilon}\,'), \tag{2.48}$$

where σ_T is the Thomson cross section, $\hat{\epsilon}$ and $\hat{\epsilon}\,'$ are the polarization vectors of the initial and final photons, respectively. For simplicity, we average over all polarizations and angular dependence which results in a constant amplitude

$$|\mathcal{M}|^2 = 8\pi\sigma_T m_e^2. \tag{2.49}$$

Thus, using this amplitude and the expansion of the distribution function (2.41), the collision term can be written as

$$\begin{aligned}C[f(\vec{p})] = \frac{2\pi^2 n_e\sigma_T}{p}\int\frac{d^3p'}{(2\pi)^3p'}\times\left\{\delta(p-p')+(\vec{p}-\vec{p}\,')\cdot\vec{v}_b\frac{\partial\delta(p-p')}{\partial p'}\right\} \\ \times\left\{f^{(0)}(\vec{p}\,')-f^{(0)}(\vec{p})-p'\frac{\partial f^{(0)}}{\partial p'}\Theta(\hat{p}\,')+p\frac{\partial f^{(0)}}{\partial p}\Theta(\hat{p})\right\}, \end{aligned} \tag{2.50}$$

where we did the integrals over momentum $\vec{q}$ using the number density definition (1.37) and we define the velocity as

$$v^i \equiv \frac{g_*}{n}\int\frac{d^3p}{(2\pi)^3}f\frac{p\hat{p}^i}{E}. \tag{2.51}$$

The spin degeneracy g_* can be incorporated into the phase space distribution f.

To solve the integral over $\vec{p}'$ in Eq. (2.50), we split the radial and angular parts of the differential d^3p'. Then, keeping only first-order terms in perturbations, the integral over the solid angle yields

$$C[f(\vec{p})] = \frac{n_e\sigma_T}{p}\int_0^\infty dp'p'\left\{\delta(p-p')\left[-p'\frac{\partial f^{(0)}}{\partial p'}\Theta_0 + p\frac{\partial f^{(0)}}{\partial p}\Theta(\hat{p})\right]\right. \\ \left. +\vec{p}\cdot\vec{v}_b\frac{\partial\delta(p-p')}{\partial p'}\left[f^{(0)}(p') - f^{(0)}(p)\right]\right\}, \quad (2.52)$$

where we define the multipoles

$$\Theta_l \equiv \frac{1}{(-i)^l}\int_{-1}^{1}\frac{d\mu}{2}P_l(\mu)\Theta(\mu), \quad (2.53)$$

such that P_l is the Legendre polynomial of order l and instead of the unit vector $\hat{p}$, we used the direction cosine

$$\mu \equiv \frac{\vec{k}\cdot\hat{p}}{k}. \quad (2.54)$$

Finally, the p' integral can be done in the first line of Eq. (2.52) with the delta function and in the second line integrating by parts, the result is [60]

$$C[f(\vec{p})] = -p\frac{\partial f^{(0)}}{\partial p}n_e\sigma_T\left[\Theta_0 - \Theta(\hat{p}) + \hat{p}\cdot\vec{v}_b\right], \quad (2.55)$$

where n_e is the electron density and $\vec{v}_b$ is the velocity of the electrons, which is associated with the baryons.

At last the first-order Boltzmann equation (2.29) for photons can be obtained equating Eq. (2.42) and Eq. (2.55)

$$\frac{\partial\Theta}{\partial t} + \frac{\hat{p}^i}{a}\frac{\partial\Theta}{\partial x^i} + \frac{\partial\Phi}{\partial t} + \frac{\hat{p}^i}{a}\frac{\partial\Psi}{\partial x^i} = n_e\sigma_T\left[\Theta_0 - \Theta(\hat{p}) + \hat{p}\cdot\vec{v}_b\right]. \quad (2.56)$$

As usual we assume the fluid to be irrotational, which means we can write $v_b^i = v_b k^i/k$. Thus, passing to the conformal time and Fourier space we obtain

$$\tilde{\Theta}' + ik\mu\tilde{\Theta} + \tilde{\Phi}' + ik\mu\tilde{\Psi} = -\tau'\left[\tilde{\Theta}_0 - \tilde{\Theta}(\hat{p}) + \mu\tilde{v}_b\right], \quad (2.57)$$

where we defined the *optical depth*

$$\tau \equiv \int_{\eta}^{\eta_0} n_e \sigma_T a d\tilde{\eta}. \tag{2.58}$$

When deriving Eq. (2.57) we use a constant amplitude given by (2.49). Actually, the Compton scattering has an angular dependence and it also couples the temperature field to the strength of the polarization field Θ_P. The general expression can be obtained following the same procedure we did, but using the complete amplitude (2.48). The answer is [60]

$$\tilde{\Theta}' + ik\mu\tilde{\Theta} + \tilde{\Phi}' + ik\mu\tilde{\Psi} = -\tau'[\tilde{\Theta}_0 - \tilde{\Theta} + \mu\tilde{v}_b - \frac{P_2(\mu)}{2}\Pi], \tag{2.59}$$

where $\Pi = \tilde{\Theta}_2 + \tilde{\Theta}_{P2} + \tilde{\Theta}_{P0}$. Θ_{P0} and Θ_{P2} are the monopole and quadrupole of the polarization field, which satisfies

$$\tilde{\Theta}'_P + ik\mu\tilde{\Theta}_P = -\tau'[-\tilde{\Theta}_P + \frac{1 - P_2(\mu)}{2}\Pi]. \tag{2.60}$$

The above equations show that even if we are interested only in the temperature field, it is influenced by the polarization field.

2.3.2 Baryons

The formalism presented in the last subsection can be used to obtain the Boltzmann equation for any constituent in the Universe. We now move to consider the behavior of massive particles, for which we have

$$P^2 = g_{\mu\nu}P^\mu P^\nu = -m^2. \tag{2.61}$$

Defining the energy

$$E \equiv \sqrt{p^2 + m^2}, \tag{2.62}$$

where p^2 is the same as in equation (2.36), the four-momentum of a massive particle is given by

$$P^\mu = \left[(1 - \Psi)E,\ \frac{1 - \Phi}{a} p\hat{p}^i\right]. \tag{2.63}$$

Instead of the momentum p, massive particles must be described by the energy E. Therefore, the left hand side of the Boltzmann equation (2.29) is expanded as

$$\frac{df}{dt} = \frac{\partial f}{\partial t} + \frac{\partial f}{\partial x^i} \cdot \frac{dx^i}{dt} + \frac{\partial f}{\partial E} \cdot \frac{dE}{dt} + \frac{\partial f}{\partial \hat{p}^i} \cdot \frac{d\hat{p}^i}{dt}. \tag{2.64}$$

Following the same steps as for the case of photons, we can obtain the coefficients dx^i/dt and dE/dt such that Eq. (2.64) can be rewritten as

$$\frac{df}{dt} = \frac{\partial f}{\partial t} + \frac{\hat{p}^i}{a}\frac{p}{E}\frac{\partial f}{\partial x^i} - p\frac{\partial f}{\partial E}\left(H\frac{p}{E} + \frac{p}{E}\frac{\partial \Phi}{\partial t} + \frac{\hat{p}^i}{a}\frac{\partial \Psi}{\partial x^i}\right). \tag{2.65}$$

Once again we neglected the last term in Eq. (2.64) as it does not contribute at first order. The main difference of this equation to the photon case is the presence of factors p/E, which arise from the energy-momentum constraint. The massless case can be recovered from Eq. (2.65) with $E = p$.

When we considered photons, to complete the left hand side of the Boltzmann equation, we needed the knowledge of the distribution function. For massive particles, the treatment can be simplified if they are nonrelativistic. In this case, we do not need a detailed information about the distribution function, all we need is to take moments of the Boltzmann equation taking into account that terms second-order in $v = p/E$ must be neglected because of the nonrelativistic behavior.

The zeroth moment is obtained integrating the Boltzmann equation as

$$\int \frac{d^3p}{(2\pi)^3}\frac{df}{dt} = \frac{\partial}{\partial t}\int \frac{d^3p}{(2\pi)^3} f + \frac{1}{a}\frac{\partial}{\partial x^i}\int \frac{d^3p}{(2\pi)^3} f\frac{p\hat{p}^i}{E} - \left[H + \frac{\partial \Phi}{\partial t}\right]\int \frac{d^3p}{(2\pi)^3}\frac{\partial f}{\partial E}\frac{p^2}{E} - \frac{1}{a}\frac{\partial \Psi}{\partial x^i}\int \frac{d^3p}{(2\pi)^3}\frac{\partial f}{\partial E} p\hat{p}^i. \tag{2.66}$$

From the definitions (1.37) and (2.51), the first two terms of the right hand side of equation (2.66) can be written in terms of the number density and velocity, respectively [2]. To integrate the third term of the r.h.s. of Eq. (2.66) we observe that $dE/dp = p/E$, thus

$$\int \frac{d^3p}{(2\pi)^3}\frac{\partial f}{\partial E}\frac{p^2}{E} = \int \frac{d^3p}{(2\pi)^3} p\frac{\partial f}{\partial p} = \int \frac{d\Omega}{(2\pi)^3}\int_0^\infty dp p^3 \frac{\partial f}{\partial p} = -3\int \frac{d\Omega}{(2\pi)^3}\int_0^\infty dp\, p^2 f = -3n, \tag{2.67}$$

[2] The spin degeneracy g_* can be incorporated in the phase space distribution f.

where in the third step we integrated by parts. The last term of (2.66) does not contribute at first order since the integral over the direction vector is null at zeroth order and that integral multiplies a metric perturbation, thus this term is at least of second order. Finally, we obtain

$$\int \frac{d^3p}{(2\pi)^3}\frac{df}{dt} = \frac{\partial n}{\partial t} + \frac{1}{a}\frac{\partial (nv^i)}{\partial x^i} + 3\left(H + \frac{\partial \Phi}{\partial t}\right) n. \tag{2.68}$$

The above result for the zeroth moment of the Boltzmann equation has introduced two unknown variables: n and v^i. Thus, we need one more equation to close the system. This additional equation can be obtained taking the first moment

$$\begin{aligned}\int \frac{d^3p}{(2\pi)^3}\frac{p\hat{p}^j}{E}\frac{df}{dt} = \frac{\partial}{\partial t}\int \frac{d^3p}{(2\pi)^3} f \frac{p\hat{p}^j}{E} + \frac{1}{a}\frac{\partial}{\partial x^i}\int \frac{d^3p}{(2\pi)^3} f \frac{p^2\hat{p}^i\hat{p}^j}{E^2} \\ - \left[H + \frac{\partial \Phi}{\partial t}\right]\int \frac{d^3p}{(2\pi)^3}\frac{\partial f}{\partial E}\frac{p^3\hat{p}^j}{E^2} - \frac{1}{a}\frac{\partial \Psi}{\partial x^i}\int \frac{d^3p}{(2\pi)^3}\frac{\partial f}{\partial E}\frac{p^2\hat{p}^i\hat{p}^j}{E}.\end{aligned} \tag{2.69}$$

The first term on the r.h.s. can be identified with the partial time derivative of nv^j. The second one is neglected at first order since it depends on $(p/E)^2$. To calculate the last terms, we follow the same procedure used in Eq. (2.67). Therefore, keeping only first-order terms, the first moment of the Boltzmann equation is

$$\int \frac{d^3p}{(2\pi)^3}\frac{p\hat{p}^j}{E}\frac{df}{dt} = \frac{\partial (nv^j)}{\partial t} + 4Hnv^j + \frac{n}{a}\frac{\partial \Psi}{\partial x^j}. \tag{2.70}$$

An interesting fact can be observed by taking moments of the Boltzmann equation: the lth moment depends on the $(l+1)$th moment. Thus, in principle, they constitute an infinite hierarchy of equations. However, as we are considering nonrelativistic particles, we neglected terms of second order and higher in (p/E) which correspond to the higher moments. Therefore, Eqs. (2.68) and (2.70) form a closed system for n and v^i.

Until now we restricted the analysis to the left hand side of the Boltzmann equation. The results presented in equations (2.68) and (2.70) are general for any massive and nonrelativistic component in the Universe. To proceed further let us restrict the study to the case of baryons.

Electrons and protons are coupled by Coulomb scattering whose rate is much larger than the expansion rate at all epochs of interest. Because of this tight coupling, electrons

and protons have the same overdensities

$$\frac{\rho_e - \rho_e^{(0)}}{\rho_e^{(0)}} = \frac{\rho_p - \rho_p^{(0)}}{\rho_p^{(0)}} \equiv \delta_b \tag{2.71}$$

and velocities

$$\vec{v}_e = \vec{v}_p \equiv \vec{v}_b. \tag{2.72}$$

Besides the Coulomb scattering, baryons interact with photons through the Compton scattering. Thus, the unintegrated Boltzmann equation for baryons is given by

$$\frac{df_b(t, \vec{x}, \vec{q})}{dt} = \langle c_{e\gamma} \rangle_{pp'q'} \,, \tag{2.73}$$

where $\langle c_{e\gamma} \rangle_{pp'q'}$ represents the Compton collision term, as in Eq. (2.44), and the subscripts represent which momenta are being integrated. In principle, the collision term should have an additional term account for the proton-photon Compton scattering, however, the cross section for this process is much smaller than the electron-photon scattering and can be ignored. We are also considering a simplified model with all electrons ionized.

To solve Eq. (2.73) we first take the zeroth moment integrating in the electron momentum $\vec{q}$. Thus, using Eq. (2.68) we obtain

$$\frac{\partial n_b}{\partial t} + \frac{1}{a}\frac{\partial (n_b v_b^i)}{\partial x^i} + 3\left(H + \frac{\partial \Phi}{\partial t}\right) n_b = \langle c_{e\gamma} \rangle_{pp'q'q} \,. \tag{2.74}$$

The collision term in the right hand side vanishes since the integration is symmetric under the interchange of $p \leftrightarrow p'$ and $q \leftrightarrow q'$ while it is antisymmetric in the distribution function factors. The number density can be split into a background part and a perturbed part as $n_b = n_b^{(0)}[1 + \delta_b]$. Thus, collecting the zeroth order and first-order terms, and passing to conformal time and Fourier space, the perturbed part gives us

$$\tilde{\delta}_b' + ik\tilde{v}_b + 3\tilde{\Phi}' = 0. \tag{2.75}$$

The second equation, which describes the evolution of the velocity field, is obtained taking the first moment of Eq. (2.73). In Eq. (2.70) we found the first moment of the left-hand side of the Boltzmann equation. There we first multiplied by $\vec{p}/E$ and then integrated. For baryons we multiply Eq. (2.73) by the momentum $\vec{q}$ instead of $\vec{q}/E$. This

will produce the same result as (2.70) except for a factor of m_b

$$m_b \frac{\partial(n_b v_b^j)}{\partial t} + 4H m_b n_b v_b^j + \frac{m_b n_b}{a}\frac{\partial \Psi}{\partial x^j} = \left\langle c_{e\gamma} q^j \right\rangle_{pp'q'q}. \tag{2.76}$$

Using the conservation of the total momentum $\vec{q} + \vec{p}$, we have that $\langle c_{e\gamma}\vec{q}\rangle_{pp'q'q} = -\langle c_{e\gamma}\vec{p}\rangle_{pp'q'q}$. Passing to Fourier space and multiplying Eq. (2.76) by $\hat{k}^j$, the right-hand side becomes $-\langle c_{e\gamma} p\mu\rangle_{pp'q'q}$. In equation (2.55), we already computed $\langle c_{e\gamma}\rangle_{p'q'q}$, thus we just need to multiply that result by $p\mu$ and integrate over all $\vec{p}$,

$$\begin{aligned} -\langle c_{e\gamma} p\mu\rangle_{pp'q'q} &= n_e \sigma_T \int \frac{d^3p}{(2\pi)^3} p^2 \frac{\partial f^{(0)}}{\partial p} \mu \left[\tilde{\Theta}_0 - \tilde{\Theta}(\mu) + \mu \tilde{v}_b\right] \\ &= n_e \sigma_T \int_0^\infty \frac{dp}{2\pi^2} p^4 \frac{\partial f^{(0)}}{\partial p} \int_{-1}^{1} \frac{d\mu}{2} \mu \left[\tilde{\Theta}_0 - \tilde{\Theta}(\mu) + \mu \tilde{v}_b\right]. \end{aligned} \tag{2.77}$$

In the second line we split the integration over $\vec{p}$ into a radial part and an angular part. The integral over the radial part p can be made integrating by parts similar to Eq.(2.67), the result is $-4\rho_\gamma$. The first term in the μ-integration vanishes, the second term is the dipole component of Θ and the last term reduces to $v_b/3$. Therefore, collecting these results in Eq. (2.76) and switching to conformal time, we obtain

$$\tilde{v}_b' + \frac{a'}{a}\tilde{v}_b + ik\tilde{\Psi} = \tau' \frac{4\rho_\gamma}{3\rho_b}\left[3i\tilde{\Theta}_1 + \tilde{v}_b\right]. \tag{2.78}$$

2.3.3 Neutrinos

Equation (2.59) can be extended to massless neutrinos. They obey a similar equation without a collision term,

$$\tilde{\mathcal{N}}' + ik\mu\tilde{\mathcal{N}} + \tilde{\Phi}' + ik\mu\tilde{\Psi} = 0, \tag{2.79}$$

where $\mathcal{N}$ is the perturbation in the neutrino temperature. On the other hand, if neutrinos are massive, the left-hand side of the Boltzmann equation will be given by Eq. (2.65). However, unlike the baryon case, neutrinos are relativistic particles, then we cannot neglect terms of order $(p/E)^2$ and higher, we have to take into account the whole hierarchy of moments. A discussion about massive neutrinos can be found in [88].

2.3.4 Dark Matter

Cold dark matter behaves like baryons. However, it does not interact electromagnetically, then the perturbations are not affected by a collision term [3]. Thus, the density contrast of cold dark matter obeys an equation identical to (2.75)

$$\tilde{\delta}_c' + ik\tilde{v}_c + 3\tilde{\Phi}' = 0 \tag{2.80}$$

and the velocity equation is similar to (2.78) without a collision term

$$\tilde{v}_c' + \frac{a'}{a}\tilde{v}_c + ik\tilde{\Psi} = 0. \tag{2.81}$$

We observe that to obtain Eqs. (2.80) and (2.81) we use the Boltzmann equation, however, cold dark matter always behaves like a fluid, which means that it can be described completely by the energy-momentum tensor $T_{\mu\nu}$. Thus, we could obtain the evolution equations above using the conservation of the energy-momentum tensor as we did in the homogeneous case.

2.3.5 Energy-Momentum Tensor

Now that we know the equations governing the evolution of perturbations in the components of the Universe, we are in position to complete the Einstein equations (2.27) and (2.28) with the perturbed energy-momentum tensor. In general, the energy-momentum tensor of a fluid with a distribution function $f(t, \vec{x}, \vec{p})$ is given by

$$T^{\mu}_{\nu}(t, \vec{x}) = g_* \int \frac{d^3p}{(2\pi)^3} \frac{p^{\mu} p_{\nu}}{E} f(t, \vec{x}, \vec{p}). \tag{2.82}$$

Remember that the Einstein equations take into account the contributions of all species in the Universe, thus from the time-time component of (2.82), we obtain

$$T^0_0 = -\sum_{all\ species\ i} g_{*i} \int \frac{d^3p}{(2\pi)^3} E_i(p) f_i(t, \vec{x}, \vec{p}). \tag{2.83}$$

The distribution functions above consist in a background part and a perturbed part. For nonrelativistic particles, the integral produces $-\rho_i(1 + \delta_i)$, while for relativistic ones,

[3] In the next chapter we will extend this model assuming an interaction in the dark sector.

the integral can be done using the expansion (2.41). Considering only the first-order perturbations, the Einstein equation (2.27) results

$$k^2\tilde{\Phi} + 3\frac{a'}{a}\left(\tilde{\Phi}' - \tilde{\Psi}\frac{a'}{a}\right) = 4\pi G a^2\left[\rho_c\tilde{\delta}_c + \rho_b\tilde{\delta}_b + 4\rho_\gamma\tilde{\Theta}_0 + 4\rho_\nu\tilde{\mathcal{N}_0}\right], \tag{2.84}$$

where $\tilde{\mathcal{N}_0}$ is the monopole term of the neutrino temperature perturbations.

The second Einstein equation (2.28) needs the longitudinal traceless projection of the space-space energy-momentum tensor

$$\left(\hat{k}_i\hat{k}^j - \frac{1}{3}\delta_i^j\right)T_j^i = \sum_{all\ \ species\ \ i} g_{*i}\int\frac{d^3p}{(2\pi)^3}p^2\frac{\mu^2-1/3}{E_i(p)}f_i(t,\vec{x},\vec{p}). \tag{2.85}$$

We observe that the factor $\mu^2-1/3$ is equal to $2/3P_2(\mu)$, where $P_2(\mu)$ is the second Legendre polynomial. Therefore, the integral picks out the quadrupole part of the distributions. We already saw that nonrelativistic particles do not contribute to the second moment and higher, thus only photons and neutrinos must be taken into account. For example, let us calculate the integral in the case of photons:

$$-2\int\frac{dp}{2\pi^2}p^4\frac{\partial f^{(0)}}{\partial p}\int_{-1}^{1}\frac{d\mu}{2}\frac{2P_2(\mu)}{3}\Theta(\mu) = \frac{4\Theta_2}{3}\int\frac{dp}{2\pi^2}p^4\frac{\partial f^{(0)}}{\partial p} = -\frac{8\rho_\gamma\Theta_2}{3}. \tag{2.86}$$

Finally, combining (2.28) and (2.85) we obtain the second Einstein equation

$$k^2(\tilde{\Phi}+\tilde{\Psi}) = -32\pi G a^2\left[\rho_\gamma\tilde{\Theta}_2 + \rho_\nu\tilde{\mathcal{N}_2}\right]. \tag{2.87}$$

We emphasize that, in principle, we should have a term for perturbations in the dark energy in the Einstein equations above. However, until now, we consider it to be smooth and important only very recently as described by the cosmological constant model.

2.4 Initial Conditions

Equations (2.59), (2.60), (2.75), (2.78), (2.79), (2.80), (2.81), (2.84) and (2.87) form a system of nine first-order differential equations. To solve them we need a set of nine initial conditions. However, in the early Universe, we can relate all perturbation variables to the gravitational potential Φ, such that we will actually need just one initial condition.

Considering times so early that for all k-modes of interest $k\eta \ll 1$, we can neglect all terms in the Boltzmann equations multiplied by k. This condition means that on early times all perturbations of interest had wavelengths much larger than the distance of causal contact. Thus, an observer within the causal horizon sees a uniform sky, which means that higher multipoles, e.g. Θ_1, Θ_2, ..., are much smaller than the monopole term. Therefore, using these considerations, equations (2.59), (2.79), (2.75) and (2.80) can be written as

$$\tilde{\Theta}_0' + \tilde{\Phi}' = 0, \tag{2.88}$$

$$\tilde{\mathcal{N}}_0' + \tilde{\Phi}' = 0, \tag{2.89}$$

$$\tilde{\delta}_b' + 3\tilde{\Phi}' = 0, \tag{2.90}$$

$$\tilde{\delta}_c' + 3\tilde{\Phi}' = 0, \tag{2.91}$$

respectively. The velocities v_b and v_c are of the same order of magnitude of the dipole moment of the temperature distribution, thus they can be neglected at first. We are also setting the polarization equal to zero.

Using the Einstein equation (2.84) at early times, and knowing that radiation dominates the energy content at those epochs, we obtain

$$\tilde{\Phi}''\eta + \tilde{\Phi}' - \tilde{\Psi}' = -2\tilde{\Phi}', \tag{2.92}$$

where we used equations (2.88) and (2.89). On the other hand, the second Einstein equation (2.87) tells us that $\Psi = -\Phi$, because the terms of quadrupole can be neglected at those epochs. Therefore, the equation above implies

$$\tilde{\Phi}''\eta + 4\tilde{\Phi}' = 0, \tag{2.93}$$

which has solution $\tilde{\Phi} = A + B\eta^{-3}$, where A and B are constants. The second term is a decaying mode, consequently any contribution to it will vanish very quickly. Thus, we will consider solutions with $\tilde{\Phi} = constant$.

If $\tilde{\Phi} = constant$, Eqs. (2.88) and (2.89) imply that $\tilde{\Theta}_0$ and $\tilde{\mathcal{N}}_0$ are constants too. On the other hand, most models of structure formation consider that $\tilde{\Theta}_0 = \tilde{\mathcal{N}}_0$. Using such

arguments in (2.84) we are led to

$$\tilde{\Phi}(\eta_i, k) = 2\tilde{\Theta}_0(\eta_i, k), \tag{2.94}$$

where η_i means that this is valid for some initial conformal time. Combining (2.88) with (2.75) and (2.80), we obtain that their initial conditions are given by

$$\tilde{\delta}_b = 3\tilde{\Theta}_0 + constant \tag{2.95}$$

and

$$\tilde{\delta}_c = 3\tilde{\Theta}_0 + constant. \tag{2.96}$$

If the constants above are zero we have *adiabatic* initial conditions, but if they are nonzero the initial conditions are called *isocurvature* ones.

Although we have neglected the initial conditions for velocities, there are situations where they must be taken into account. Using (2.59), (2.78), (2.79) and (2.81), we can show they are given by

$$\tilde{\Theta}_1 = \tilde{\mathcal{N}}_1 = \frac{i\tilde{v}_b}{3} = \frac{i\tilde{v}_c}{3} = -\frac{k\tilde{\Phi}}{6aH}. \tag{2.97}$$

The above equations relate all variables of the initial perturbations to the initial gravitational potential $\tilde{\Phi}(\eta_i, k)$. Then, it remains to be known how these primordial perturbations were generated and which initial value they should have. The theory of *inflation*, which was created to account with the *horizon problem*, also provides a mechanism responsible for the origin of perturbations in the Universe. In this theory, quantum mechanical fluctuations during inflation are responsible for the variations around the smooth background. At any given time, there are regions where the fields are slightly larger and regions where they are smaller, so that the average value is zero

$$\left\langle \tilde{\Phi}(\vec{k}) \right\rangle = 0. \tag{2.98}$$

However, the variance is nonzero

$$\left\langle \tilde{\Phi}(\vec{k})\tilde{\Phi}^*(\vec{k'}) \right\rangle = (2\pi)^3 P_\Phi(k)\delta^3(\vec{k} - \vec{k'}), \tag{2.99}$$

where $P_\Phi(k)$ is the *power spectrum* of the primordial perturbations to the gravitational

potential Φ.

To account with an inflationary scenario we need a field with a negative equation of state, the *inflaton*, which is responsible for the exponential acceleration of the Universe at early times. Quantum mechanical fluctuations on this field feed perturbations in the metric. Assuming a canonical scalar field is responsible for inflation, we can obtain the post-inflation power spectrum of Φ from the horizon-crossing spectrum of the scalar field as [60]

$$P_\Phi(k) = \left.\frac{8\pi G H^2}{9k^3\epsilon}\right|_{aH=k} \equiv \frac{50\pi^2}{9k^3}\left(\frac{k}{H_0}\right)^{n_s-1}\delta_H^2, \tag{2.100}$$

where $\epsilon = -H'/aH^2$ is the slow roll parameter of the scalar field. In the second equality, we rewrote the primordial power spectrum defining the scalar spectral index n_s and the scalar amplitude δ_H[4]. This convention means that a scale-invariant scalar spectrum corresponds to $n_s = 1$.

2.5 Inhomogeneities: Matter Power Spectrum

The perturbation equations developed in sections 2.2 and 2.3, with the initial conditions obtained in the last section, allow us to calculate the inhomogeneities and anisotropies in the Universe. Inhomogeneities in the matter density at the early Universe will grow up due to gravitational instabilities and they will build the structures we observe. Actually, to describe correctly the structures observed, e.g. galaxy distributions, we have to take into account nonlinearities and gas dynamics, but even on small scales the linear regime is a starting point.

Solving the cosmological perturbations it is verified that their evolution can be divided in three stages. Thus, the density contrast of matter at some conformal time η, or equivalently with scale factor a, $\tilde{\delta}_m(a,\vec{k})$, is related to the primordial density contrast $\tilde{\delta}_{mP}(\vec{k})$ by

$$\tilde{\delta}_m(a,\vec{k}) = \tilde{\delta}_{mP}(\vec{k})T(k)D_\delta(a), \tag{2.101}$$

where the transfer function $T(k)$ describes the evolution of perturbations through the epochs of horizon crossing and transition from radiation to matter. On the other hand, the

[4]Camb code parameterizes the primordial super-horizon power spectrum $P_\Phi(k)$ of curvature perturbations as $P_\Phi(k) = A_s(\frac{k}{k_s})^{(n_s-1)}$. The input parametes are the pivot scale k_s, the spectral index n_s and the amplitude at the pivot scale A_s. As we are interested in using the Camb code for numerical calculations, we shall use such convention for the primordial power spectrum in the next chapters.

growth function $D_\delta(a)$ describes the late time growth which is independent of wavelength.

To compare with observations we note that, as for the gravitational potential $\tilde{\Phi}(\vec{k})$, the density contrast of matter also has a vanishing average,

$$\left\langle \tilde{\delta}_m(a,\vec{k}) \right\rangle = 0. \tag{2.102}$$

Its variance equals

$$\left\langle \tilde{\delta}_m(a,\vec{k})\tilde{\delta}^*_m(a,\vec{k'}) \right\rangle = (2\pi)^3 P_{\delta_m}(a,k)\delta^3(\vec{k}-\vec{k'}). \tag{2.103}$$

Therefore, combining (2.101) with the above variance, we see that the matter power spectrum is given by

$$P_{\delta_m}(a,k) = |T(k)|^2 |D_\delta(a)|^2 P_{\delta_m}(\eta_i,k). \tag{2.104}$$

2.6 Anisotropies: CMB Power Spectrum

One way to solve the perturbation equation for photons (2.59) is expanding the Θ function in Legendre polynomials

$$\tilde{\Theta}(\eta,\vec{k},\hat{p}) = \sum_{l=0}^{\infty}(-i)^l(2l+1)\tilde{\Theta}_l(\eta,\vec{k})P_l(\mu), \tag{2.105}$$

such that (2.59) is split in a hierarchical system of differential equations as

$$\begin{aligned}
\tilde{\Theta}'_0 &= -k\tilde{\Theta}_1 - \tilde{\Phi}', \\
\tilde{\Theta}'_1 &= \frac{k}{3}\left(\tilde{\Theta}_0 - 2\tilde{\Theta}_2 + \tilde{\Psi}\right) + \tau'\left(\tilde{\Theta}_1 - \frac{i}{3}\tilde{v}_b\right), \\
\tilde{\Theta}'_2 &= \frac{k}{5}\left(2\tilde{\Theta}_1 - 3\tilde{\Theta}_3\right) + \tau'\left(\tilde{\Theta}_2 - \frac{\Pi}{10}\right), \\
\tilde{\Theta}'_l &= -\frac{k}{2l+1}\left[(l+1)\tilde{\Theta}_{l+1} - l\tilde{\Theta}_{l-1}\right] + \tau'\tilde{\Theta}_l, \quad l > 2.
\end{aligned} \tag{2.106}$$

In fact this was done in the first numerical programs to calculate the anisotropies in the CMB. However, this method requires to solve thousands coupled differential equations for small angular scales $\theta \approx 1/l$, besides the need of a small time step to obtain good results. Therefore, nowadays, another method is used, the *line of sight approach*. Following this

strategy we can obtain an approximate analytic solution given by [60]

$$\begin{aligned}\tilde{\Theta}_l(\eta_0,\vec{k}) \approx & \left[\tilde{\Theta}_0(\eta_*,\vec{k})+\tilde{\Psi}(\eta_*,\vec{k})\right] j_l[k(\eta_0-\eta_*)] \\ & + 3\tilde{\Theta}_1(\eta_*,\vec{k})\left\{j_{l-1}[k(\eta_0-\eta_*)] - \frac{(l+1)j_l[k(\eta_0-\eta_*)]}{k(\eta_0-\eta_*)}\right\} \\ & + \int_0^{\eta_0} d\eta e^{-\tau}\left[\tilde{\Psi}'(\eta,\vec{k})-\tilde{\Phi}'(\eta,\vec{k})\right] j_l[k(\eta_0-\eta)], \end{aligned} \tag{2.107}$$

where η_* is the conformal time at recombination and j_l is the spherical Bessel function.

The solutions of (2.59) are given by Θ_l. We need to know how to make comparisons with the observations. We thus first expand the temperature perturbation in spherical harmonics,

$$\Theta(\eta,\vec{x},\hat{p}) = \sum_{l=1}^{\infty}\sum_{m=-l}^{l} a_{lm}(\eta,\vec{x})Y_{lm}(\hat{p}). \tag{2.108}$$

Using the orthogonality property of the spherical harmonics, we can invert the expansion above to obtain

$$a_{lm}(\eta,\vec{x}) = \int d\Omega Y^*_{lm}(\hat{p})\Theta(\eta,\vec{x},\hat{p}). \tag{2.109}$$

However, we cannot make predictions for a particular a_{lm}, only their distributions are known which are originated in quantum mechanical fluctuations at the inflationary epoch. Therefore, in the linear regime, they have a gaussian distribution, where

$$\langle a_{lm}(\eta,\vec{x})\rangle = 0 \tag{2.110}$$

and

$$\langle a_{lm}(\eta,\vec{x})a^*_{l'm'}(\eta,\vec{x})\rangle = \delta_{ll'}\delta_{mm'}C_l. \tag{2.111}$$

Finally, substituting (2.109) in (2.111), going to the Fourier space and using the expansion (2.105), we can write

$$C_l = (4\pi)\int \frac{d^3k}{(2\pi)^3} P_\Phi(\eta_i,k)|\tilde{\Theta}_l(\eta,k)|^2. \tag{2.112}$$

The matter power spectrum obtained in the last section and the CMB power spectrum in the above equation give us a prediction for the variance in the matter and CMB temperature, respectively. Both depend on the whole system of Einstein-Boltzmann equations developed in this chapter. Thus, their predictions take into account all the components

in the Universe. In the next chapter, we will extend the standard scenario presented so far, considering models with an interaction in the dark sector. Using these power spectra we will be able to make predictions about the behavior of an interaction and constraint the models comparing with some observational data.

Chapter 3

Interacting Dark Energy

In the last years several works on the possibility of an interaction between dark energy and dark matter have appeared [3, 10, 18, 21, 22, 36, 42, 89–94]. One of the motivations is that a model with an interaction in the dark sector can provide a mechanism to solve, or at least to alleviate, the coincidence problem. Moreover, because both dark energy and dark matter are, until now, two unknown components, when considering that they are originated by physical fields from quantum field theory it is natural to assume that they interact.

3.1 Phenomenological Model

The first chapters dealt with general aspects of cosmology. We started with a homogeneous and isotropic model of the Universe and treated its components. Then, in order to explain the structures around us, we introduced inhomogeneities and anisotropies about this background through a perturbation theory. We pass now to discuss a specific model which consists in a universe filled with baryons, photons, neutrinos, dark matter and dark energy where we introduce an interaction between the components in the dark sector.

If dark matter and dark energy are coupled with each other, the energy-momentum tensor $T^{\mu\nu}_{(\lambda)}$ of each individual component $\lambda = c, d$ is no longer conserved. Instead,

$$\nabla_\mu T^{\mu\nu}_{(\lambda)} = Q^\nu_{(\lambda)}\,, \tag{3.1}$$

where ∇_μ is the covariant derivative, $Q^\nu_{(\lambda)}$ is the four-vector governing the energy-momentum transfer between dark components and the subscript (λ) can refer to dark matter (c) or

dark energy (d), respectively. Including an interaction in the dark sector, dark matter and dark energy components are not separately conserved, while the energy-momentum tensor of the whole dark sector is still conserved:

$$\sum_{\lambda} \nabla_{\mu} T^{\mu\nu}_{(\lambda)} = \sum_{\lambda} Q^{\nu}_{(\lambda)} = 0, \tag{3.2}$$

thus, $Q^{\nu}_{(c)} = -Q^{\nu}_{(d)}$.

We assume a spatially flat Friedmann-Lemaitre-Robertson-Walker background given by Eq. (1.2) and an energy-momentum tensor of a perfect fluid (1.7). From the energy conservation of the full energy-momentum tensor, we can derive the equations of evolution of the background dark matter and dark energy densities,

$$\begin{aligned} \rho'_c + 3\mathcal{H}\rho_c =& a^2 Q^0_c = +aQ\,, \\ \rho'_d + 3\mathcal{H}\left(1+\omega\right)\rho_d =& a^2 Q^0_d = -aQ\,, \end{aligned} \tag{3.3}$$

where the derivatives and the Hubble parameter $\mathcal{H}$ are in conformal time, ρ_c and ρ_d are the energy densities for dark matter and dark energy, respectively, $\omega = p_d/\rho_d$ is the equation of state of dark energy and Q was chosen to be the energy transfer in cosmic time coordinates. We emphasize that the homogeneity and isotropy of the background require the spatial components of $Q^{\nu}_{(\lambda)}$ to be zero.

In this section we concentrate on the phenomenological interaction as a linear combination of energy densities of dark sectors with the form of $Q = 3H(\xi_1\rho_c + \xi_2\rho_d)$, describing the energy transfer. With the above expression for the continuity equations, if $Q > 0$, we have that the dark energy transfers energy to the dark matter. In studying the curvature perturbation, it has been made clear that when the interaction is proportional to the energy density of dark energy ($Q = 3H\xi_2\rho_d$), we get a stable curvature perturbation except for $\omega = -1$; however, when the interaction is proportional to the dark matter density ($Q = 3H\xi_1\rho_c$) or total dark sectors ($Q = 3H\xi(\rho_c + \rho_d)$), the curvature perturbation can only be stable when the constant dark energy equation of state satisfies $\omega < -1$ [13]. For the case of a time-dependent dark energy equation of state, the stability of curvature perturbations was discussed in [14, 15]. With the interaction, the effective background

equations of state for the dark matter and dark energy change to

$$\omega_{c,eff} = -\frac{a^2 Q_c^0}{3\mathcal{H}\rho_c}\,, \qquad \omega_{d,eff} = \omega - \frac{a^2 Q_d^0}{3\mathcal{H}\rho_d}\,. \tag{3.4}$$

We summarize different forms of the interaction with the effective background equation of state in Table 3.1; we label our models with Roman numerals [44].

In order to solve the coincidence problem, we require the ratio of the energy densities of dark matter and dark energy, $\varrho = \rho_c/\rho_d$, to be a constant in the expansion history of our Universe, $\varrho' = \frac{\rho_c'}{\rho_d} - \varrho\frac{\rho_d'}{\rho_d} = 0$. This leads to a quadratic equation,

$$\xi_1\varrho^2 + (\xi_1 + \xi_2 + \omega)\,\varrho + \xi_2 = 0. \tag{3.5}$$

The solutions of this equation can lead to unphysical results, such as negative energy density of cold dark matter in the past or complex roots. For different phenomenological models of the interaction between dark sectors, the conditions to obtain physical results, positive energy densities and real roots were obtained in [44] as shown in Table 3.1. Figure 3.1 illustrates the behavior of ϱ for the four interacting models. We observe that, for the interaction proportional to the energy density of dark energy, a positive interaction can help to alleviate the coincidence problem as there is a longer period for the energy densities of dark matter and dark energy to be comparable. In contrast, a negative interaction can not alleviate the coincidence problem. For the interaction proportional to the energy density of dark matter or to the sum of both energies, the ratio ϱ presents a scaling behavior.

Table 3.1: Different coupling models with their constraints, dark energy equation of state and the effective equation of state for both dark sector fluids.

Model	Q	DE EoS	$\omega_{c,eff}$	$\omega_{d,eff}$	Constraints
I	$3\xi_2 H\rho_d$	$-1 < \omega < 0$	$-\xi_2/\varrho$	$\omega + \xi_2$	$\xi_2 < -2\omega\Omega_c$
II	$3\xi_2 H\rho_d$	$\omega < -1$	$-\xi_2/\varrho$	$\omega + \xi_2$	$\xi_2 < -2\omega\Omega_c$
III	$3\xi_1 H\rho_c$	$\omega < -1$	$-\xi_1$	$\omega + \xi_1\varrho$	$0 < \xi_1 < -\omega/4$
IV	$3\xi H\,(\rho_d + \rho_c)$	$\omega < -1$	$-\xi\,(1 + 1/\varrho)$	$\omega + \xi\,(\varrho + 1)$	$0 < \xi < -\omega/4$

From the background dynamics we see that when we introduce the phenomenological interaction between dark sectors, it is possible to have the scaling solution of the ratio between dark matter and dark energy, which can help to alleviate the coincidence problem. However, in the background dynamics there appears an inevitable degeneracy between the

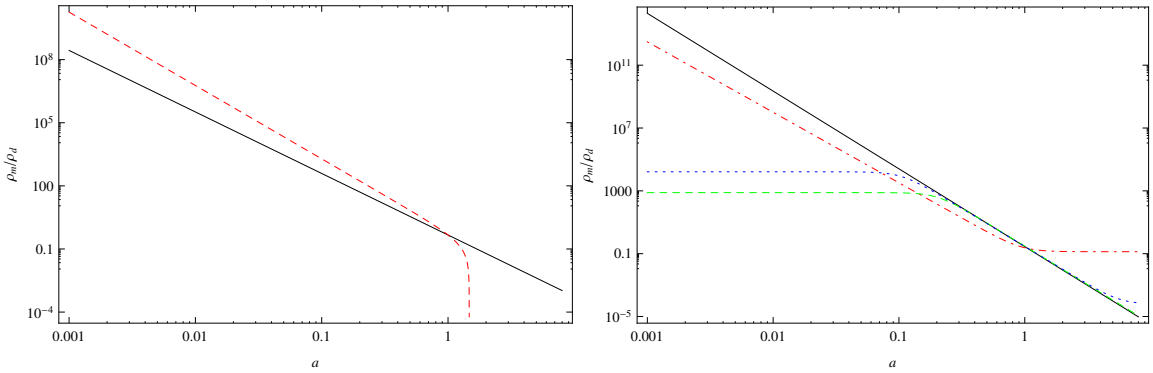

(a) **(b)**

Figure 3.1: Evolution of the dark energy to dark matter energy density ratio $\varrho \equiv \rho_c/\rho_d$ in a model with $Q = 3H(\xi_1\rho_c + \xi_2\rho_d)$ for different coupling constants. (a) The red dashed line corresponds to Planck best-fit Model I, with $\xi_2 = -0.1881$ corresponding to the lowest value in the 68% C.L. as in Table 4.2. The black solid line has the same parameters but no interaction. (b) The black solid line corresponds to a noninteracting model with $w = -1.65$ and $\Omega_d = 0.78$. The red dot-dashed line describes Model II listed in the first column of Table 4.3 with $\xi_2 = 0.2$. The green dashed line corresponds to Planck best-fit Model III (see Table 4.4), and the blue dotted line, to Planck best-fit Model IV (see Table 4.5).

coupling in dark sectors and the dark energy equation of state. In general this degeneracy cannot be broken by just investigating the dynamics of the background spacetime, except in the case when the coupling is proportional to the dark matter density (Model III) [44]. It is expected that the degeneracy between the coupling and other cosmological parameters can be solved in the perturbed spacetime by considering the evolution of the perturbations of dark energy and dark matter.

Although we introduced perturbations in the components of the Universe through the Boltzmann equation in the last chapter, the dark matter could be completely described using the energy-momentum tensor as we observed earlier. Thus, for the interacting model, we will consider perturbations through the conservation equation (3.1). To calculate the covariant derivative we use the perturbed metric (2.6) and we assume that the energy-momentum tensor is given by a perfect fluid even in the perturbed case:

$$T^{\mu\nu}_{(\lambda)}(\eta,\vec{x}) = \{\rho(\eta)[1+\delta(\eta,\vec{x})] + [P(\eta)+\delta P(\eta,\vec{x})]\}u^\mu u^\nu + [P(\eta)+\delta P(\eta,\vec{x})]g^{\mu\nu}, \quad (3.6)$$

where $\delta(\eta,\vec{x})$ is the density contrast $\delta \equiv \delta\rho/\rho$ and the four-velocity reads

$$u^\mu = a^{-1}(1-\psi,\vec{v}_{(\lambda)}) \quad \text{and} \quad u_\mu = a(-1-\psi,\vec{v}_{(\lambda)}+\partial_i B). \quad (3.7)$$

$\vec{v}_{(\lambda)}$ can be written as minus the gradient of a peculiar velocity potential $v_{(\lambda)}$ plus a zero divergence vector. Only the first one contributes to scalar perturbations. Thus, taking the perturbed part of the energy-momentum conservation results

$$\begin{aligned}\delta\nabla_\mu T^{\mu 0}_{(\lambda)} =&\frac{1}{a^2}\left\{-2\left[\rho'_\lambda + 3\mathcal{H}\left(\rho_\lambda + P_\lambda\right)\right]\psi + (\rho_\lambda\delta_\lambda)' - (\rho_\lambda + P_\lambda)\nabla^2 v_\lambda + 3\mathcal{H}(\rho_\lambda\delta_\lambda + \delta P_\lambda)\right.\\ &\left.+3(\rho_\lambda + P_\lambda)\phi'\right\} = \delta Q^0_{(\lambda)}\end{aligned} \tag{3.8}$$

and

$$\begin{aligned}\partial_i\delta\nabla_\mu T^{\mu i}_{(\lambda)} =&\frac{1}{a^2}\left\{\left[P'_\lambda + \mathcal{H}(\rho_\lambda + P_\lambda)\right]\nabla^2 B - \left[(\rho'_\lambda + P'_\lambda) + 4\mathcal{H}(\rho_\lambda + P_\lambda)\right]\nabla^2 v_\lambda\right.\\ &\left.+(\rho_\lambda + P_\lambda)\nabla^2 B' + \nabla^2\delta P_\lambda - (\rho_\lambda + P_\lambda)\nabla^2 v'_\lambda + (\rho_\lambda + P_\lambda)\nabla^2\psi\right\} = \partial_i\delta Q^i_{(\lambda)}.\end{aligned} \tag{3.9}$$

To solve equations (3.8) and (3.9) we need a relation for δP_λ. In order to find such a relation, we first observe that the sound speed c_s of a fluid or scalar field is the propagation speed of pressure fluctuations in its rest frame [12]:

$$c_s^2 = \left.\frac{\delta P}{\delta\rho}\right|_{rf}. \tag{3.10}$$

For a scalar field φ, the sound speed is equal to the speed of light, $c^2_{s\varphi} = 1$. On the other hand, we can define the "adiabatic sound speed" for any medium as

$$c_a^2 = \frac{P'}{\rho'} = \omega + \frac{\omega'\rho}{\rho'}. \tag{3.11}$$

If a fluid is barotropic, the sound speed is equal to the adiabatic sound speed, $c_s^2 = c_a^2$, and if its equation of state is constant, then $c_a^2 = \omega$. At first sight, the dark-energy fluid with $\omega = const.$ is a barotropic adiabatic model. However, this results in an imaginary sound speed which leads to instabilities in the dark energy. Thus, we impose that $c^2_{sd} > 0$ by hand and it is natural to adopt the scalar field value.

The rest frame is defined as the comoving ($v|_{rf} = 0$) and orthogonal ($B|_{rf} = 0$) frame, which implies $T^i_0|_{rf} = T^0_i|_{rf} = 0$. Making a gauge transformation, $x^\mu \to x^\mu + (\delta\eta, \partial^i\delta x)$,

from the rest frame to a general gauge, we obtain [1]

$$-v+B=(-v+B)|_{rf}+\delta\eta\,,\qquad \delta P=\delta P|_{rf}-P'\delta\eta\,,\qquad \delta\rho=\delta\rho|_{rf}-\rho'\delta\eta. \quad (3.12)$$

Using the definition of the rest frame, the first equality above results $\delta\eta=-v+B$. Thus, following [12], the perturbed pressure of dark energy is given by

$$\begin{aligned}\delta P_d &= \delta P_d|_{rf}-P'_d(-v_d+B)\\ &= \frac{\delta P_d|_{rf}}{\delta\rho_d|_{rf}}\delta\rho_d|_{rf}-\frac{P'_d}{\rho'_d}\rho'_d(-v_d+B)\\ &= c^2_{sd}[\rho_d\delta_d+\rho'_d(-v_d+B)]-c^2_{ad}\rho'_d(-v_d+B)\\ &= c^2_{ad}\rho_d\delta_d+(c^2_{sd}-c^2_{ad})[\rho_d\delta_d+\rho'_d(-v_d+B)]\\ &= c^2_{ad}\rho_d\delta_d+\delta P_{(nad)},\end{aligned} \quad (3.13)$$

where $\delta P_{(nad)}$ is the intrinsic non-adiabatic pressure perturbation in the dark energy fluid. For the coupled case, we have

$$\delta P_d=c^2_{sd}\rho_d\delta_d+(c^2_{sd}-c^2_{ad})\left[-3\mathcal{H}(1+\omega)\rho_d+a^2Q^0_d\right](-v_d+B), \quad (3.14)$$

where $\delta_d=\delta\rho_d/\rho_d$ is the density contrast, c^2_{sd} is the effective sound speed at the rest frame, which we set to one, and c^2_{ad} is the adiabatic sound speed, all with respect to dark energy.

The perturbed four-vector $\delta Q^\nu_{(\lambda)}$ can be decomposed into

$$\delta Q^0_{(\lambda)}=\pm\left(-\frac{\psi}{a}Q+\frac{1}{a}\delta Q\right),\qquad \delta Q_{p(\lambda)}=Q^I_{p(\lambda)}\Big|_t+Q^0_{(\lambda)}v_t. \quad (3.15)$$

Here the $\pm$ sign refers to dark matter or dark energy, respectively, and $\delta Q_{p(\lambda)}$ is the potential of the perturbed energy-momentum transfer $\delta Q^i_{(\lambda)}$. $Q^I_{p(\lambda)}\Big|_t$ is the external non-gravitational force density and v_t is the average velocity of the energy transfer. In this section we consider that there is no nongravitational interaction between dark energy and dark matter; only an inertial drag effect appears due to stationary energy transfer. Thus $Q^I_{p(\lambda)}\Big|_t$ and v_t vanish, which implies that $\delta Q^i_{(\lambda)}=0$.

[1] The minus sign in v comes from our convention to define the velocity as minus the gradient of a peculiar velocity potential.

Finally we are in position to write the equations governing the evolution of linear perturbations for dark matter and dark energy. As we are interested to implement the interacting model in the public code CAMB [95], it will be more appropriate to obtain the perturbed equations in the synchronous gauge. Thus, collecting equations (3.14) and (3.15) in (3.8) and (3.9), and passing to the Fourier space[2], we obtain

$$\dot{\delta}_c = -(kv_c + \frac{\dot{h}}{2}) + 3\mathcal{H}\xi_2\frac{1}{r}\left(\delta_d - \delta_c\right) , \tag{3.16}$$

$$\begin{aligned}\dot{\delta}_d = &-\left(1+\omega\right)\left(kv_d + \frac{\dot{h}}{2}\right) + 3\mathcal{H}(\omega - c_e^2)\delta_d + 3\mathcal{H}\xi_1 r\left(\delta_d - \delta_c\right) \\ &- 3\mathcal{H}\left(c_e^2 - c_a^2\right)\left[3\mathcal{H}\left(1+\omega\right) + 3\mathcal{H}\left(\xi_1 r + \xi_2\right)\right]\frac{v_d}{k} ,\end{aligned} \tag{3.17}$$

$$\dot{v}_c = -\mathcal{H}v_c - 3\mathcal{H}(\xi_1 + \frac{1}{r}\xi_2)v_c , \tag{3.18}$$

$$\dot{v}_d = -\mathcal{H}\left(1 - 3c_e^2\right)v_d + \frac{3\mathcal{H}}{1+\omega}\left(1 + c_e^2\right)\left(\xi_1 r + \xi_2\right)v_d + \frac{kc_e^2\delta_d}{1+\omega} , \tag{3.19}$$

where $h = 6\phi$ is the synchronous gauge metric perturbation. In practice, we fix the remaining freedom in the synchronous gauge setting a comoving frame with respect to the dark matter fluid, such that the peculiar velocity of dark matter v_c vanishes.

To solve equations (3.16)-(3.19) we set initial conditions according to [13]. Using the gauge-invariant quantity [96]

$$\zeta = \phi - \mathcal{H}\frac{\delta\rho}{\rho'} \tag{3.20}$$

and the gauge-invariant relative entropy perturbation

$$S_{AB} = 3\mathcal{H}\left(\frac{\delta\rho_B}{\rho'_B} - \frac{\delta\rho_A}{\rho'_A}\right) = 3(\zeta_A - \zeta_B), \tag{3.21}$$

we get adiabatic initial conditions

$$\frac{\delta_c}{1 - \xi_1 - \xi_2/r} = \frac{\delta_d}{1 + \omega + \xi_1 r + \xi_2} = \frac{3\delta_\gamma}{4} \tag{3.22}$$

and

$$v_d = v_\gamma. \tag{3.23}$$

In the linear perturbation formalism, the influence of the interaction between dark energy

[2]In the Fourier space, we use the convention to divide the velocity potential by an additional factor of $k \equiv |\vec{k}|$ so that it has the same dimension as the vector part. Thus, $\theta \equiv \nabla \cdot \vec{v} = -\nabla^2 v = kv$.

and dark matter on the CMB and the matter power spectrum can be calculated by modifying the CAMB code [95]. Figures 3.2-3.5 present the behavior of the power spectra for different phenomenological models. The appendix A shows the most important steps to introduce the phenomenological model in the CAMB code.

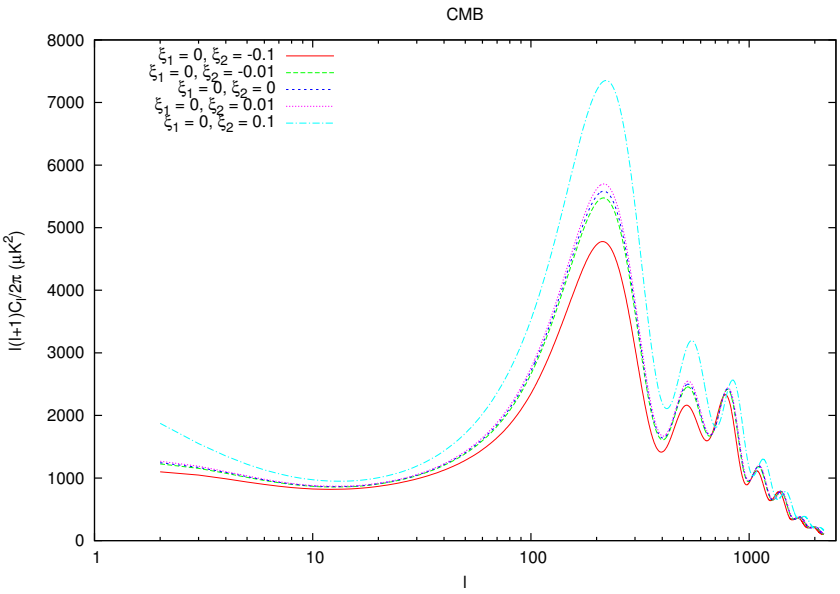

(a)

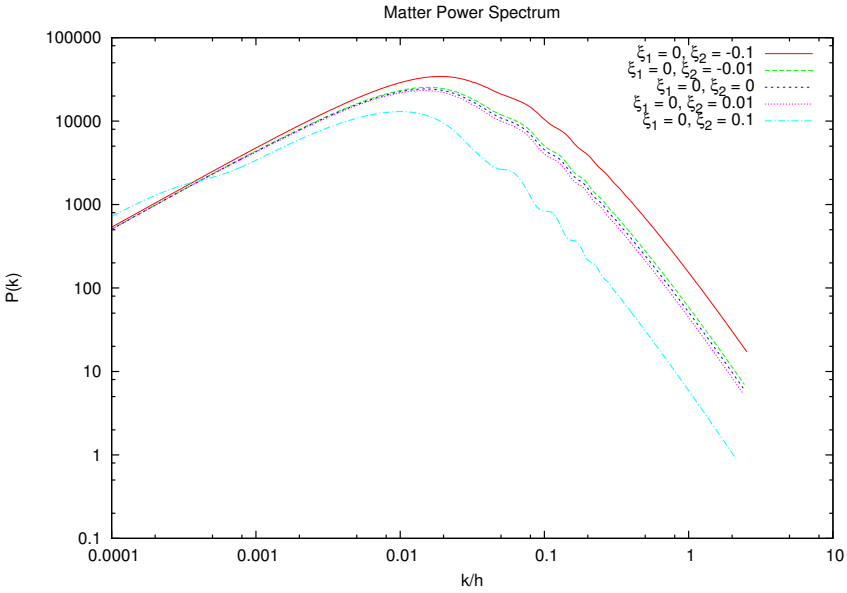

(b)

Figure 3.2: Power spectra for the phenomenological Model I with $\omega = -0.8$ and different values of the interaction parameters.

Figures 3.2-3.5 show that in addition to modifying the CMB spectrum at small l, the coupling between dark sectors can shift the acoustic peaks at large multipoles. While the change of equation of state of dark energy can only modify the low l CMB power

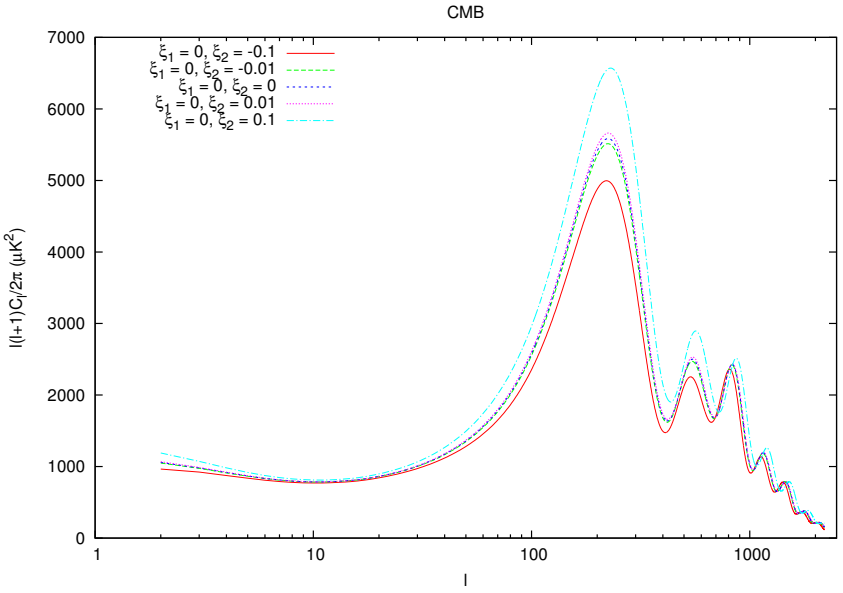

(a)

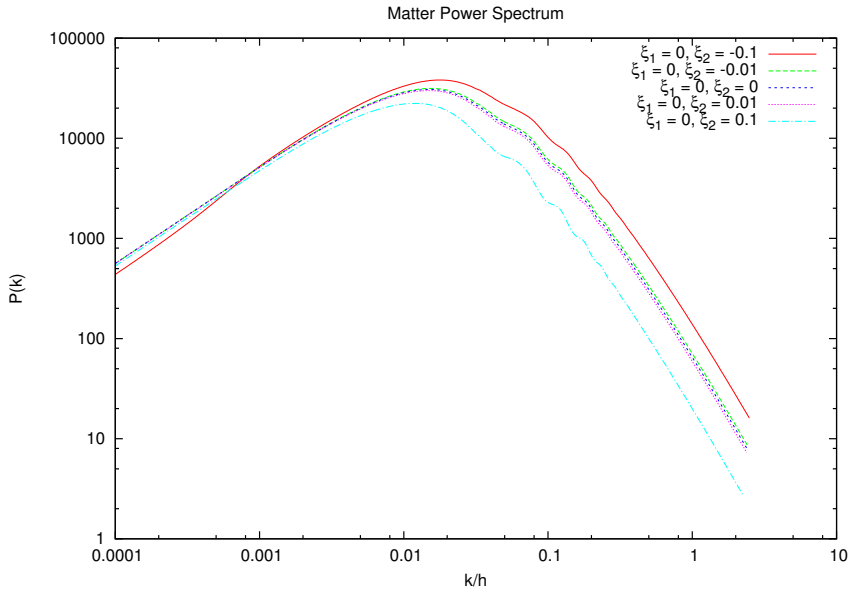

(b)

Figure 3.3: Power spectra for the phenomenological Model II with $\omega = -1.2$ and different values of the interaction parameters.

spectrum, it leaves the acoustic peaks basically unchanged. This provides the possibility to break the degeneracy between the coupling and the equation of state of dark energy in the linear perturbation theory. Furthermore, it was observed that the abundance of dark matter can influence the acoustic peaks in CMB, especially the first and the second ones. The degeneracy between the abundance of the dark matter and the coupling between dark sectors can be broken by examining the CMB spectrum at large scale, since only the coupling between dark sectors influences the large scale CMB spectrum. Theoretically it

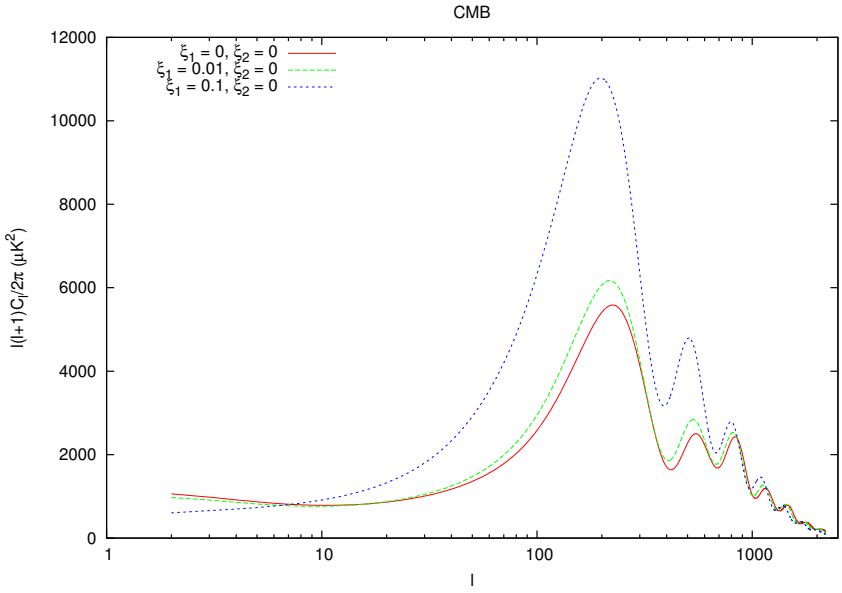

(a)

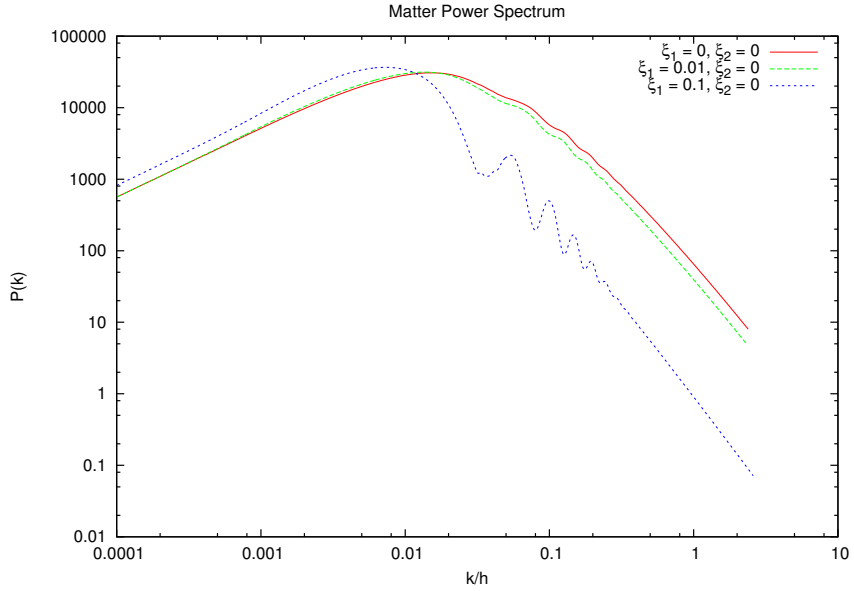

(b)

Figure 3.4: Power spectra for the phenomenological Model III with $\omega = -1.2$ and different values of the interaction parameters.

was observed that there are possible ways to break the degeneracy between the interaction, dark energy equation of state and the dark matter abundance in the perturbation theory [44]. This can help to get tight constraint on the interaction between dark energy and dark matter.

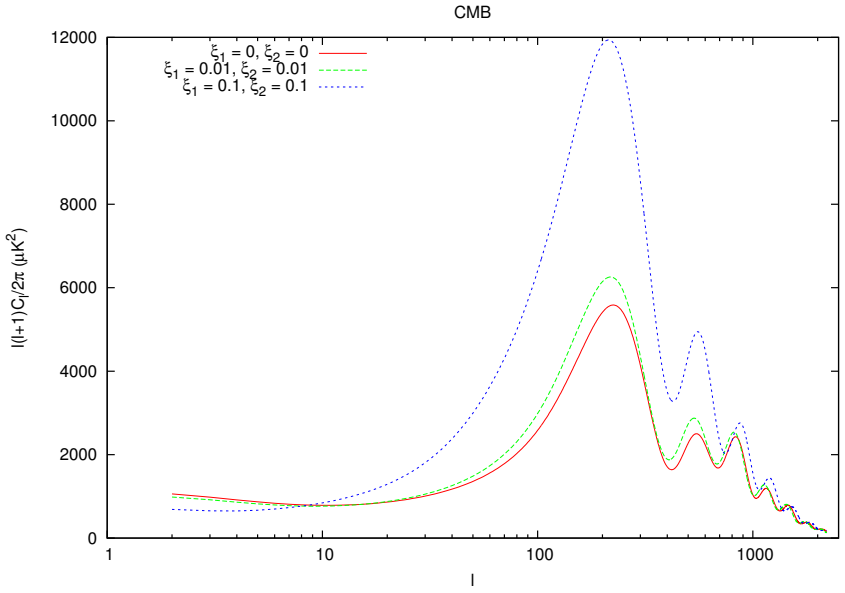

(a)

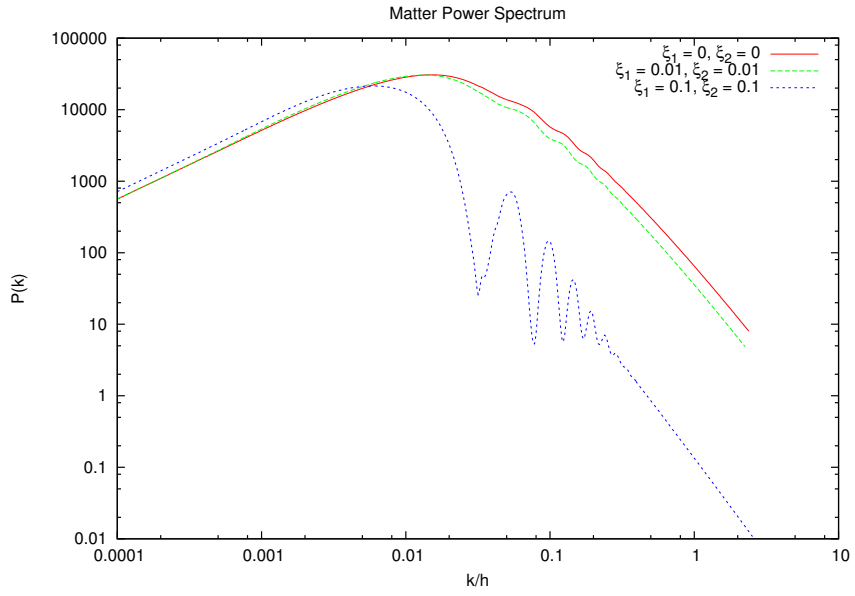

(b)

Figure 3.5: Power spectra for the phenomenological Model IV with $\omega = -1.2$ and different values of the interaction parameters.

3.2 Lagrangian Model

It would be desirable to construct a more fundamental model for dark matter, dark energy and a possible interaction between them. As we know, the fundamental particles and the corresponding interactions in the standard model are described by quantum field theories. In the same way, we would like to account with dark matter and dark energy in the context of a quantum field theory. However, as we already saw, the standard model of particle

physics have no explanation for the dark sector. Thus, in this section, we postulate a model for dark matter interacting with dark energy.

3.2.1 The Tetrad Formalism

We are interested in the behavior of the fields on cosmological scale which means we need a field theory on a curved spacetime. We could be tempted to follow the general approach to transform the special-relativistic equations into general-relativistic equations changing the tensors $T^{\alpha\cdots}_{\beta\cdots}$, the derivatives ∂/∂^α and the metric $\eta_{\alpha\beta}$ to tensors $T^{\mu\cdots}_{\nu\cdots}$, covariant derivatives ∇_μ and metric $g_{\mu\nu}$ in the general coordinate frame. However, there are no representations of the general-coordinate transformation group which behave like spinors under the Lorentz subgroup. Thus, to deal with a fermionic field in the context of general relativity we need the tetrad formalism [57].

Using the *Principle of Equivalence*, we can establish, at every point X, a set of coordinates ξ^α_X that are locally inertial. In the locally inertial frame, the metric is the Minkowski one, $\eta_{\alpha\beta}$. Thus, we can obtain the metric in a general noninertial coordinate system x^μ as [3]

$$g_{\mu\nu}(x) = e^\alpha_\mu(x) e^\beta_\nu(x) \eta_{\alpha\beta}, \tag{3.24}$$

where

$$e^\alpha_\mu(X) \equiv \left(\frac{\partial \xi^\alpha_X(x)}{\partial x^\mu} \right)_{x=X}. \tag{3.25}$$

Fixing the locally inertial coordinates ξ^α_X at each physical point X, the partial derivatives e^α_μ change under a general coordinate transformation $x^\mu \to x'^\mu$ as

$$e^\alpha_\mu \to e'^\alpha_{\ \mu} = \frac{\partial x^\nu}{\partial x'^\mu} e^\alpha_\nu. \tag{3.26}$$

Thus, we can identify e^α_μ with four covariant vector fields, and this set of four vectors is called a *tetrad*, or *vierbien*. On the other hand, the tetrad behaves like a Lorentz contravariant vector under a Lorentz transformation $\Lambda^\alpha_\beta(x)$ of the locally inertial frame:

$$e^\alpha_\mu \to e'^\alpha_{\ \mu} = \Lambda^\alpha_\beta(x) e^\beta_\mu. \tag{3.27}$$

[3] We use Greek letters from the beginning of the alphabet $(\alpha, \beta, \cdots)$ to describe coordinates in the locally inertial frame, while we use Greek letters from the end of the alphabet $(\mu, \nu, \cdots)$ to describe a general coordinate system.

Given a contravariant vector A^μ, we can contract it with the tetrad e^α_μ such that the resulting object $A^\alpha = e^\alpha_\mu A^\mu$ transforms as a set of four scalars under a general coordinate transformation, while it transforms as a Lorentz contravariant vector under a Lorentz transformation of the locally inertial coordinate system. In general, a tensor n times contravariant and m times covariant $T^{\mu_1\cdots\mu_n}_{\nu_1\cdots\nu_m}$, having its contravariant indices contracted with e^α_μ and its covariant indices contracted with the inverse tetrad $e^\nu_\beta = \eta_{\alpha\beta}g^{\mu\nu}e^\alpha_\mu$, will transform as a set of $n \times m$ scalars under a general transformation, and as a Lorentz tensor n times contravariant and m times covariant under a Lorentz transformation of the local frame.

A matter action physically acceptable must be both a scalar under a general coordinate transformation and under a locally inertial Lorentz transformation. If an action could be obtained solely from fields, this condition would be automatically achieved. However, any physically sensible action must also involve derivatives of the fields. Let us consider a field Ψ (where Ψ can be a field of multiple components), which transforms under a Lorentz transformation as $\Psi'(x) = D(\Lambda(x))\Psi(x)$, where $D(\Lambda)$ is a matrix representation of the Lorentz group. What we need is to define a covariant derivative that for a local Lorentz transformation behaves as $\tilde{\nabla}'_\beta\Psi' = \Lambda^\alpha_\beta D(\Lambda)\tilde{\nabla}_\alpha\Psi$. We can verify that the following covariant derivative obeys such a condition [57]:

$$\tilde{\nabla}_\alpha \equiv e^\mu_\alpha(\partial_\mu + \Gamma_\mu) = e^\mu_\alpha\left[\partial_\mu + \frac{1}{2}\sigma^{\beta\delta}e^\nu_\beta(x)\left(\nabla_\mu e_{\delta\nu}(x)\right)\right], \tag{3.28}$$

where $\nabla_\mu e_{\delta\nu}(x) \equiv \partial_\mu e_{\delta\nu}(x) - \Gamma^\lambda_{\mu\nu}e_{\delta\lambda}(x)$ and $\sigma^{\beta\delta}$ are the generators of the Lorentz group. For example, scalars have $\sigma^{\beta\delta} = 0$ and $\tilde{\nabla}_\alpha = \partial_\alpha$, while spinors have $\sigma^{\beta\delta} = \frac{1}{4}[\gamma^\beta, \gamma^\delta]$, where γ^β are Dirac matrices.

Finally we have a prescription to generalize a field theory to curved spacetimes: given a Lagrangian which is a function of the fields and their derivatives, we contract all vectors, tensors, etc., with the tetrad (e.g. $A^\alpha \to e^\alpha_\mu A^\mu$) and substitute the derivatives ∂_α for covariant derivatives $\tilde{\nabla}_\alpha$. Using this prescription, the action will be a scalar under a general coordinate transformation and under a local Lorentz transformation.

The energy-momentum tensor can be defined as [57]

$$T_{\mu\nu}(x) \equiv -\frac{e_{\alpha\mu}(x)}{\det[e(x)]}\frac{\delta S_M}{\delta e^\nu_\alpha(x)}, \tag{3.29}$$

where S_M denotes the action of the matter fields and $\det[e(x)] = \sqrt{-g}$, where g is the determinant of the metric tensor. It is possible to show that the energy-momentum tensor defined in this way is symmetric and obeys the conservation equation $\nabla_\mu T^{\mu\nu} = 0$. Using the definition above, we can obtain the energy-momentum tensor for fields with spin in a curved spacetime.

3.2.2 Yukawa-Type Interaction

Let us consider now a model of interaction between dark energy and dark matter from a Lagrangian density. In this model, the dark energy will be described by a scalar field ϕ and the dark matter will be described by a massive fermionic field of spin-$\frac{1}{2}$ Ψ [4]. We will suppose that the interaction between them is realized by an Yukawa type interaction, which is the only interaction between a scalar field and a fermionic field of spin-$\frac{1}{2}$ that is renormalizable. Thus, the action for this model will be given by

$$S_M = \int d^4x\sqrt{-g}\left\{-\frac{1}{2}\partial_\mu\phi\partial^\mu\phi - V(\phi) + \frac{i}{2}\left[\bar{\Psi}\gamma^\mu\tilde{\nabla}_\mu\Psi - (\tilde{\nabla}_\mu\bar{\Psi})\gamma^\mu\Psi\right] - (M-\beta\phi)\bar{\Psi}\Psi\right\}, \tag{3.30}$$

where β is a dimensionless interaction constant and $V(\phi)$ is the scalar potential. γ^μ are matrices in the curved spacetime identified with the Dirac matrices γ^α multiplied by the tetrad as $\gamma^\mu \equiv e^\mu_\alpha\gamma^\alpha$ and they obey the anti-comutation relation

$$\{\gamma^\mu, \gamma^\nu\} = -2g^{\mu\nu}(x). \tag{3.31}$$

Varying the action S_M with respect to the Dirac field Ψ and the adjoint $\bar{\Psi}$, we obtain the equations of motion for the fermionic fields

$$i\gamma^\mu\tilde{\nabla}_\mu\Psi - \bar{M}\Psi = 0 \tag{3.32}$$

and

$$i(\tilde{\nabla}_\mu\bar{\Psi})\gamma^\mu + \bar{M}\bar{\Psi} = 0, \tag{3.33}$$

where $\bar{M} \equiv M - \beta\phi$. Using these equations, we can show that the current defined as

[4] Note that ϕ and Ψ here are scalar and fermionic fields, respectively. Do not confuse with the metric perturbations defined in the previous chapter.

$j^\mu(x) = \sqrt{-g}\bar{\Psi}\gamma^\mu\Psi$ is conserved

$$\partial_\mu j^\mu(x) = 0. \tag{3.34}$$

On the other hand, varying the action with respect to the scalar field ϕ, we obtain its equation of motion

$$\nabla_\mu \partial^\mu \phi - \frac{dV}{d\phi} = -\beta\bar{\Psi}\Psi, \tag{3.35}$$

where ∇_μ is the covariant derivative in the curved spacetime.

The energy-momentum tensor of the system can be calculated using Eq. (3.29). For our scalar and fermionic fields described by the action (3.30), we can show that [97]

$$T^\phi_{\mu\nu}(x) = \partial_\mu\phi\partial_\nu\phi - g_{\mu\nu}(\frac{1}{2}g^{\alpha\beta}\partial_\alpha\phi\partial_\beta\phi + V(\phi)) \tag{3.36}$$

and

$$T^\Psi_{\mu\nu}(x) = \frac{i}{4}\left[(\tilde{\nabla}_\mu\bar{\Psi})\gamma_\nu\Psi + (\tilde{\nabla}_\nu\bar{\Psi})\gamma_\mu\Psi - \bar{\Psi}\gamma_\mu\tilde{\nabla}_\nu\Psi - \bar{\Psi}\gamma_\nu\tilde{\nabla}_\mu\Psi\right]. \tag{3.37}$$

We have split the energy-momentum tensor by defining a scalar part and a fermionic part such that

$$T_{\mu\nu}(x) = T^\phi_{\mu\nu}(x) + T^\Psi_{\mu\nu}(x) \tag{3.38}$$

and the interaction was included in the fermionic part.

On large scales, we assume that the components in the Universe can be described by a fluid with energy-momentum tensor given by Eq. (1.7). Thus, from the energy-momentum tensor of a perfect fluid, we find that

$$\rho = -T^0_0 \qquad \text{and} \qquad P = \frac{1}{3}T^i_i. \tag{3.39}$$

Therefore, using the energy-momentum tensor of the scalar field (3.36), we can identify an energy density and a pressure given by

$$\rho_\phi = -\frac{1}{2}\left(\partial_\mu\phi\partial^\mu\phi\right) + V(\phi) \tag{3.40}$$

and

$$P_\phi = -\frac{1}{2}\left(\partial_\mu\phi\partial^\mu\phi\right) - V(\phi). \tag{3.41}$$

On the other hand, from the energy-momentum tensor of the fermionic field (3.37), we

have

$$\rho_\Psi = \bar{M}\bar{\Psi}\Psi + \frac{i}{2}\left[\left(\tilde{\nabla}^i\bar{\Psi}\right)\gamma_i\Psi - \bar{\Psi}\gamma^i\tilde{\nabla}_i\Psi\right] \tag{3.42}$$

and

$$P_\Psi = \frac{i}{6}\left[\left(\tilde{\nabla}^i\bar{\Psi}\right)\gamma_i\Psi - \bar{\Psi}\gamma^i\tilde{\nabla}_i\Psi\right]. \tag{3.43}$$

We observe that in the relativistic limit $\bar{M} = 0$, we recover the equation of state for an ideal relativistic gas, $P_\Psi = \rho_\Psi/3$.

Let us assume that the Universe obeys the FLRW metric and the fields are homogeneous such that $\partial_i\phi = 0$, $\partial_i\Psi = \partial_i\bar{\Psi} = 0$ and $\left(\tilde{\nabla}^i\bar{\Psi}\right)\gamma_i\Psi - \bar{\Psi}\gamma^i\tilde{\nabla}_i\Psi = 0$. Thus, the energy density and pressure of the fields result

$$\rho_\phi = \frac{1}{2}\dot{\phi}^2 + V(\phi) \tag{3.44}$$

$$P_\phi = \frac{1}{2}\dot{\phi}^2 - V(\phi) \tag{3.45}$$

$$\rho_\Psi = \bar{M}\bar{\Psi}\Psi \tag{3.46}$$

$$P_\Psi = 0. \tag{3.47}$$

From the above equations we observe that the scalar field possesses an equation of state given by

$$\omega_\phi \equiv \frac{P_\phi}{\rho_\phi} = \frac{\dot{\phi}^2 - 2V}{\dot{\phi}^2 + 2V}. \tag{3.48}$$

Besides the relations above, in a FLRW universe, the equation of motion for the scalar field (3.35) yields

$$\ddot{\phi} + 3H\dot{\phi} + \frac{dV}{d\phi} = \beta\bar{\Psi}\Psi \tag{3.49}$$

and the current conservation of the fermionic field (3.34) gives

$$\frac{d(a^3\Psi^\dagger\Psi)}{dt} = 0. \tag{3.50}$$

Deriving equations (3.44) and (3.46) with respect to the cosmic time and using the equations of motion for the scalar and fermionic fields, we obtain the energy balance equations

$$\dot{\rho}_\phi + 3H\rho_\phi(1 + \omega_\phi) = \beta\dot{\phi}\bar{\Psi}\Psi = Q \tag{3.51}$$

and

$$\dot{\rho}_\Psi + 3H\rho_\Psi = -\beta\dot{\phi}\bar{\Psi}\Psi = -Q. \tag{3.52}$$

From Eq. (3.46), we see that the interaction $Q \equiv \beta\dot{\phi}\bar{\Psi}\Psi$ can be rewritten as

$$Q \equiv \beta\dot{\phi}\bar{\Psi}\Psi = -\frac{\partial \ln \bar{M}}{\partial\phi}\rho_\Psi\dot{\phi} = \frac{\beta}{M-\beta\phi}\rho_\Psi\dot{\phi}. \tag{3.53}$$

Thus, we observe that the fermionic field can be completely described by a fluid, since the energy balance equations depend on the fermionic field only through the energy density ρ_Ψ and a constant mass M. On the other hand, the scalar field cannot be completely described by the energy balance equations because the equation of state ω_ϕ and the interaction term Q depend on the scalar field and its derivative. Therefore, the background equations describing the evolution of the fermionic and scalar fields are

$$\dot{\rho}_\Psi + 3H\rho_\Psi = -\frac{\beta}{M-\beta\phi}\rho_\Psi\dot{\phi} \tag{3.54}$$

and

$$\ddot{\phi} + 3H\dot{\phi} + \frac{dV}{d\phi} = \frac{\beta}{M-\beta\phi}\rho_\Psi. \tag{3.55}$$

Let us introduce now linear perturbations in our model. To facilitate the study of linear perturbations, we assume that the fermionic field can be completely described by the fluid equations even in the perturbed level. The interaction between the dark energy and dark matter can be generalized into a covariant form as

$$Q^\mu = \frac{\partial \ln \bar{M}}{\partial\phi}\rho_\Psi\partial^\mu\phi. \tag{3.56}$$

Thus, the balance equations can be generalized to

$$\nabla_\mu T^{\mu\nu}_\phi = Q^\nu = \frac{\beta}{M-\beta\phi}\rho_\Psi\nabla^\nu\phi \tag{3.57}$$

and

$$\nabla_\mu T^{\mu\nu}_\Psi = -Q^\nu = -\frac{\beta}{M-\beta\phi}\rho_\Psi\nabla^\nu\phi, \tag{3.58}$$

where $T^{\mu\nu}_\Psi$ assumes the form of a perfect fluid as in Eq. (3.6). The scalar field can be decomposed into a homogeneous part and a perturbed part, $\phi(t) + \varphi(t,\vec{x})$. Thus, using

the metric (2.6) in the synchronous gauge, the balance equations (3.57) and (3.58) yield the perturbed equations

$$\varphi'' + 2\mathcal{H}\varphi' + k^2\varphi + a^2\frac{d^2V}{d\phi^2}\varphi + \frac{h'\phi'}{2} = -a^2\frac{\beta^2}{(M-\beta\phi)^2}\varphi\rho_\Psi + a^2\frac{\beta}{M-\beta\phi}\rho_\Psi\delta_\Psi, \tag{3.59}$$

$$\delta'_\Psi = -\frac{h'}{2} - kv_\Psi - \frac{\beta}{M-\beta\phi}\varphi' + \frac{\beta^2}{(M-\beta\phi)^2}\phi'\varphi, \tag{3.60}$$

$$v'_\Psi = -\mathcal{H}v_\Psi + \frac{\beta}{M-\beta\phi}v_\Psi\phi' - k\frac{\beta}{M-\beta\phi}\varphi, \tag{3.61}$$

in the Fourier space and conformal time.

To complete the discussion about the linear perturbations we need the initial conditions of the perturbed quantities. We assume that the dark matter and the dark energy satisfy adiabatic initial conditions

$$\frac{\delta\rho_\phi}{\rho_\phi + P_\phi} = \frac{\delta\rho_\Psi}{\rho_\Psi + P_\Psi}, \tag{3.62}$$

where using equations (3.44) and (3.45) in the conformal time, we have

$$\delta\rho_\phi = \frac{\phi'\varphi'}{a^2} + \frac{dV}{d\phi}\varphi \qquad \text{and} \qquad \delta P_\phi = \frac{\phi'\varphi'}{a^2} - \frac{dV}{d\phi}\varphi. \tag{3.63}$$

Thus, the adiabatic initial condition (3.62) can be rewritten as

$$\frac{\phi'\varphi' + a^2\frac{dV}{d\phi}\varphi}{\phi'^2} = \delta_\Psi. \tag{3.64}$$

As the scalar field obeys a second-order differential equation, we need two initial conditions. The second initial condition can be obtained considering that the intrinsic entropy is null

$$\frac{\delta\rho_\phi}{\rho_\phi} - \frac{\delta P_\phi}{P_\phi} = 0, \tag{3.65}$$

which implies

$$\frac{\phi'\varphi' + a^2\frac{dV}{d\phi}\varphi}{\frac{\phi'^2}{2} + a^2V} = \frac{\phi'\varphi' - a^2\frac{dV}{d\phi}\varphi}{\frac{\phi'^2}{2} - a^2V}. \tag{3.66}$$

Finally, solving equations (3.64) and (3.66) for φ and φ', we obtain the perturbed initial conditions for the scalar field

$$\varphi = \frac{2\delta_\Psi\phi'^2V}{(\phi'^2 + 2a^2V)\frac{dV}{d\phi}} \tag{3.67}$$

and

$$\varphi' = \frac{\delta_\Psi \phi'^3}{\phi'^2 + 2a^2 V}. \tag{3.68}$$

We modified the CAMB code to include the Lagrangian model above. We considered that the scalar potential is given by

$$V(\phi) = Ae^{-\lambda\phi/M_{pl}}, \tag{3.69}$$

where A is a normalization constant, λ is a dimensionless parameter and M_{pl} is the reduced Planck mass. We set A to the value of the cosmological constant energy density $A = \rho_\Lambda$. Thus, $\lambda \neq 0$ and $\beta \neq 0$ is a measurement of how our model differ from the cosmological constant model. We also see from Eq. (3.53) that the interaction β and the fermion mass M are degenerate, we can only know the ratio $r \equiv \frac{\beta}{M} M_{pl}$. Therefore, we use r instead of β as our interaction parameter. This has the advantage of decreasing one degree of freedom in the analysis, at the cost that we are unable to know the individual values of β or M.

The appendix B shows the most import steps to introduce the Lagrangian model in the CAMB code. Below we present some graphs for the CMB and matter power spectrum obtained from the Lagrangian model for different values of the parameters. Figure 3.6 shows that the scalar potential parameter λ has a small effect on the CMB and matter power spectrum, affecting mainly the low-l CMB power spectrum. On the other hand, as observed in the phenomenological case, we see from Fig. 3.7 that in addition to modifying the CMB spectrum at low l, the coupling between dark sectors can shift the acoustic peaks at large multipoles. However, comparing with the phenomenological models, the Yukawa interaction has a more dramatic effect on low multipoles and less effect on the acoustic peaks. We also observe that the power spectra present an almost symmetric behavior around the zero value for the interaction. However, such a symmetry is broken when we look at background quantities, e.g. the age of the Universe.

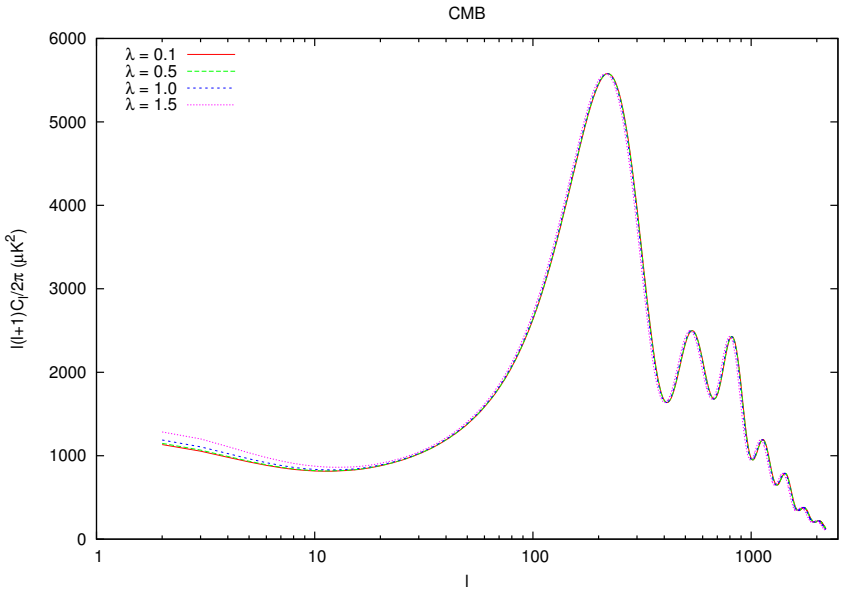

(a)

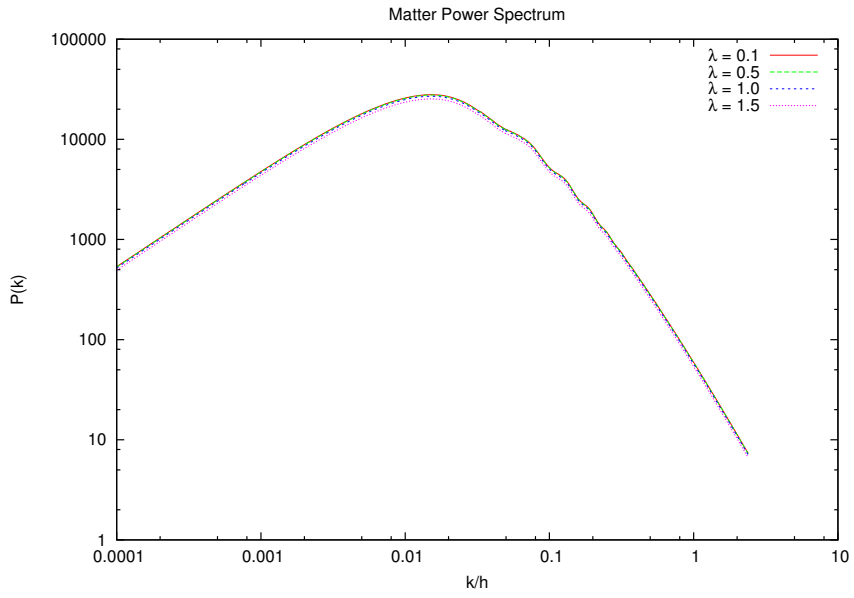

(b)

Figure 3.6: Power spectra for the Lagrangian model with $r = \frac{\beta}{M} M_{pl} = 0$ and different values for the scalar potential parameter.

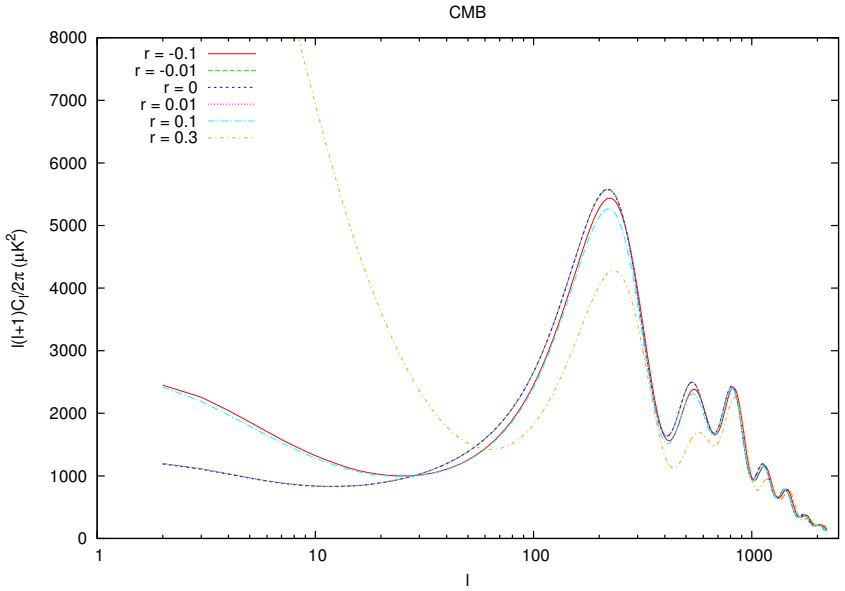

(a)

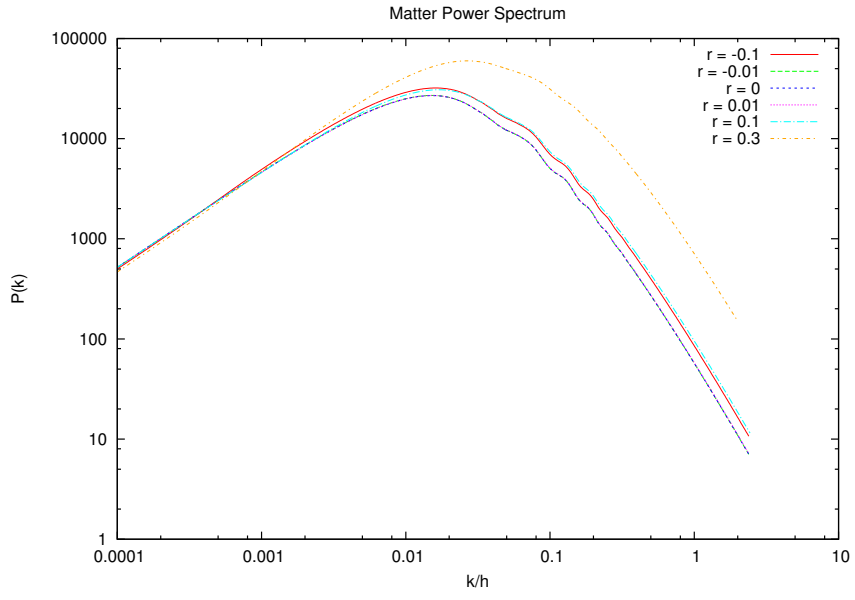

(b)

Figure 3.7: Power spectra for the Lagrangian model with $\lambda = 1$ and different values for the dimensioless interaction parameter $r = \frac{\beta}{M} M_{pl}$.

Chapter 4

Analysis

In the previous chapter we presented some models of interacting dark energy. We showed some aspects of their behavior, especially on the power spectra. We now wish to test such models with current observational data in order to constrain the cosmological parameters. The results of this chapter are matter of publication in [98–100].

4.1 Methods for Data Analysis

Let us suppose we want to estimate a random physical quantity x with a *probability density function* (PDF) $f(x|\theta)$ that depends on an unknown parameter θ. Naturally, we cannot know the exact value of x, since there are several uncertainties in the measurement, which we denote as σ. Then, the probability of obtaining x in the interval Δx around x is

$$P = \int_{x_1}^{x_2} f(x|\theta)dx. \tag{4.1}$$

Such a probability is called a *conditional probability* of having the data x given the theoretical parameter θ. If the interval of integration above is small, we can approximate the probability as $P \approx f(x|\theta)\Delta x$.

The law of joint probability tells us that for several measurements x_i, $i = 1, ..., N$, the probability of having x_1 in the interval Δx_1 around x_1, x_2 in the interval Δx_2 around x_2 and so forth is

$$P(x_i|\theta) \approx (\Delta x)^N \prod_{i=1}^{N} f(x_i|\theta) \equiv (\Delta x)^N \mathcal{L}(x_i|\theta). \tag{4.2}$$

This procedure is correct given the fact that the measurements are mutually independent

and considering equally spaced small intervals Δx_i. In the above expression we defined the *likelihood function*, $\mathcal{L}(x_i|\theta) \equiv \prod_{i=1}^{N} f(x_i|\theta)$. Except for a constant value, the likelihood function gives us the probability of having the outcomes x_i given the parameter θ. In general, the data can be correlated and depend on several parameters θ_j. For correlated data, $\mathcal{L}(x_i|\theta_j)$ will not be the simple product of the PDFs, but its statistical interpretation remains the same.

For every set of parameters θ_j, the likelihood function $\mathcal{L}(x_i|\theta_j)$ will assume a different value. It is logic to define the best θ_js as the parameters that maximize the likelihood. Thus, the maximum likelihood method of parameter estimation consists in finding the parameters that maximize the likelihood solving the system

$$\frac{\partial \mathcal{L}(x_i|\theta_j)}{\partial \theta_j} = 0, \qquad j = 1, \cdots, m. \tag{4.3}$$

The solutions of these equations, $\hat{\theta}_j$s, are functions of the random data x_is, therefore they are random too. In the *frequentist* approach, one tries to find the distribution of the $\hat{\theta}_j$s given the distribution of the data x_is; if this is possible, one can associate probabilities to intervals of $\hat{\theta}_j$s, for instance determine the interval of $\hat{\theta}_j$ that has 95% probability that a set of data were obtained from the theoretical distribution. However, it is often too difficult to derive the $\hat{\theta}_j$'s distributions analytically and very demanding to derive them numerically using simulated datasets. Moreover, this approach does not take into account our previous knowledge about the theoretical parameters, e.g. the results of preceding experiments. These issues can be worked more appropriately using the *Bayesian* approach.

In the Bayesian approach, instead of looking for the probability of having the data given the model, $\mathcal{L}(x_i|\theta_j)$, we look for the probability of the model given the data, $P(\theta_j|x_i)$. This is possible thanks to the Bayes's theorem,

$$P(B|A, I) = \frac{P(A|B, I)P(B|I)}{P(A|I)}, \tag{4.4}$$

which relates the conditional probability of having an event B given the event A occurred, $P(B|A, I)$, with the conditional probability $P(A|B, I)$ of A given B and the probabilities $P(B|I)$ and $P(A|I)$ of the events B and A, respectively. The letter "I" denotes that these probabilities depend on some information I we assume to be true.

In our case we have the data $A \equiv x_i$ and the parameters $B \equiv \theta_j$ for some theoretical

model $I \equiv M$, thus

$$p(\theta_j|x_i, M) = \frac{\mathcal{L}(x_i|\theta_j)p(\theta_j|M)}{p(x_i|M)}. \tag{4.5}$$

The function $p(\theta_j|x_i, M)$ is the *posterior* probability distribution, $p(x_i|M)$ is the PDF of the data x_i, sometimes called *evidence*, and $p(\theta_j|M)$ is the *prior* probability for the parameters θ_j, it represents our previous knowledge for the parameters before we make the experiment. Therefore, the posterior contains the information we are looking for: the probability of having the parameters θ_j given the data x_i and some previous knowledge about the parameters.

The posterior is a probability distribution and consequently it must be normalized to unity

$$\int p(\theta_j|x_i, M)d^m\theta_j = \frac{\int \mathcal{L}(x_i|\theta_j)p(\theta_j|M)d^m\theta_j}{p(x_i|M)} = 1, \tag{4.6}$$

which implies

$$\int \mathcal{L}(x_i|\theta_j)p(\theta_j|M)d^m\theta_j = p(x_i|M). \tag{4.7}$$

Thus, we can think the evidence as a normalization factor. On the other hand, the prior is often unknown. Usually, if we know nothing about the parameters we want to estimate, we choose a uniform prior in some interval and zero outside it. However, if we have some estimate of the parameters from previous experiments, we can adopt a Gaussian centered at the estimated value as our prior. In general, the choice of priors affect the posterior distribution, but if we have enough data they will dominate the posterior.

Given the posterior $p(\theta_j|x_i, M)$ we can find the maximum likelihood estimators $\hat{\theta}_j$ as

$$\frac{\partial p(\theta_j|x_i, M)}{\partial \theta_j} = 0 \qquad j = 1, \cdots, m. \tag{4.8}$$

We can also derive the regions of confidence for the parameters, which are defined as regions $R(\alpha)$ such that

$$\int_{R(\alpha)} p(\theta_j|x_i, M)d^m\theta = \alpha, \tag{4.9}$$

where the posterior must be normalized, which means $0 < \alpha < 1$. To find these regions, the limits of integration must be the lowest ones such that the integral is valid. Typical choices of α are $\alpha = 0.683,\ 0.954,\ 0.997$ which denote the 1σ, 2σ and 3σ confidence levels. Frequently, we are interested in a subset of the parameter space and we consider the others as "nuisance", thus we integrate (marginalize) over the uninterested parameters.

In general, the distribution function depends on the characteristics of the quantity it describes and its uncertainties. In cosmology we usually assume a Gaussian distribution for the data even when each data was not extracted from a Gaussian distribution. This is possible thanks to the *central limit theorem* [101, 102], which establishes that for a set of N variables with some distribution each one with a finite variance, in the limit $N \to \infty$, the average distribution tends to a Gaussian one. Thus, if the data have a Gaussian distribution and are independent of each other, then

$$\begin{aligned}\mathcal{L}(x_i|\theta_j) &= \prod_{i=1}^{N} \frac{1}{\sqrt{2\pi\sigma_i}} \exp\left[-\frac{1}{2}\left(\frac{x_i - x_i(\theta_j)}{\sigma_i}\right)^2\right] \\ &= \left(\prod_{i=1}^{N} \frac{1}{\sqrt{2\pi\sigma_i}}\right) \exp\left[-\frac{1}{2}\sum_{i=1}^{N}\left(\frac{x_i - x_i(\theta_j)}{\sigma_i}\right)^2\right]. \end{aligned} \tag{4.10}$$

Therefore, maximizing the posterior distribution (4.5) is equivalent to minimizing the above exponent

$$\chi^2 \equiv \sum_{i=1}^{N}\left(\frac{x_i - x_i(\theta_j)}{\sigma_i}\right)^2. \tag{4.11}$$

If the data are correlated, the above likelihood must be generalized as

$$\mathcal{L}(x_i|\theta_j) \propto \frac{1}{\sqrt{\det C}} \exp\left(-\frac{1}{2}\mathbf{X}^T C^{-1}\mathbf{X}\right), \tag{4.12}$$

where $\mathbf{X}$ is the data vector and C is the covariance matrix.

4.2 Data

To constrain the cosmological parameters in our interacting models, we use several data sets, the measurements of CMB anisotropies, BAO, SNIa, the direct measurement of the Hubble constant H_0 and Lookback Time. Below we describe the likelihood for these measurements.

4.2.1 CMB Measurements

The Planck data set we use is a combination of the low-l TT likelihood, which includes measurements for $l = 2 - 49$, combined with the high-l TT likelihood, which includes measurements from $l = 50$ up to a maximum multipole number of $l_{max} = 2500$ [47–49].

Together with the Planck data, we include the polarization measurements from the nine year Wilkinson Microwave Anisotropy Probe (WMAP) [103], the low-l ($l < 32$) TE, EE, BB likelihoods.

The CMB power spectrum likelihood for low-l multipoles can be written as

$$\mathcal{L}(C_l) = p(\mathbf{m}|C_l) = \frac{1}{2\pi^{n/2}|\mathbf{M}|^{1/2}} \exp\left(-\frac{1}{2}\mathbf{m}^t\mathbf{M}^{-1}\mathbf{m}\right), \tag{4.13}$$

where n is the number of observed pixels, $\mathbf{M}(C_l) = \mathbf{C}(C_l) + \mathbf{N}$ is the data covariance matrix, which is split into the CMB, $\mathbf{C}$, and noise, $\mathbf{N}$, covariance matrices, and $\mathbf{m} = \mathbf{s} + \mathbf{n}$ is the observed map. Actually, the estimated C_l distribution is not well approximate by a Gaussian at low l ($l < 50$), because of the limited degrees of freedom per l. However, if foregrounds and instrumental systematics are negligible, then the CMB signal $\mathbf{s}$ and instrumental noise $\mathbf{n}$ are nearly Gaussian and the above likelihood is valid.

In the general case, the data vector $\mathbf{m}$ includes both temperature and linear polarization. For the temperature, the signal covariance matrix gives

$$\langle T_{i_1} T_{i_2} \rangle = \sum_{l=2}^{l_{max}} \frac{2l+1}{4\pi} C_l^{th} b_l^2 W_l^2 P_l(\theta_{i_1 i_2}) + \mathbf{N_{i_1 i_2}}, \tag{4.14}$$

where P_l are Legendre polynomials calculated at angle $\theta_{i_1 i_2}$ between the centers of pixels i_1 and i_2, b_l is the effect of instrumental beam and W_l is the window function. For polarization correlations, we obtain similar expressions.

4.2.2 BAO Measurements

In addition to the CMB data sets, we also consider measurements of Baryon Acoustic Oscillations (BAO) in the matter power spectrum. We combine the results from three redshift surveys: the 6dF Galaxy Survey measurement at redshift $z = 0.106$ [50], the SDSS DR7 BAO measurement at redshift $z = 0.35$ as analysed by Padmanabhan et al. [51] and the BOSS DR9 measurement at $z = 0.57$ [52].

These redshift surveys measure the distance ratio

$$d_z = \frac{r_s(z_{drag})}{D_V(z)}, \tag{4.15}$$

where $r_s(z_{drag})$ is the comoving sound horizon at the baryon drag epoch, the epoch when

baryons became dynamically decoupled from photons, and $D_V(z)$ combines the angular diameter distance $d_A(z)$ and the Hubble parameter $H(z)$, in a way appropriate for the analysis of spherically-averaged two-point statistics,

$$D_V(z) = \left[(1+z)^2 d_A^2(z)\frac{cz}{H(z)}\right]^{1/3}. \tag{4.16}$$

The comparison with BAO measurements is made using χ^2 statistics

$$\chi^2_{BAO} = (\mathbf{x} - \mathbf{x}^{obs})^T C^{-1}_{BAO}(\mathbf{x} - \mathbf{x}^{obs}), \tag{4.17}$$

where $\mathbf{x}$ is our theoretical predictions and $\mathbf{x}^{obs}$ denotes the data vector. The data vector is composed by the measurements of the three data sets above: For the 6dF $D_V(0.106) = (457 \pm 27)Mpc$, for the DR7 $D_V(0.35)/r_s = 8.88 \pm 0.17$ and for the DR9 $D_V(0.57)/r_s = 13.67 \pm 0.22$.

4.2.3 SNIa Measurements

We use the SNIa data from the Supernova Cosmology Project (SCP) Union 2.1 compilation [53], which has 580 samples. The Union 2.1 uses SALT2 [104] to fit supernova lightcurves. The SALT2 model fits three parameters to each supernova: an overall normalization, x_0, to the time dependent spectral energy distribution of a SNIa, the deviation from the average lightcurve shape x_1 and the deviation from the mean SNIa B - V color c. Combining these parameters, the distance modulus is given by

$$\mu_B = m_B^{max} + \alpha \cdot x_1 - \beta \cdot c + \delta \cdot P(m_\star^{true} < m_\star^{threshold}) - M_B, \tag{4.18}$$

where m_B^{max} is the integrated B-band flux at maximum light, $P(m_\star^{true} < m_\star^{threshold})$ gives the correlation of SNIa luminosity to the mass of the host galaxy and M_B is the absolute B-band magnitude. The nuisance parameters α, β, δ and M_B are fitted simultaneously with cosmological parameters.

The best-fit cosmology is determined by minimizing the χ^2,

$$\chi^2_{SN} = \sum_{i=1}^{580} \frac{[\mu_B(\alpha,\beta,\delta,M_B) - \mu(z,\Omega_m,\Omega_d,w)]^2}{\sigma^2}. \tag{4.19}$$

To test our interacting dark energy models we use the CosmoMC [105, 106] module associated with the Union 2.1 sample. In this module the nuisance parameters are hold fixed with values $\alpha = 0.1218$, $\beta = 2.4657$ and $\delta = -0.03634$.

4.2.4 H_0 Measurements

From observations of Cepheid variables and low-redshift Type Ia surpernovae, the Hubble Space Telescope (HST) determined the Hubble constant with 3.3% uncertainty including systematic errors [54]

$$H_0 = 73.8 \pm 2.4 kms^{-1}Mpc^{-1}. \tag{4.20}$$

We use this measurement of the Hubble constant as an additional data.

4.2.5 Lookback Time Measurements

The background observables treated so far, the measurements of H_0 and SNIa, are firmed on distance measurements. To pin down the cosmological parameters we will consider another indicator, the *lookback time*, which is based on ages instead of distances. The lookback time $t_L(z)$ is the difference between the present age of the Universe, t_0, and its age at redshift z, $t(z)$,

$$t_L(z) = t_0 - t(z) = \int_0^\infty \frac{dz'}{(1+z')H(z')} - \int_z^\infty \frac{dz'}{(1+z')H(z')} = \int_0^z \frac{dz'}{(1+z')H(z')}. \tag{4.21}$$

For an object at redshift z_i, we can calculate its age from the difference between the age of the Universe at redshift z_i and the age of the Universe when the object was formed at redshift z_F,

$$t(z_i) = \int_{z_i}^\infty \frac{dz'}{(1+z')H(z')} - \int_{z_F}^\infty \frac{dz'}{(1+z')H(z')} = \int_{z_i}^{z_F} \frac{dz'}{(1+z')H(z')} = t_L(z_F) - t_L(z_i), \tag{4.22}$$

where we used the lookback time definition (4.21). Thus, the above equation tells us that the observed lookback time $t_L^{obs}(z_i)$ to an object i at redshift z_i is

$$t_L^{obs}(z_i) = t_L(z_F) - t(z_i) = [t_0^{obs} - t(z_i)] - [t_0^{obs} - t_L(z_F)] = t_0^{obs} - t(z_i) - df, \tag{4.23}$$

where $df \equiv t_0^{obs} - t_L(z_F)$ is the *delay factor* which encodes our ignorance of the formation redshift z_F.

In order to constrain the cosmological parameters, we implement a CosmoMC module to calculate the likelihood for lookback time measurements (Appendix C shows the details of this module). We use the data of 32 passively evolving galaxies in the redshift interval $0.117 \leq z \leq 1.845$ with an uncertainty in the age measurements of 12% at one standard deviation [56]. Additionally, we use the ages of 6 galaxy clusters in the redshift range $0.10 \leq z \leq 1.27$ with an uncertainty of 1Gyr at one standard deviation [55]. The likelihood is a Gaussian with

$$\chi^2_{LBT} = \sum_{i=1}^{38} \frac{[t_L(z_i, \vec{p}) - t_L^{obs}(z_i, df)]^2}{\sigma_i^2 + \sigma_{t_0^{obs}}^2} + \frac{[t_0(\vec{p}) - t_0^{obs}]^2}{\sigma_{t_0^{obs}}^2}, \tag{4.24}$$

where $\vec{p}$ denotes the theoretical cosmological parameters. The delay factor is a nuisance parameter that is fitted simultaneously with the cosmological parameters.

4.3 Results

4.3.1 Phenomenological Model

We would like to put constraints on the four phenomenological coupled dark energy models listed in Table 3.1. For this purpose, we will use the recent measurements of the cosmic microwave background anisotropies as measured by the Planck satellite mission. We will also consider the combined constraints from the Planck data plus BAO, SNIa and H_0 measurements. In our analysis, we will choose our priors of different cosmological parameters as listed in Table 4.1. The results were published in [98].

We will allow the equation of state of dark energy to vary. We also choose the helium abundance Y_p from a big bang nucleosynthesis (BBN) consistent scenario. Thus, the primordial helium abundance Y_p is predicted as a function of the baryon density $\Omega_b h^2$ and number of extra radiation degrees of freedom ΔN. We will use interpolated results from the PArthENoPE code [107] to set Y_p, following [108]. We will take the relativistic number of degrees of freedom $N_{eff} = 3.046$, the total neutrino mass $\sum m_\nu = 0.06eV$ and the spectrum lensing normalization $A_L = 1$. To compare theory with observations, we employ the Markov chain Monte Carlo (MCMC) methodology through a modified version

Table 4.1: Priors for the cosmological parameters considered in the analysis of the phenomenological interaction models.

Parameters	Prior			
$\Omega_b h^2$	$[0.005, 0.1]$			
$\Omega_c h^2$	$[0.001, 0.5]$			
100θ	$[0.5, 10]$			
τ	$[0.01, 0.8]$			
n_s	$[0.9, 1.1]$			
$log(10^{10} A_s)$	$[2.7, 4]$			
	Model I	Model II	Model III	Model IV
ω	$[-1, -0.1]$	$[-2.5, -1]$	$[-2.5, -1]$	$[-2.5, -1]$
ξ	$[-0.4, 0]$	$[0, 0.4]$	$[0, 0.01]$	$[0, 0.01]$

of the program CosmoMC [105, 106]. We set the statistical convergence of the chains from the Gelman and Rubin criterion $R - 1 = 0.03$. After running the MCMC, we list our fitting results in Tables 4.2-4.5.

Table 4.2: Cosmological parameters - Model I.

	Planck		Planck+BAO		Planck+BAO+SNIa+H0	
Parameter	Best fit	68% limits	Best fit	68% limits	Best fit	68% limits
$\Omega_b h^2$	0.02213	$0.02202^{+0.000272}_{-0.000273}$	0.02225	$0.02203^{+0.000261}_{-0.000261}$	0.0221	$0.02202^{+0.000251}_{-0.000251}$
$\Omega_c h^2$	0.1188	$0.06889^{+0.0483}_{-0.0252}$	0.1121	$0.0608^{+0.038}_{-0.0311}$	0.07199	$0.04824^{+0.0256}_{-0.0319}$
$100\theta_{MC}$	1.041	$1.045^{+0.00174}_{-0.00351}$	1.042	$1.045^{+0.00179}_{-0.00309}$	1.044	$1.046^{+0.00195}_{-0.00256}$
τ	0.08951	$0.08843^{+0.0123}_{-0.0136}$	0.09803	$0.08835^{+0.0121}_{-0.0139}$	0.09492	$0.08866^{+0.012}_{-0.0136}$
n_s	0.9596	$0.9601^{+0.00747}_{-0.00739}$	0.9643	$0.9606^{+0.00639}_{-0.00642}$	0.964	$0.9598^{+0.00616}_{-0.00624}$
$\ln(10^{10} A_s)$	3.088	$3.087^{+0.0237}_{-0.0256}$	3.106	$3.086^{+0.0238}_{-0.0265}$	3.102	$3.088^{+0.0236}_{-0.0261}$
w	-0.9747	$-0.8797^{+0.0287}_{-0.119}$	-0.9934	$-0.9141^{+0.0221}_{-0.0849}$	-0.9935	$-0.9362^{+0.0171}_{-0.0628}$
ξ_2	-0.0006633	$-0.1353^{+0.128}_{-0.0528}$	-0.02123	$-0.1546^{+0.0743}_{-0.0947}$	-0.1359	$-0.1854^{+0.0524}_{-0.0793}$
Ω_d	0.6829	$0.7918^{+0.112}_{-0.0937}$	0.7103	$0.8234^{+0.0852}_{-0.072}$	0.8106	$0.8569^{+0.0706}_{-0.0478}$
Ω_m	0.3171	$0.2082^{+0.0957}_{-0.114}$	0.2897	$0.1766^{+0.072}_{-0.0852}$	0.1894	$0.1431^{+0.0478}_{-0.0706}$
z_{re}	11.05	$10.99^{+1.08}_{-1.07}$	11.74	$10.96^{+1.1}_{-1.08}$	11.55	$10.99^{+1.08}_{-1.06}$
H_0	66.81	$67.66^{+4.7}_{-3.55}$	68.26	$69.26^{+2.04}_{-1.99}$	70.72	$70.71^{+1.36}_{-1.37}$
Age/Gyr	13.83	$13.82^{+0.0762}_{-0.116}$	13.78	$13.78^{+0.0458}_{-0.0468}$	13.75	$13.76^{+0.0371}_{-0.0374}$
$\chi^2_{min}/2$	4903.07		4903.61		4970.24	

The constraints on the parameters and the best fit values for Model I are reported in Table 4.2. The 1-D posteriors for the parameters are shown in Fig.4.1 and the main parameter degeneracies are shown in Fig.4.2. The presence of a dark coupling is perfectly compatible with the Planck data set. The marginalized value tells us $\xi_2 < 0$. With the combined constraint by including other observational data, the negative value of the coupling keeps. Thus, for this coupling model, there is a lower value of the cold dark matter density today, since there is energy flow from dark matter to dark energy. This direction of energy flow cannot alleviate the coincidence problem. As shown in Fig.3.1,

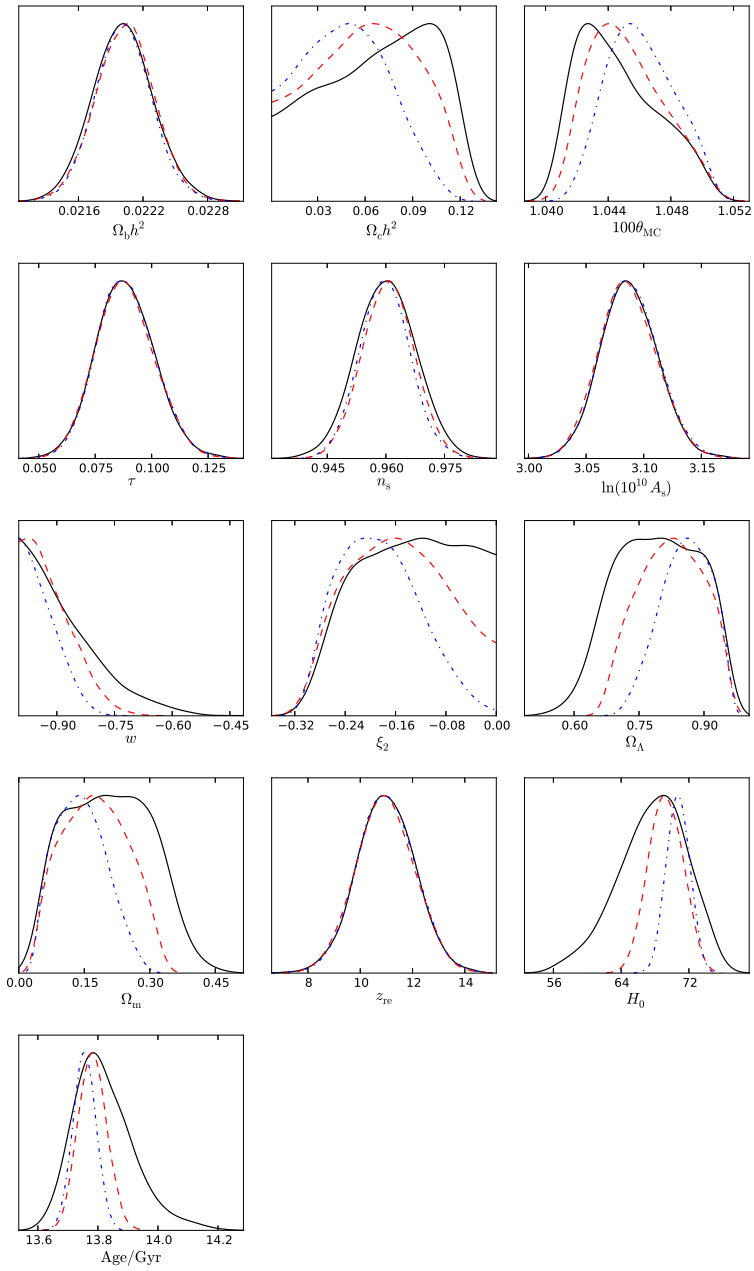

Figure 4.1: The likelihood for the parameters of the phenomenological Model I. The black solid lines correspond to the Planck constraints, the red dashed lines correspond to Planck + BAO and the blue dot-dashed lines correspond to Planck + BAO + SNIa + H_0.

there is even shorter period for the energy densities of dark matter and dark energy to be comparable. For the Hubble constant value, from the Planck data alone, H_0 is small in this interacting model, which is similar to that obtained in the ΛCDM case. This interaction model between dark sectors cannot be of much help to relax the tension on the Hubble parameter between Planck measurement and HST observation. After including other observational data at low redshift, we find that the tension between the Hubble constant measurements is alleviated.

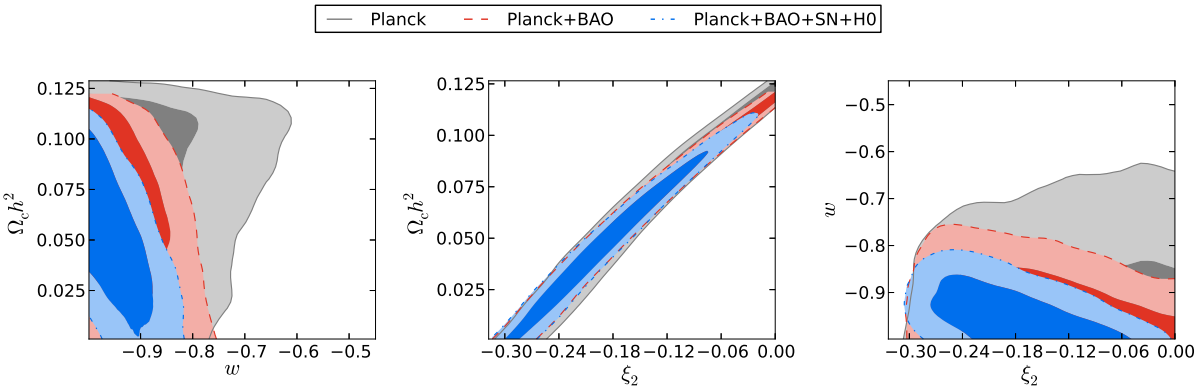

Figure 4.2: 2-D distribution for selected parameters - Model I.

Table 4.3: Cosmological parameters - Model II.

	Planck		Planck+BAO		Planck+BAO+SNIa+H0	
Parameter	Best fit	68% limits	Best fit	68% limits	Best fit	68% limits
$\Omega_b h^2$	0.02201	$0.02208^{+0.000283}_{-0.000277}$	0.02219	$0.02199^{+0.000264}_{-0.00026}$	0.02208	$0.02203^{+0.000255}_{-0.000255}$
$\Omega_c h^2$	0.1308	$0.1335^{+0.0076}_{-0.0118}$	0.132	$0.1352^{+0.00844}_{-0.0115}$	0.1432	$0.1344^{+0.00751}_{-0.0118}$
$100\theta_{MC}$	1.041	$1.041^{+0.000815}_{-0.000768}$	1.041	$1.04^{+0.000747}_{-0.000758}$	1.04	$1.04^{+0.00076}_{-0.000757}$
τ	0.08672	$0.08934^{+0.0128}_{-0.0138}$	0.08154	$0.08761^{+0.0121}_{-0.0137}$	0.08312	$0.08844^{+0.012}_{-0.0135}$
n_s	0.9615	$0.9599^{+0.00715}_{-0.00703}$	0.9598	$0.9581^{+0.00654}_{-0.00658}$	0.962	$0.9586^{+0.00632}_{-0.00637}$
$\ln(10^{10}A_s)$	3.085	$3.089^{+0.0245}_{-0.0267}$	3.078	$3.088^{+0.0234}_{-0.0261}$	3.079	$3.089^{+0.0232}_{-0.0263}$
w	-1.696	$-1.516^{+0.312}_{-0.305}$	-1.166	$-1.189^{+0.152}_{-0.0721}$	-1.181	$-1.192^{+0.0771}_{-0.0715}$
ξ_2	0.02837	$0.03923^{+0.0121}_{-0.0392}$	0.03522	$0.04818^{+0.0164}_{-0.0482}$	0.0784	$0.04562^{+0.0155}_{-0.0456}$
Ω_d	0.806	$0.762^{+0.0799}_{-0.0384}$	0.69	$0.6849^{+0.0292}_{-0.0296}$	0.6653	$0.6901^{+0.0253}_{-0.0201}$
Ω_m	0.194	$0.238^{+0.0384}_{-0.0799}$	0.31	$0.3151^{+0.0296}_{-0.0292}$	0.3347	$0.3099^{+0.0201}_{-0.0253}$
z_{re}	10.81	$11.^{+1.11}_{-1.1}$	10.35	$10.92^{+1.08}_{-1.08}$	10.5	$10.98^{+1.07}_{-1.07}$
H_0	88.93	$82.69^{+9.78}_{-11.9}$	70.68	$70.92^{+2.08}_{-3.19}$	70.42	$71.25^{+1.48}_{-1.48}$
Age/Gyr	13.53	$13.6^{+0.0942}_{-0.148}$	13.74	$13.76^{+0.0489}_{-0.0487}$	13.75	$13.75^{+0.0373}_{-0.0378}$
$\chi^2_{min}/2$	4901.08		4903.02		4968.20	

Now we present the fitting results for the coupling Model II in Table 4.3. In this model, the interaction between the dark sectors is still proportional to the energy density of dark energy but with equation of state of dark energy smaller than -1. From the Planck data analysis alone, we obtain the Hubble constant value significantly larger than that in the standard ΛCDM case, $H_0 = 82.69^{+9.78}_{-11.9}$ km $\cdot$ s^{-1} $\cdot$ Mpc^{-1}. This is different from what we observed in the fitting results of Model I, where the H_0 is much smaller and consistent with the ΛCDM case. The lower fitting range of the H_0 in Model II is consistent with the observations in the low redshift. We have explored the degeneracy between the Hubble value and the equation of state of dark energy and found that smaller equation of state of dark energy leads to higher value of the Hubble parameter. The coupling constant ξ_2 is found to be positive, which shows that there is an energy flow from dark energy to dark matter. This is required to alleviate the coincidence problem, because with this

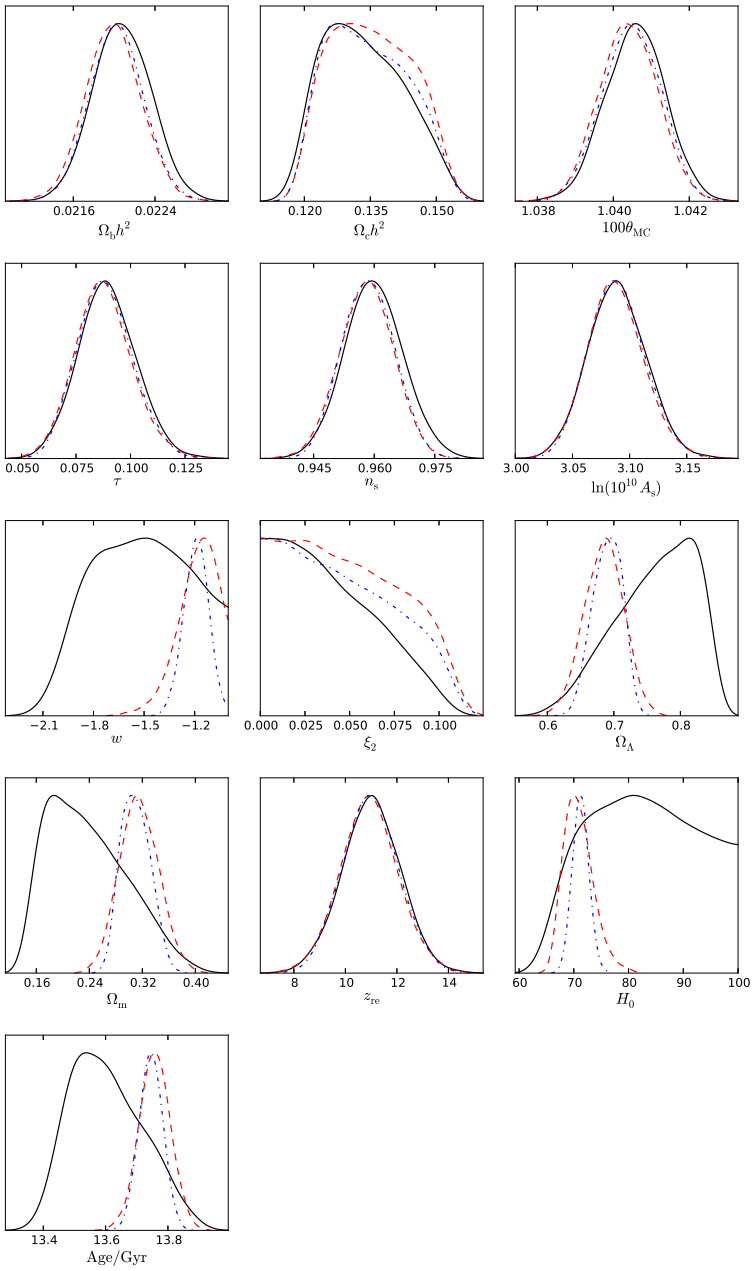

Figure 4.3: The likelihood for the parameters of the phenomenological Model II. The black solid lines correspond to the Planck constraints, the red dashed lines correspond to Planck + BAO and the blue dot-dashed lines correspond to Planck + BAO + SNIa + H_0.

interaction there is longer period for the energy densities of dark matter and dark energy to be comparable, which was illustrated in the Fig.3.1. Combined with other observational data, we show that a combined analysis provides significant evidence for this coupled dark energy with positive non-zero value of the coupling parameter, consistent Hubble constant and equation of state of dark energy. The 1-D posteriors for the parameters are shown in Fig.4.3 and the main parameter degeneracies are shown in Fig.4.4.

Now we turn our discussion to the coupled dark energy Model III, where the interaction

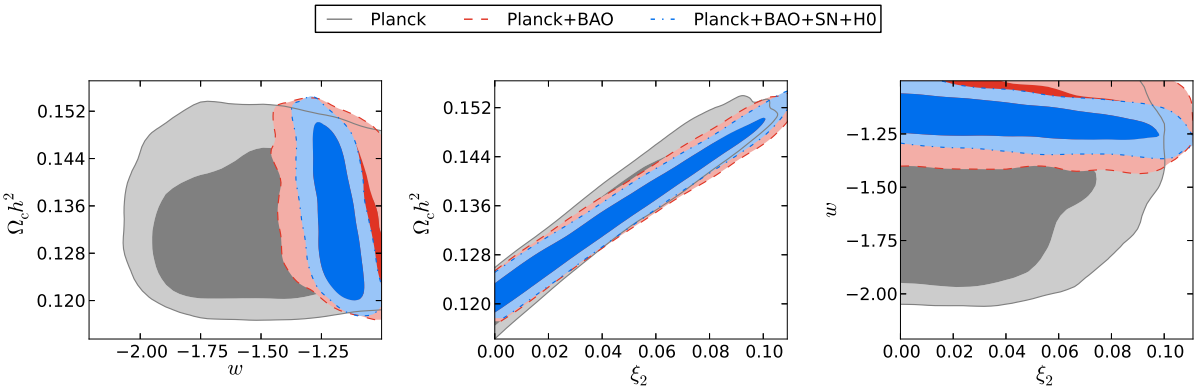

Figure 4.4: 2-D distribution for selected parameters - Model II.

Table 4.4: Cosmological parameters - Model III.

	Planck		Planck+BAO		Planck+BAO+SNIa+H0	
Parameter	Best fit	68% limits	Best fit	68% limits	Best fit	68% limits
$\Omega_b h^2$	0.02225	$0.02265^{+0.000412}_{-0.000506}$	0.02248	$0.02244^{+0.000347}_{-0.000399}$	0.02227	$0.02235^{+0.000314}_{-0.000372}$
$\Omega_c h^2$	0.1258	$0.1292^{+0.00516}_{-0.00857}$	0.1254	$0.1251^{+0.00256}_{-0.00257}$	0.1237	$0.123^{+0.00212}_{-0.00212}$
$100\theta_{MC}$	1.041	$1.041^{+0.000676}_{-0.000689}$	1.041	$1.041^{+0.000591}_{-0.000589}$	1.041	$1.041^{+0.000587}_{-0.000584}$
τ	0.08378	$0.08887^{+0.013}_{-0.0131}$	0.09507	$0.08956^{+0.0126}_{-0.0142}$	0.08342	$0.09011^{+0.0124}_{-0.0141}$
n_s	0.9584	$0.9563^{+0.00756}_{-0.00758}$	0.9603	$0.9587^{+0.00651}_{-0.00667}$	0.9631	$0.9599^{+0.00614}_{-0.0062}$
$\ln(10^{10}A_s)$	3.075	$3.081^{+0.0252}_{-0.0269}$	3.095	$3.084^{+0.0246}_{-0.0269}$	3.071	$3.086^{+0.0239}_{-0.0273}$
w	-1.638	$-1.779^{+0.457}_{-0.341}$	-1.48	$-1.455^{+0.275}_{-0.139}$	-1.296	$-1.254^{+0.0944}_{-0.0695}$
ξ_1	0.002118	< 0.004702	0.002266	$0.002272^{+0.00103}_{-0.00137}$	0.001781	$0.001494^{+0.00065}_{-0.00116}$
Ω_d	0.7668	$0.7393^{+0.111}_{-0.0365}$	0.7431	$0.7361^{+0.0219}_{-0.0281}$	0.719	$0.717^{+0.0127}_{-0.0115}$
Ω_m	0.2332	$0.2607^{+0.0365}_{-0.111}$	0.2569	$0.2639^{+0.0281}_{-0.0219}$	0.281	$0.283^{+0.0115}_{-0.0127}$
z_{re}	10.57	$10.91^{+1.11}_{-1.11}$	11.49	$10.99^{+1.1}_{-1.1}$	10.51	$11.04^{+1.1}_{-1.09}$
H_0	79.85	$79.35^{+12.4}_{-12.1}$	76.02	$75.23^{+2.73}_{-4.91}$	72.24	$71.88^{+1.44}_{-1.43}$
Age/Gyr	13.81	$13.93^{+0.189}_{-0.362}$	13.82	$13.84^{+0.0709}_{-0.0715}$	13.85	$13.82^{+0.0575}_{-0.0702}$
$\chi^2_{min}/2$	4902.23		4903.24		4969.78	

is proportional to the energy density of dark matter. In this model, to ensure stability of the curvature perturbation, if the equation of state of dark energy is constant, it has to be smaller than -1 [13]. Looking at the new constraints on this coupled dark energy model from the recent measurements of CMB from the Planck satellite mission alone, in Table 4.4, we find that the Hubble constant value is consistent with low redshift observations, but it is much higher than that of the ΛCDM result. The coupling constant is more tightly constrained in this coupled dark energy model than those in Models I and II, which is in agreement with the findings in the WMAP constraints [25, 44]. The value of the coupling parameter ξ_1 is small positive, which meets the requirement to alleviate the coincidence problem. The evolution of the ratio between energy densities of dark matter and dark energy with this small positive coupling was shown in the Fig.3.1, which has a longer period for the dark matter and dark energy energy densities to be comparable

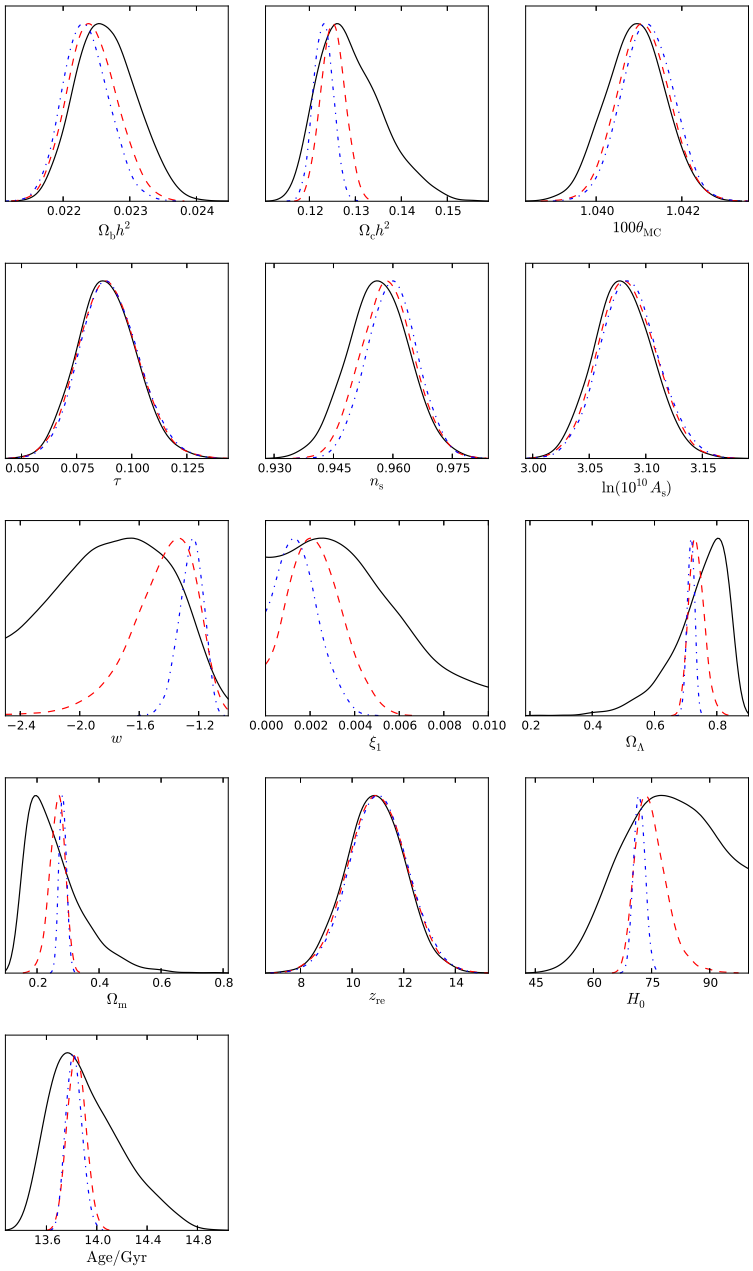

Figure 4.5: The likelihood for the parameters of the phenomenological Model III. The black solid lines correspond to the Planck constraints, the red dashed lines correspond to Planck + BAO and the blue dot-dashed lines correspond to Planck + BAO + SNIa + H_0.

when ξ is positive and has the attractor solution with the ratio between dark energy and dark matter energy densities $\varrho \sim constant$ in the past. We also consider the combined constraints from the Planck data plus other measurements. The results are listed in Table 4.4, which shows stronger evidence for this coupled dark energy model with small positive coupling. We plot the 1-D posteriors for the parameters in Fig.4.5 and show the main parameter degeneracies in Fig.4.6.

Finally, we present the fitting results for the coupled dark energy Model IV, where

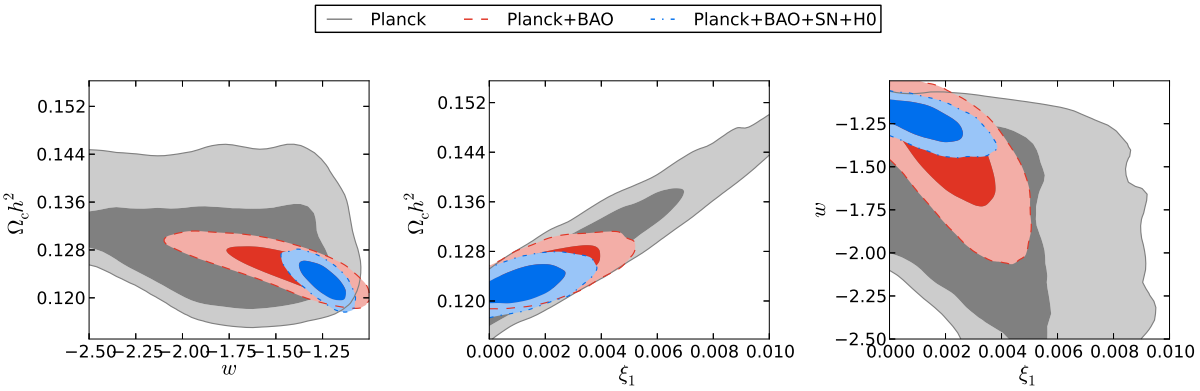

Figure 4.6: 2-D distribution for selected parameters - Model III.

Table 4.5: Cosmological parameters - Model IV.

	Planck		Planck+BAO		Planck+BAO+SNIa+H0	
Parameter	Best fit	68% limits	Best fit	68% limits	Best fit	68% limits
$\Omega_b h^2$	0.02047	$0.02037^{+0.000275}_{-0.00027}$	0.02041	$0.02042^{+0.000257}_{-0.000263}$	0.02053	$0.02056^{+0.000253}_{-0.000265}$
$\Omega_c h^2$	0.1251	$0.1273^{+0.00309}_{-0.00321}$	0.125	$0.1261^{+0.00254}_{-0.0025}$	0.1245	$0.1242^{+0.00204}_{-0.00208}$
$100\theta_{MC}$	1.04	$1.04^{+0.000618}_{-0.000607}$	1.04	$1.04^{+0.000574}_{-0.000572}$	1.04	$1.04^{+0.000537}_{-0.000541}$
τ	0.0883	$0.07771^{+0.011}_{-0.0129}$	0.06756	$0.07785^{+0.0112}_{-0.0124}$	0.07537	$0.07899^{+0.0112}_{-0.0127}$
n_s	0.9305	$0.9309^{+0.00746}_{-0.00743}$	0.9295	$0.9332^{+0.00643}_{-0.00655}$	0.9338	$0.9368^{+0.00592}_{-0.00594}$
$\ln(10^{10}A_s)$	3.086	$3.068^{+0.0221}_{-0.0253}$	3.045	$3.066^{+0.0228}_{-0.0248}$	3.06	$3.064^{+0.0227}_{-0.0233}$
w	-1.613	$-1.763^{+0.385}_{-0.432}$	-1.267	$-1.472^{+0.229}_{-0.147}$	-1.305	$-1.286^{+0.082}_{-0.074}$
ξ	0.00009881	< 0.0004618	0.00001943	< 0.0004260	0.0000671	< 0.0003314
Ω_d	0.7735	$0.772^{+0.0793}_{-0.0319}$	0.7079	$0.7365^{+0.0238}_{-0.0267}$	0.7199	$0.7149^{+0.0126}_{-0.0115}$
Ω_m	0.2265	$0.228^{+0.0319}_{-0.0793}$	0.2921	$0.2635^{+0.0267}_{-0.0238}$	0.2801	$0.2851^{+0.0115}_{-0.0126}$
z_{re}	11.61	$10.65^{+1.14}_{-1.12}$	9.624	$10.63^{+1.14}_{-1.1}$	10.35	$10.66^{+1.11}_{-1.11}$
H_0	80.35	$82.5^{+12.4}_{-9.95}$	70.71	$75._{-4.59}^{+3.07}$	72.11	$71.45^{+1.48}_{-1.46}$
Age/Gyr	13.8	$13.85^{+0.0891}_{-0.136}$	13.92	$13.9^{+0.046}_{-0.0532}$	13.89	$13.92^{+0.0385}_{-0.0391}$
$\chi^2_{min}/2$	4991.13		4991.28		5058.81	

we consider the interaction between dark energy and dark matter is proportional to the energy density of the total dark sectors. In order to ensure the stability of the curvature perturbation, the constant equation of state of dark energy has to be in the phantom range. This was disclosed in [13]. As observed in the WMAP fitting results, this type of interaction has very similar constraints to the Model III [25, 44]. Confronting the model to the Planck data alone and the combined observational data, we list the constraints in Table 4.5. We show the 1-D posteriors for the parameters in Fig.4.7 and plot the main parameter degeneracies in Fig.4.8. From the Planck data alone, we again see that the Hubble constant is much higher than that of the ΛCDM model. This is consistent with the observations from Model II and Model III. The coupling constant is more tightly constrained in Model IV to be very small but positive, what is needed to alleviate the coincidence problem with longer period for the dark energy and dark matter energy den-

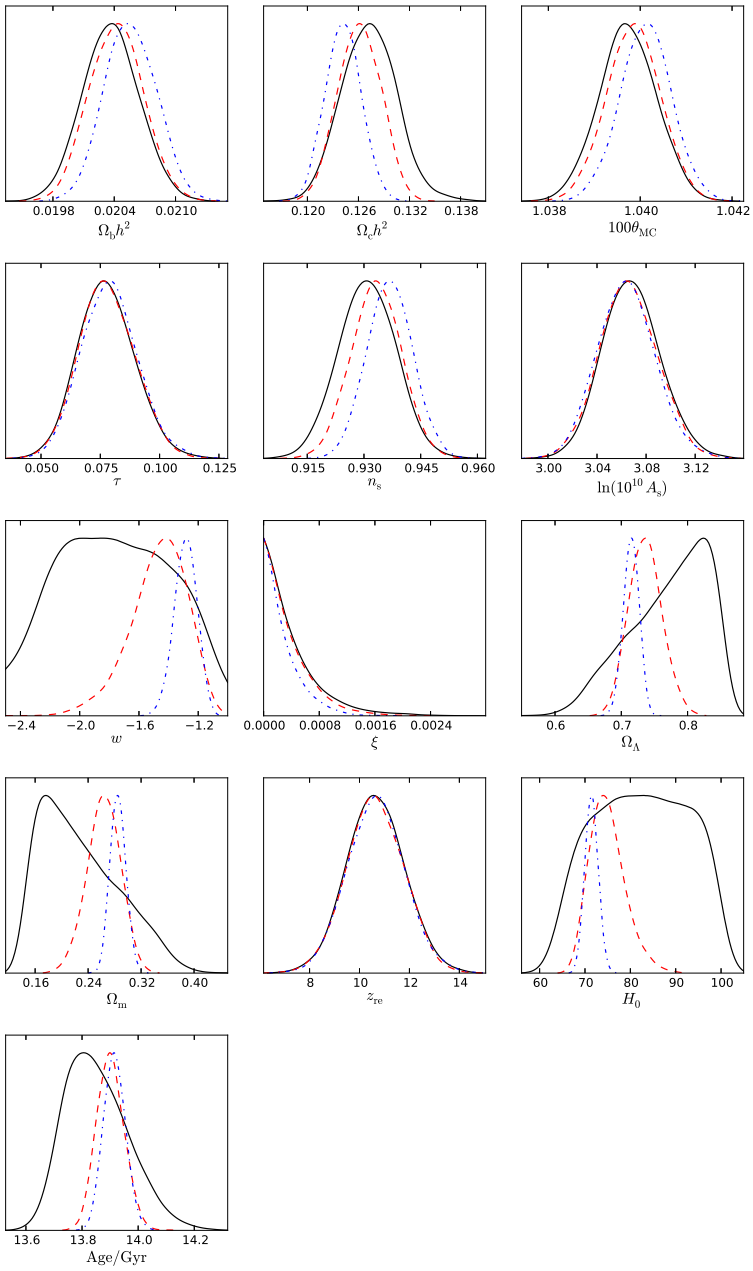

Figure 4.7: The likelihood for the parameters of the phenomenological Model IV. The black solid lines correspond to the Planck constraints, the red dashed lines correspond to Planck + BAO and the blue dot-dashed lines correspond to Planck + BAO + SNIa + H_0.

sities to be comparable in the expansion of the Universe as shown in Fig.3.1. The Model IV has an attractor solution with $\varrho \sim constant$ in the future. In the joint constraints, by including other observational data, we find that the coupled dark energy model IV is fully compatible with astronomical observations. It is a viable model.

We constrained, up to now, the four phenomenological models based on Planck measurements and additional data from BAO, SNIa and $H0$. These additional data sets are based on measurements of distances. As we pointed out in the previous section, another

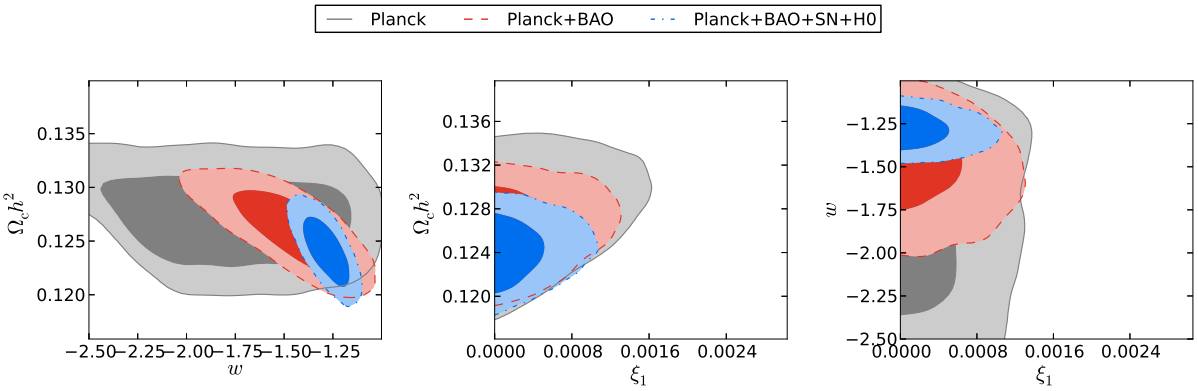

Figure 4.8: 2-D distribution for selected parameters - Model IV.

Table 4.6: Priors for the cosmological parameters considered in the analysis with lookback time of the phenomenological models.

Parameters	Prior			
$\Omega_b h^2$	$[0.005, 0.99]$			
$\Omega_c h^2$	$[0.001, 0.99]$			
H_0	$[20, 100]$			
df	$[0, 5]$			
	Model I	Model II	Model III	Model IV
ω	$[-1, -0.1]$	$[-2.5, -1]$	$[-2.5, -1]$	$[-2.5, -1]$
ξ	$[-0.4, 0.4]$	$[-0.4, 0.4]$	$[-0.4, 0.4]$	$[-0.4, 0.4]$

kind of data can be obtained based on measurements of ages instead of distances. One such technique is the lookback time. Thus, to take this kind of data into account we implemented the likelihood for lookback time in the CosmoMC code (see Appendix C). We choose our priors for the different cosmological parameters as listed in Table 4.6. The equation of state of dark energy is set constant, but it can have any value inside the prior interval. We also take the relativistic number of degrees of freedom $N_{eff} = 3.046$ and the total neutrino mass $\sum m_\nu = 0.06eV$. The MCMC will run until the chains reach the statistical convergence for Gelman and Rubin criterion $R - 1 = 0.01$. We list our fitting results in Tables 4.7-4.10. These results will be part of publication in [100].

The lookback time constraints for Model I are reported in Table 4.7. The 1-D posterior distributions are shown in Fig. 4.9 and the main parameter degeneracies appear in Fig. 4.10. The first columns of Table 4.7 present the best fit and 68% C.L. for the prior given in Table 4.6. The columns in the middle redo the calculations with a restrict prior for ξ_2 as that in Table 4.1. The last columns show the results including the Planck measurements, in this case the others parameters are set according to Table 4.1. For

Table 4.7: Cosmological parameters - LBT analysis for Model I.

	LBT+H0		LBT+H0 ($\xi_2 = [-0.4, 0]$)		LBT+H0+Planck	
Parameter	Best fit	68% limits	Best fit	68% limits	Best fit	68% limits
$\Omega_b h^2$	0.1693	$0.09288^{+0.0277}_{-0.0879}$	0.009321	$0.03423^{+0.00737}_{-0.0292}$	0.02185	$0.02203^{+0.000252}_{-0.000251}$
$\Omega_c h^2$	0.05315	$0.08679^{+0.0244}_{-0.0858}$	0.006469	$0.03003^{+0.00751}_{-0.029}$	0.04167	$0.04524^{+0.0168}_{-0.04}$
H_0	73.22	$73.15^{+2.42}_{-2.42}$	72.85	$72.94^{+2.44}_{-2.5}$	71.69	$71.06^{+1.82}_{-1.82}$
w	-0.6778	$-0.7319^{+0.143}_{-0.165}$	-0.4277	$-0.7098^{+0.184}_{-0.141}$	-0.9621	$-0.9346^{+0.016}_{-0.0644}$
ξ_2	0.2708	$0.1992^{+0.197}_{-0.0635}$	-0.008092	$-0.05135^{+0.0513}_{-0.00763}$	-0.2048	$-0.1878^{+0.0479}_{-0.0812}$
df	2.461	$2.205^{+0.31}_{-0.259}$	2.387	$1.831^{+0.27}_{-0.268}$	1.376	$1.381^{+0.0993}_{-0.0991}$
Ω_d	0.5838	$0.6623^{+0.0794}_{-0.154}$	0.969	$0.8772^{+0.0623}_{-0.0465}$	0.8751	$0.8637^{+0.0784}_{-0.0389}$
Ω_m	0.4162	$0.3377^{+0.154}_{-0.08}$	0.03097	$0.1228^{+0.047}_{-0.0627}$	0.1249	$0.1363^{+0.0389}_{-0.0784}$
$\chi^2_{min}/2$	13.48		13.60		4921.61	

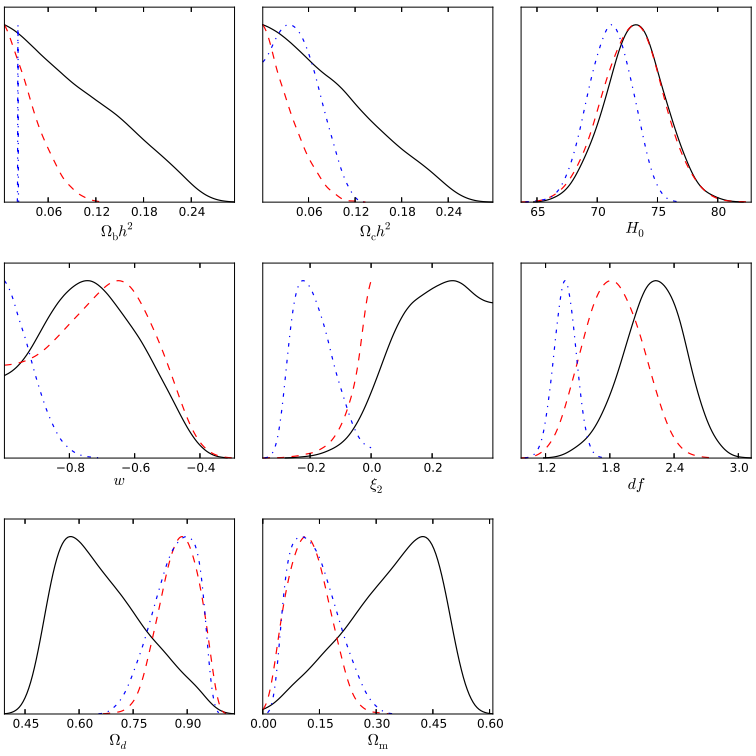

Figure 4.9: The likelihood for the parameters of the phenomenological Model I using lookback time measurements. The black solid lines correspond to the LBT + H_0 constraints, the red dashed lines correspond to LBT + H_0 with a restricted prior to $\xi_2 = [-0.4, 0]$ and the blue dot-dashed lines correspond to LBT + H_0 + Planck.

lookback time calculations of Model I, we use the age of the Universe obtained with Planck data $t_0^{obs} = 13.821 Gyr$ with one standard deviation $\sigma_{t_0^{obs}} = 0.101 Gyr$. From the fitting results, we observe that Planck measurements provide narrower constraints than lookback time, especially for $\Omega_b h^2$. This would be expected since baryon perturbations are coupled to photons and thus the CMB anisotropies depend on the amount of baryons. On the other hand, lookback time only takes into account the background evolution. We also see that lookback time prefers a dark energy equation of state in the quintessence regime

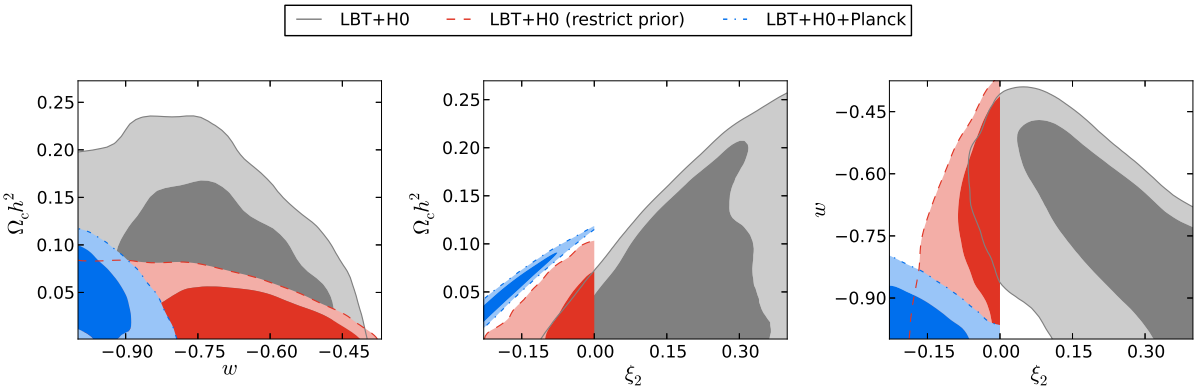

Figure 4.10: 2-D distribution for selected parameters - LBT analysis for Model I.

Table 4.8: Cosmological parameters - LBT analysis for Model II

	LBT+H0		LBT+H0 ($\xi_2 = [0, 0.4]$)		LBT+H0+Planck	
Parameter	Best fit	68% limits	Best fit	68% limits	Best fit	68% limits
$\Omega_b h^2$	0.2548	$0.098^{+0.0294}_{-0.093}$	0.1355	$0.1095^{+0.0346}_{-0.104}$	0.02228	$0.0222^{+0.000264}_{-0.000263}$
$\Omega_c h^2$	0.005993	$0.0958^{+0.0305}_{-0.0948}$	0.1255	$0.1054^{+0.036}_{-0.104}$	0.1372	$0.1335^{+0.00814}_{-0.0125}$
H_0	74.34	$74.06^{+2.5}_{-2.52}$	74.12	$74.04^{+2.52}_{-2.53}$	77.88	$74.94^{+2.23}_{-2.24}$
w	-1.009	$-1.482^{+0.481}_{-0.148}$	-1.015	$-1.413^{+0.412}_{-0.0657}$	-1.359	$-1.274^{+0.0972}_{-0.0886}$
ξ_2	0.3967	$0.144^{+0.255}_{-0.0715}$	0.398	$0.2475^{+0.151}_{-0.0496}$	0.05431	$0.04451^{+0.0146}_{-0.0445}$
df	1.961	$1.312^{+0.291}_{-0.421}$	1.937	$1.405^{+0.325}_{-0.346}$	1.338	$1.27^{+0.1}_{-0.101}$
Ω_d	0.5269	$0.6441^{+0.0552}_{-0.115}$	0.5237	$0.6058^{+0.0444}_{-0.0692}$	0.7359	$0.7209^{+0.0271}_{-0.0221}$
Ω_m	0.4731	$0.3559^{+0.115}_{-0.0553}$	0.4763	$0.3942^{+0.0692}_{-0.0444}$	0.2641	$0.2791^{+0.0221}_{-0.0271}$
$\chi^2_{min}/2$	14.12		14.03		4919.71	

at 68% C. L., while Planck is consistent with a cosmological constant. The lookback time measurements favor a positive interaction parameter, which is in tension with more than 2σ as compared with the result from Planck. Such difference in the interaction has an effect in the time when the structures were formed, as described by the delay factor df, and also in the amount of dark matter and dark energy at present.

We pass now to consider the behaviour of Model II with respect to LBT data. Table 4.8 presents the best fit values and marginalizations for the parameters. Figure 4.11 plots the 1-D posterior distributions and Fig. 4.12 plots the main parameters degeneracies. The age of the Universe is set to $t_0^{obs} = 13.604Gyr$ with standard deviation $\sigma_{t_0^{obs}} = 0.115Gyr$. From the fitting results, we observe that the dark energy equation of state tends to larger values consistent with a cosmological constant. However, we note that our prior prevents the EoS to be larger than $\omega = -1$. Thus, this result is in agreement with that obtained for Model I. On the other hand, the Planck likelihood constrains the EoS of dark energy in the phantom region with more than 95% C.L.. At first sight, we could combine Models

I and II into one single model with EoS from quintessence to phantom regions and an interaction from negative to positive ones. This is true for the background, however Eq. (3.19) diverges for $\omega = -1$ and also appears several divergences in the power spectra for a positive interaction for Model I and negative interaction for Model II, this is the reason why we restricted the priors for the Planck data. Finally, as for Model I, we observe that lookback time data prefer larger values for the interaction in opposite to Planck.

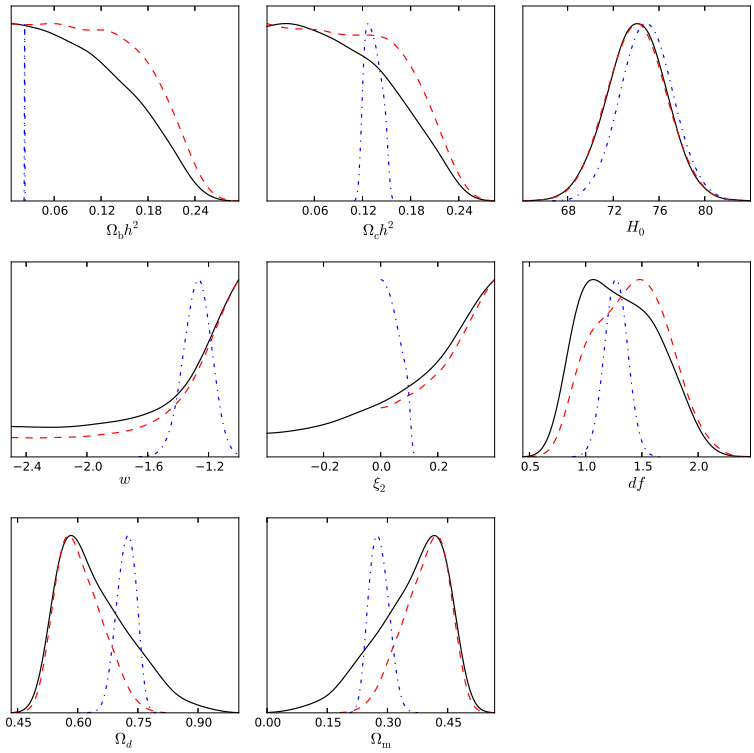

Figure 4.11: The likelihood for the parameters of the phenomenological Model II using lookback time measurements. The black solid lines correspond to the LBT + H_0 constraints, the red dashed lines correspond to LBT + H_0 with a restricted prior to $\xi_2 = [0, 0.4]$ and the blue dot-dashed lines correspond to LBT + H_0 + Planck.

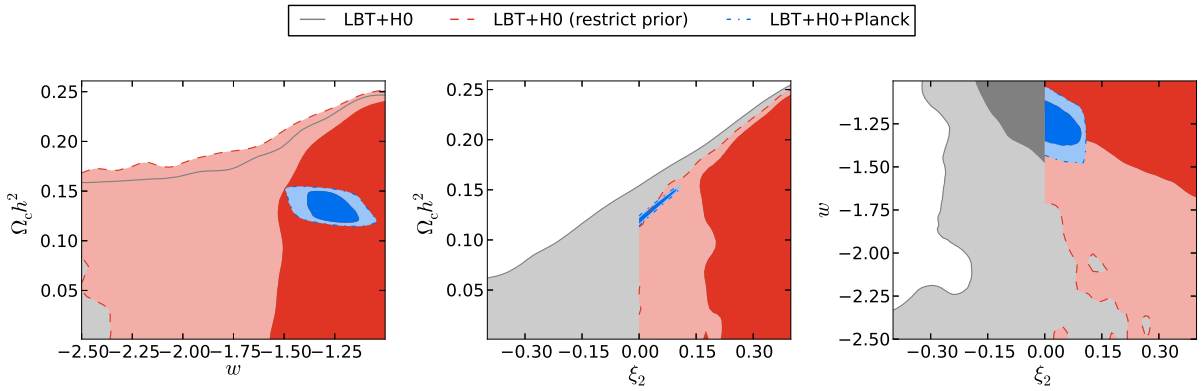

Figure 4.12: 2-D distribution for selected parameters - LBT analysis for Model II.

Table 4.9: Cosmological parameters - LBT analysis for Model III

	LBT+H0		LBT+H0 ($\xi_1 = [0, 0.4]$)		LBT+H0+Planck	
Parameter	Best fit	68% limits	Best fit	68% limits	Best fit	68% limits
$\Omega_b h^2$	0.006805	$0.0378^{+0.00592}_{-0.0328}$	0.009584	$0.03848^{+0.0059}_{-0.0335}$	0.02248	$0.02244^{+0.000332}_{-0.000399}$
$\Omega_c h^2$	0.3828	$0.252^{+0.106}_{-0.0793}$	0.386	$0.2503^{+0.105}_{-0.0759}$	0.1199	$0.1251^{+0.00331}_{-0.00462}$
H_0	73.1	$73.69^{+2.65}_{-2.6}$	73.25	$73.65^{+2.61}_{-2.59}$	74.27	$74.26^{+2.46}_{-2.46}$
w	-1.64	$-1.731^{+0.73}_{-0.769}$	-1.558	$-1.722^{+0.721}_{-0.778}$	-1.232	$-1.417^{+0.212}_{-0.112}$
ξ_1	0.3735	$0.3033^{+0.0957}_{-0.0199}$	0.3955	$0.3054^{+0.0936}_{-0.0215}$	0.0006722	$0.002171^{+0.000729}_{-0.00197}$
df	2.506	$2.048^{+0.379}_{-0.298}$	2.554	$2.048^{+0.369}_{-0.287}$	1.669	$1.405^{+0.181}_{-0.146}$
Ω_d	0.2698	$0.4615^{+0.156}_{-0.138}$	0.2616	$0.4628^{+0.152}_{-0.134}$	0.7406	$0.7305^{+0.0218}_{-0.0177}$
Ω_m	0.7302	$0.5385^{+0.138}_{-0.156}$	0.7384	$0.5372^{+0.134}_{-0.152}$	0.2594	$0.2695^{+0.0177}_{-0.0218}$
$\chi^2_{min}/2$	11.59		11.59		4918.55	

Table 4.10: Cosmological parameters - LBT analysis for Model IV

	LBT+H0		LBT+H0 ($\xi = [0, 0.4]$)		LBT+H0+Planck	
Parameter	Best fit	68% limits	Best fit	68% limits	Best fit	68% limits
$\Omega_b h^2$	0.007615	$0.04137^{+0.00758}_{-0.0364}$	0.005097	$0.0409^{+0.00713}_{-0.0359}$	0.0224	$0.0224^{+0.000335}_{-0.000376}$
$\Omega_c h^2$	0.4325	$0.3159^{+0.103}_{-0.0854}$	0.3857	$0.3177^{+0.106}_{-0.0835}$	0.125	$0.1251^{+0.00302}_{-0.00316}$
H_0	73.27	$73.22^{+2.59}_{-2.59}$	72.89	$73.17^{+2.52}_{-2.54}$	73.83	$74.03^{+2.29}_{-2.6}$
w	-2.384	$-1.702^{+0.701}_{-0.798}$	-1.768	$-1.702^{+0.701}_{-0.798}$	-1.341	$-1.384^{+0.167}_{-0.113}$
ξ	0.3188	$0.3011^{+0.0979}_{-0.0247}$	0.2772	$0.3014^{+0.0976}_{-0.0238}$	0.00141	$0.001953^{+0.000914}_{-0.00116}$
df	2.498	$2.188^{+0.411}_{-0.356}$	2.406	$2.192^{+0.422}_{-0.362}$	1.378	$1.323^{+0.115}_{-0.116}$
Ω_d	0.1791	$0.3287^{+0.155}_{-0.153}$	0.2632	$0.3251^{+0.157}_{-0.155}$	0.7284	$0.7289^{+0.0191}_{-0.0167}$
$\chi^2_{min}/2$	13.39		13.39		4920.34	

Models III and IV present very similar behavior. The best fit values and 68% C.L. limits are presented in Tables 4.9 and 4.10 for Models III and IV, respectively. Figures 4.13 and 4.14 show the 1-D posterior distributions for the parameters, while Fig. 4.15 and Fig. 4.16 plot the main parameter degeneracies. For Model III the age of the Universe is given by $t_0^{obs} = 13.928 Gyr$ with standard deviation $\sigma_{t_0^{obs}} = 0.280$ and for Model IV the age is $t_0^{obs} = 13.854 Gyr$ and $\sigma_{t_0^{obs}} = 0.111$, which were obtained from the Planck measurements alone. We observe that Planck measurements pin the parameters down much better than lookback time data for both models, especially the dark energy equation of state which is completely unconstrained using LBT. There is still a tension in the determination of the interaction parameter over several sigmas, e.g. the 95% C.L. lower limit for the interaction using only LBT is $\xi_1 = 0.14$ for Model III, while the maximum value at 95% C.L. with Planck is $\xi_1 = 0.0047$. Note the tiny confidence regions for Planck constraints as compared with the LBT constraints, and the separation between them in the 2-D distributions.

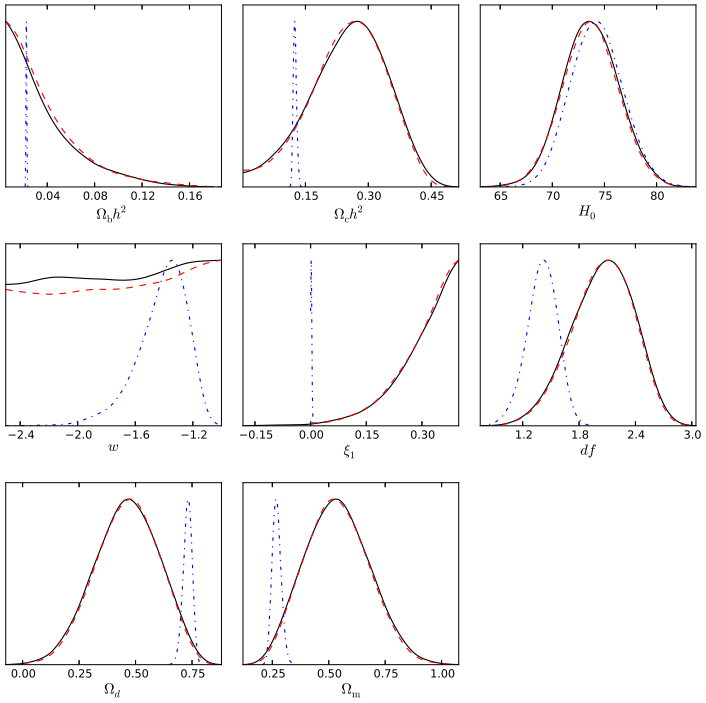

Figure 4.13: The likelihood for the parameters of the phenomenological Model III using look-back time measurements. The black solid lines correspond to the LBT + H_0 constraints, the red dashed lines correspond to LBT + H_0 with a restricted prior to $\xi_1 = [0, 0.4]$ and the blue dot-dashed lines correspond to LBT + H_0 + Planck.

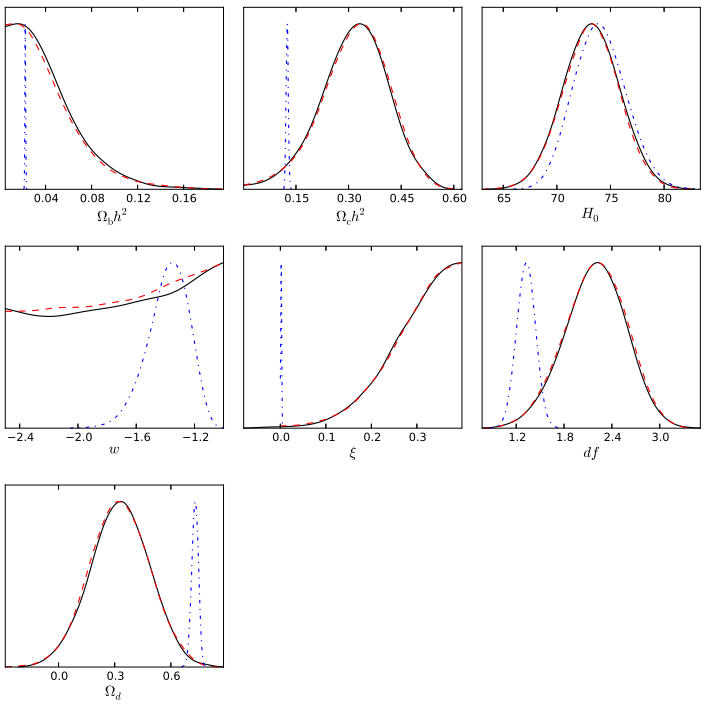

Figure 4.14: The likelihood for the parameters of the phenomenological Model IV using look-back time measurements. The black solid lines correspond to the LBT + H_0 constraints, the red dashed lines correspond to LBT + H_0 with a restricted prior to $\xi = [0, 0.4]$ and the blue dot-dashed lines correspond to LBT + H_0 + Planck .

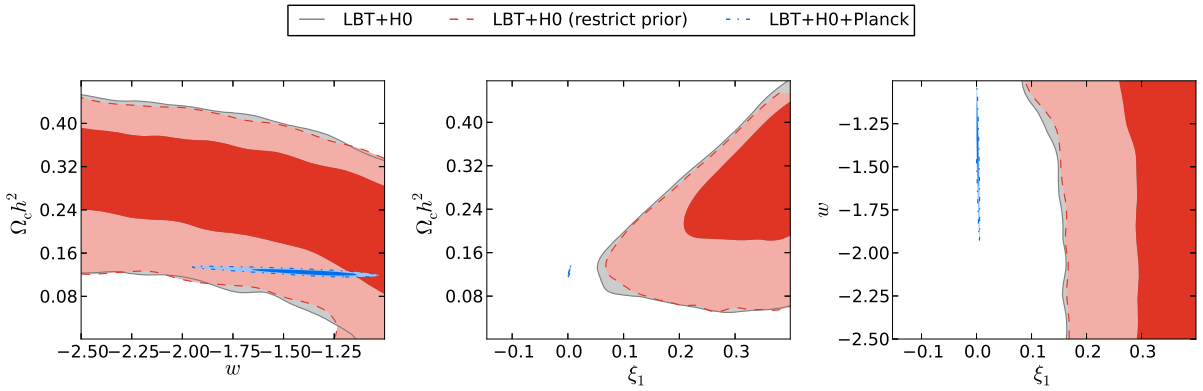

Figure 4.15: 2-D distribution for selected parameters - LBT analysis for Model III.

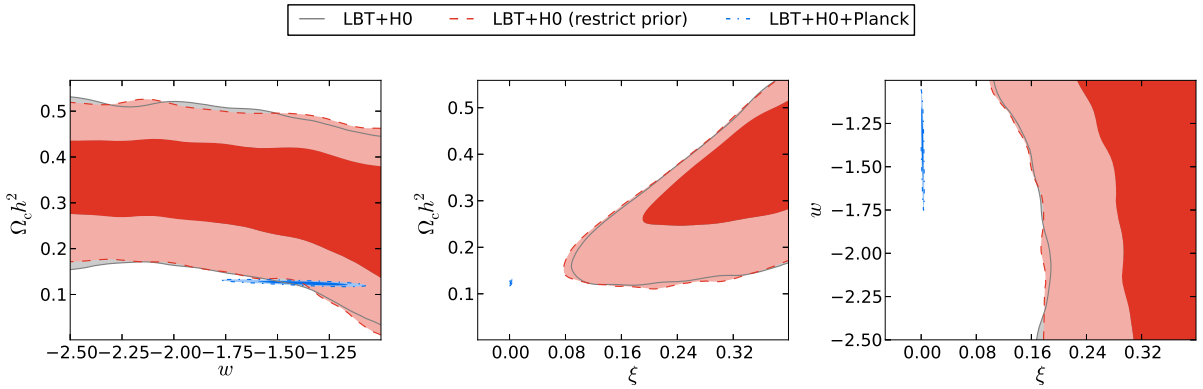

Figure 4.16: 2-D distribution for selected parameters - LBT analysis for Model IV.

4.3.2 Lagrangian Model

Let us consider now our Lagrangian model described in the previous chapter. We want to put constraints on the cosmological parameters and verify if the Yukawa interaction is favored by the observational data. The priors that we use are listed in Table 4.11. At first we allow the parameter of the scalar potential λ to vary freely. We fixed the helium

Table 4.11: Priors for the cosmological parameters considered in the analysis of the Yukawa interacting model.

Parameters	Prior
$\Omega_b h^2$	$[0.005, 0.1]$
$\Omega_c h^2$	$[0.001, 0.99]$
100θ	$[0.5, 10]$
τ	$[0.01, 0.8]$
n_s	$[0.9, 1.1]$
$log(10^{10} A_s)$	$[2.7, 4]$
λ	$[0.1, 1.5]$
$r = \frac{\beta}{M} M_{pl}$	$[-0.1, 0.1]$

Table 4.12: Cosmological parameters - Lagrangian Model

	Planck		Planck+BAO		Planck+BAO+SNIa+H0	
Parameter	Best fit	68% limits	Best fit	68% limits	Best fit	68% limits
$\Omega_b h^2$	0.02203	$0.02196^{+0.000278}_{-0.000279}$	0.02225	$0.02204^{+0.000252}_{-0.000264}$	0.02222	$0.02211^{+0.000263}_{-0.000261}$
$\Omega_c h^2$	0.1185	$0.119^{+0.00277}_{-0.00283}$	0.1181	$0.1176^{+0.00211}_{-0.00181}$	0.1171	$0.1165^{+0.00185}_{-0.00166}$
$100\theta_{MC}$	1.041	$1.041^{+0.000625}_{-0.000623}$	1.042	$1.041^{+0.000564}_{-0.000567}$	1.042	$1.041^{+0.000572}_{-0.000565}$
τ	0.09723	$0.0883^{+0.0118}_{-0.0136}$	0.09281	$0.09063^{+0.0123}_{-0.0125}$	0.08889	$0.09231^{+0.0126}_{-0.0127}$
n_s	0.9625	$0.9579^{+0.00702}_{-0.00701}$	0.9631	$0.9608^{+0.00592}_{-0.00577}$	0.9647	$0.9629^{+0.00573}_{-0.00558}$
$\ln(10^{10}A_s)$	3.101	$3.084^{+0.0229}_{-0.0256}$	3.091	$3.086^{+0.0239}_{-0.0243}$	3.086	$3.087^{+0.0249}_{-0.0247}$
λ	0.6777	$0.7451^{+0.755}_{-0.645}$	0.227	$0.6046^{+0.151}_{-0.505}$	0.3007	$0.3904^{+0.0736}_{-0.29}$
r	-0.02182	$-0.001969^{+0.0224}_{-0.0224}$	-0.003793	$-0.0008486^{+0.0238}_{-0.0281}$	0.01311	$-0.002299^{+0.033}_{-0.0338}$
Ω_d	0.6858	$0.6744^{+0.0236}_{-0.0213}$	0.6942	$0.688^{+0.0141}_{-0.0116}$	0.699	$0.701^{+0.0103}_{-0.0101}$
Ω_m	0.3142	$0.3256^{+0.0213}_{-0.0236}$	0.3058	$0.312^{+0.0116}_{-0.0141}$	0.301	$0.299^{+0.0101}_{-0.0103}$
z_{re}	11.67	$10.93^{+1.04}_{-1.05}$	11.22	$11.07^{+1.04}_{-1.07}$	10.87	$11.17^{+1.07}_{-1.07}$
H_0	67.04	$66.05^{+1.93}_{-1.77}$	67.91	$67.09^{+1.3}_{-0.968}$	68.19	$68.28^{+0.849}_{-0.839}$
Age/Gyr	13.81	$13.84^{+0.0651}_{-0.0567}$	13.79	$13.81^{+0.0414}_{-0.0417}$	13.78	$13.77^{+0.0438}_{-0.0407}$
$\chi^2_{min}/2$		4902.91		4903.89		4972.01

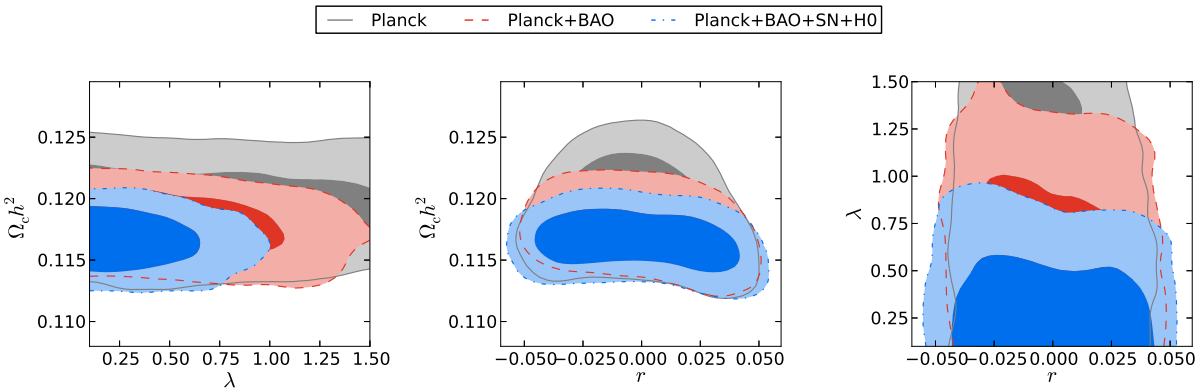

Figure 4.17: 2-D distribution for selected parameters - Lagrangian Model.

abundance as $Y_p = 0.24$. The number of relativistic degrees of freedom is adjusted to $N_{eff} = 3.046$ and the total neutrino mass is set to $\sum m_\nu = 0.06eV$. At last the spectrum lensing normalization is $A_L = 1$. To finish the MCMC we set the Gelman and Rubin criterion to $R - 1 = 0.03$. The results obtained for this model will be published soon [99].

To constrain the Yukawa-type interacting dark energy, we use the measurements of the CMB anisotropies made by Planck together with BAO, SNIa and H_0 measurements. Using the priors listed in Table 4.11 we run the MCMC. The results are shown in Table 4.12, the 1-D posteriors for the parameters are given in Fig. 4.18 and some parameter degeneracies are in Fig. 4.17. We observe that the Planck data alone is not able to constrain the scalar potential λ and it constrains the interaction parameter r symmetrically around the zero value. This is what we expected from the discussion about the power spectra of the Lagrangian model in the previous chapter, as illustrated in Figs. 3.6 and 3.7. Adding low

redshift measurements, λ tends to its lower limit, while the interaction parameter slightly breaks the symmetry around the zero value. We see that allowing the scalar potential vary freely does not favor an interacting model. In fact, it shows a tendency to $\lambda \to 0$ and $r = 0$, which is basically the ΛCDM model.

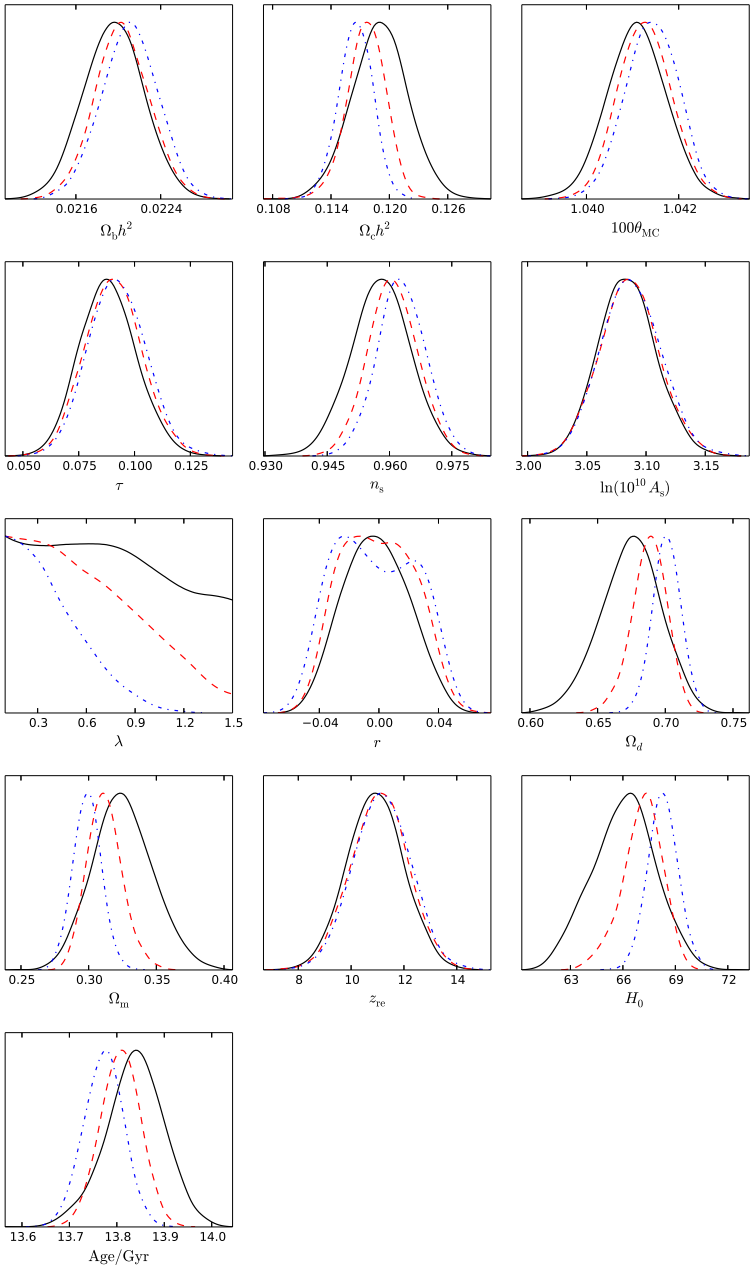

Figure 4.18: The likelihood for the parameters of the Lagrangian Model. The black solid lines correspond to the Planck constraints, the red dashed lines correspond to Planck + BAO and the blue dot-dashed lines correspond to Planck + BAO + SNIa + H_0.

We then consider the case when we fix the scalar potential parameter λ. We have learned that as we increase the value for λ, the interaction becomes more favored. For instance, $\lambda = \sqrt{3/2}$ produces the results in Table 4.13 and the 1-D posterior distributions

Table 4.13: Cosmological parameters - Lagrangian Model with Fixed λ

	Planck		Planck+BAO		Planck+BAO+SNIa+H0	
Parameter	Best fit	68% limits	Best fit	68% limits	Best fit	68% limits
$\Omega_b h^2$	0.02177	$0.02195^{+0.000276}_{-0.000274}$	0.02203	$0.02208^{+0.000265}_{-0.000263}$	0.02216	$0.02218^{+0.000272}_{-0.000267}$
$\Omega_c h^2$	0.1203	$0.1192^{+0.00288}_{-0.00282}$	0.1186	$0.1166^{+0.0026}_{-0.00202}$	0.117	$0.1155^{+0.00238}_{-0.00182}$
$100\theta_{MC}$	1.041	$1.041^{+0.000621}_{-0.000618}$	1.041	$1.041^{+0.000581}_{-0.000569}$	1.042	$1.042^{+0.00059}_{-0.000598}$
τ	0.08242	$0.08848^{+0.0117}_{-0.0144}$	0.0964	$0.09183^{+0.0124}_{-0.0142}$	0.1005	$0.09495^{+0.0127}_{-0.0145}$
n_s	0.9557	$0.9575^{+0.00727}_{-0.00734}$	0.961	$0.9629^{+0.00619}_{-0.00607}$	0.9666	$0.9662^{+0.00609}_{-0.00599}$
$\ln(10^{10}A_s)$	3.076	$3.085^{+0.0226}_{-0.0271}$	3.099	$3.086^{+0.0243}_{-0.0271}$	3.103	$3.09^{+0.0252}_{-0.0281}$
r	-0.02151	$-0.001283^{+0.0208}_{-0.0243}$	-0.01445	$-0.005535^{+0.021}_{-0.0343}$	-0.03228	$-0.02173^{+0.0105}_{-0.0346}$
Ω_d	0.654	$0.6567^{+0.0161}_{-0.0163}$	0.6632	$0.6731^{+0.0108}_{-0.0109}$	0.6804	$0.6851^{+0.0101}_{-0.0101}$
Ω_m	0.346	$0.3433^{+0.0163}_{-0.0161}$	0.3368	$0.3269^{+0.0109}_{-0.0108}$	0.3196	$0.3149^{+0.0101}_{-0.0101}$
z_{re}	10.51	$10.95^{+1.06}_{-1.17}$	11.61	$11.14^{+1.1}_{-1.08}$	11.85	$11.33^{+1.1}_{-1.09}$
H_0	64.23	$64.31^{+0.943}_{-1.06}$	64.77	$65.31^{+0.729}_{-0.72}$	66.14	$66.29^{+0.744}_{-0.866}$
Age/Gyr	13.89	$13.87^{+0.053}_{-0.0455}$	13.86	$13.83^{+0.0422}_{-0.0424}$	13.78	$13.78^{+0.0506}_{-0.045}$
$\chi^2_{min}/2$	4903.15		4905.40		4977.26	

Table 4.14: Cosmological parameters - LBT analysis for the Lagrangian Model

	LBT+H0		LBT+H0+Planck	
Parameter	Best fit	68% limits	Best fit	68% limits
$\Omega_b h^2$	0.01379	$0.04993^{+0.0501}_{-0.0449}$	0.02193	$0.02202^{+0.000223}_{-0.000227}$
$\Omega_c h^2$	0.05908	$0.04989^{+0.0211}_{-0.0407}$	0.1177	$0.1173^{+0.00213}_{-0.00212}$
H_0	73.85	$74.25^{+2.39}_{-2.38}$	67.73	$67.57^{+0.989}_{-0.978}$
λ	1.495	$1.091^{+0.409}_{-0.0893}$	0.1664	$0.482^{+0.106}_{-0.382}$
r	0.04726	$0.001707^{+0.0983}_{-0.102}$	-0.01	$-0.001682^{+0.0226}_{-0.0279}$
df	2.025	$1.819^{+0.21}_{-0.264}$	1.307	$1.339^{+0.0923}_{-0.0924}$
Ω_d	0.8652	$0.8159^{+0.0415}_{-0.0439}$	0.6942	$0.6932^{+0.0136}_{-0.0122}$
Ω_m	0.1348	$0.1841^{+0.0438}_{-0.0415}$	0.3058	$0.3068^{+0.0122}_{-0.0136}$
$\chi^2_{min}/2$	14.62		4924.29	

are plotted in Fig. 4.19. These results show that even when we fix the parameter λ, the Planck data alone is compatible with a null interaction. However, if we include low redshift measurements from BAO, SNIa and H_0, the symmetric value of r is broken and it favors a negative value of r. For this value of λ, the negative interaction parameter is favored at 68% C.L.. Augmenting the value of λ, a negative r is even more favorable. Thus, we conclude that if we are able to determine the value of λ, or if we have a theoretical model fixing it, if this value is sufficiently large, the Yukawa interaction between dark energy and dark matter will be preferred by the cosmological data.

At last we analyze the Lagrangian model comparing it with the lookback time data. The results are in Table 4.14. Figures 4.20 and 4.21 present the 1-D posteriors and the main parameter degeneracies, respectively. As expected, the lookback time yields much broader results as compared with the Planck constraints. It is not able to constrain the

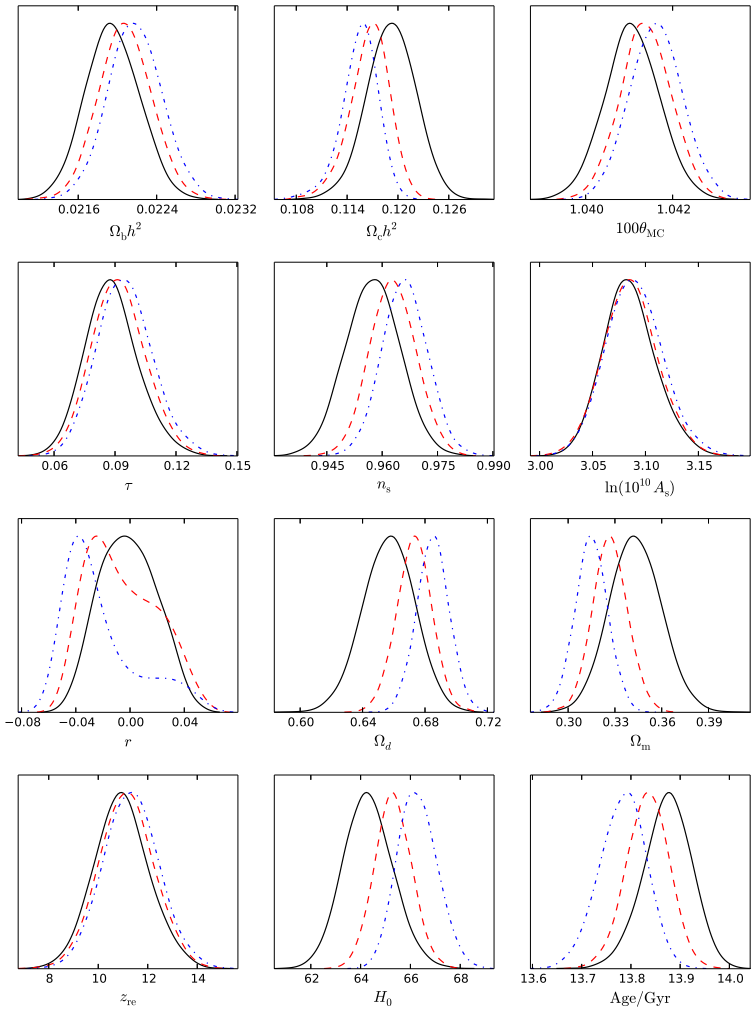

Figure 4.19: The likelihood for the parameters of the Lagrangian Model with fixed λ. The black solid lines correspond to the Planck constraints, the red dashed lines correspond to Planck + BAO and the blue dot-dashed lines correspond to Planck + BAO + SNIa + H_0.

interaction, which is completely undetermined with lookback time data alone. From the posterior distributions, we observe that LBT data prefer larger values of λ, which is in the opposite direction to the Planck measurements. Fixing the value of λ does not improve the LBT constraints for the interaction parameter, thus we do not present the results for this case here. We conclude that the LBT data alone are not of much help to constrain the Lagrangian Model with Yukawa-type interaction, but they show a tension with the Planck data in the determination of the scalar potential parameter. These results are part of a publication to appear soon[100].

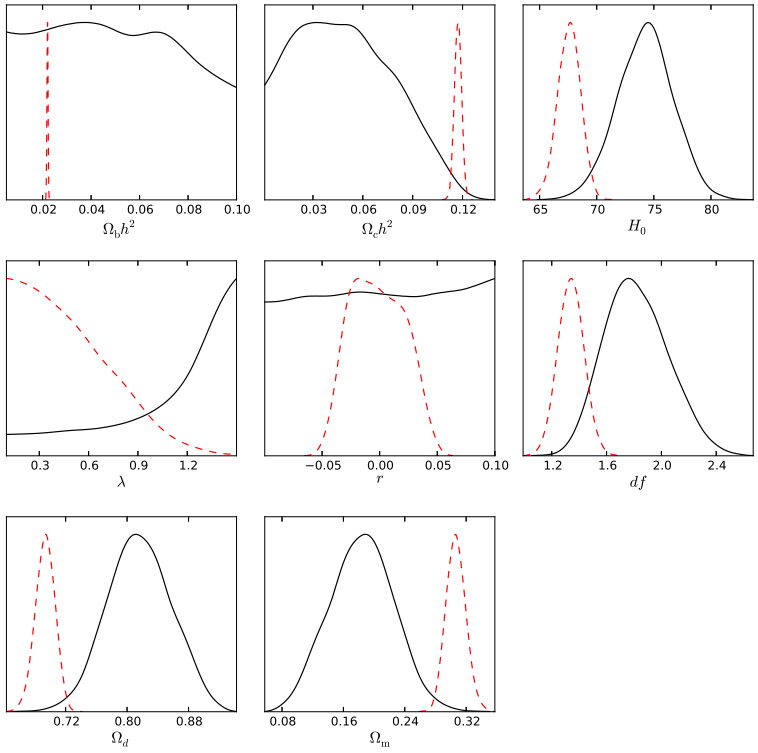

Figure 4.20: The likelihood for the parameters of the Lagrangian Model using lookback time measurements. The black solid lines correspond to the LBT + H_0 constraints and the red dashed lines correspond to LBT + H_0 + Planck.

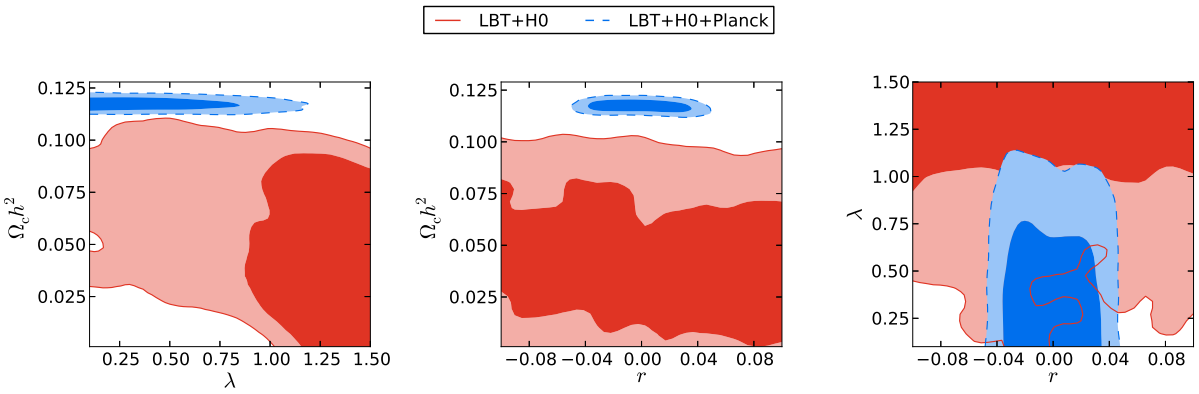

Figure 4.21: 2-D distribution for selected parameters - LBT analysis for the Lagrangian Model.

Conclusions

The aim of this thesis was to propose models of interaction between dark energy and dark matter and discover from observational data if the interaction is favored.

Chapter one dealt with basic aspects of cosmology. We introduced the simple homogeneous and isotropic model for the Universe and the equations governing its evolution. Then, in order to put the cosmological models on experimental basis, we described definitions of cosmic distances which allow us to constrain the cosmological parameters of a model from observations and make predictions that can be falsifiable. For instance, observations of surpernova type Ia put constraints from luminosity distances and measurements of baryon acustic oscillations are based on angular diameter distances. Finally, we discussed how current observations lead to the necessity of two unknown components: dark matter and dark energy.

The structures around us imply that we must go beyond the homogeneous and isotropic universe if our model intends to explain the real Universe. On large scales, we can improve our model through small perturbations in the background. Chapter two introduced such perturbations and developed their dynamical equations. The linear perturbations over the smooth background lead to predictions about the cosmic microwave background anisotropies and matter inhomogeneities which can be tested by anisotropy probes, e.g. Planck satellite, and galaxy surveys, respectively.

The first two chapters were concerned to establish the cosmological basis we needed. In chapter three we explore the possibility of an interaction in the dark sector. The simplest cosmological model, the ΛCDM, is in good agreement with current observations. However, it suffers from two theoretical problems: the cosmological constant problem and the coincidence problem. Thus, we consider alternative models: the first is a phenomenological model with an interaction given by a linear combination of the dark fluids $Q = 3H(\xi_1\rho_c + \xi_2\rho_d)$; and, as a tentative to build a more fundamental framework, the

second model comes from a Lagrangian density of a scalar field, describing dark energy, and a fermionic field, for dark matter, with an Yukawa interaction between them.

The last chapter compares the theoretical predictions of the interacting models with several observational data. The data show that an interaction is allowed and in some cases it is favored. We also observe some tension between the results from Planck with the low redshift measurements from lookback time. The lookback time favors a larger positive interaction for the phenomenological models, while for the Planck data it is more consistent with zero and even negative values for Model I. On the other hand, the lookback time data prefer larger values for the scalar potential parameter λ of the Lagrangian model, in the opposite direction to the Planck results. Appendices A, B and C present the most important parts of the computational implementation used in this thesis.

From this thesis we see at least two possible directions for future works: first, there is still much space for alternative models of dark energy and dark matter, and different kinds of interaction; second, there are other data sets that were not considered here and new techniques and probes should be taken into account. These studies will certainly augment our knowledge of the nature of dark matter and dark energy.

Appendix A

Camb Code: Phenomenological Model

```
!This appendix shows the most import steps to introduce the phenomenological
!interacting model in the CAMB code.
!We implemented the module Couple in CAMB. Its purpose is to obtain the evolution
!of rho_dm and rho_de with the scale factor "a" for the interacting model.
!The perturbations are introduced in the GaugeInterface module of CAMB.
!We only present the most important modifications to that module.

module Couple
   use precision
   use ModelParams
   use LambdaGeneral
   implicit none
   integer, parameter :: NumPoints = 2000
   real(dl) aVals(NumPoints+1),grhodm_a(NumPoints+1), grhode_a(NumPoints+1)
   real(dl) ddgrhodm_a(NumPoints+1), ddgrhode_a(NumPoints+1)
   real(dl), parameter :: amin = 1.d-9


   logical:: coupled = .true.
   real(dl) :: lambda1 = 0._dl, lambda2 = 0._dl


contains

!This is to call the parameters lambda1 and lambda2 from the params.ini file.
!lambda1 and lambda2 are the coupling constants multiplying dark matter and
!dark energy densities, respectively, in a phenomenological model.
   subroutine Couple_ReadParams(Ini)
      use IniFile
      Type(TIniFile) :: Ini


      coupled = Ini_Read_Logical_File(Ini,'coupled',.true.)
      if (coupled) then
         lambda1 = Ini_Read_Double_File(Ini,'lambda1',0.d0)
         lambda2 = Ini_Read_Double_File(Ini,'lambda2',0.d0)
         write(*,'("(lambda1, lambda2) = (", f8.5,", ", f8.5, ")")') lambda1,lambda2
      end if

   end subroutine Couple_ReadParams
```

```
!The system of differential equations for rho as a function of "a" is given here.
   subroutine EvolveBackground(dum,num,x,y,yprime)
      implicit none
      real dum
      integer num
      real(dl) x, y(num), yprime(num)
      real(dl) grhodm_ev, grhode_ev

      grhodm_ev = y(1)
      grhode_ev = y(2)

      yprime(1) = -3._dl*(1._dl/x)*grhodm_ev+3._dl*(1._dl/x)*
           (lambda1*grhodm_ev+lambda2*grhode_ev)
      yprime(2) = -3._dl*(1._dl/x)*(1._dl+w_de(x))*grhode_ev-3._dl*(1._dl/x)*
           (lambda1*grhodm_ev+lambda2*grhode_ev)

   end subroutine EvolveBackground

!The system of differential equations is solved in this subroutine.
   subroutine History
      real(dl) :: astart,aend,atol,alogmin,lnastart
      integer, parameter :: NumEqs=2
      real(dl) c(24), w(NumEqs,9), y(NumEqs)
      integer ind, i
      real dum,num

      ind = 1
      atol = 1.d-5

      alogmin = dlog(amin)

      astart = 1._dl
      lnastart = dlog(astart)

      y(1) = grhoc
      y(2) = grhov

      aVals(1) = astart
      grhodm_a(1) = y(1)
      grhode_a(1) = y(2)


!For better interpolation I go a little into the future (a > 1).
      do i=1,100
         aend = lnastart-(alogmin/NumPoints)*i
         aend = dexp(aend)
         call dverk(dum,NumEqs,EvolveBackground,astart,y,aend,atol,ind,c,NumEqs,w)
         aVals(i+1) = aend
         grhodm_a(i+1) = y(1)
         grhode_a(i+1) = y(2)
      enddo

      aVals(1) = aend
      grhodm_a(1) = y(1)
      grhode_a(1) = y(2)

      astart = aVals(1)
```

```
      lnastart = dlog(astart)


      do i=1, NumPoints
         aend = lnastart+(alogmin/NumPoints)*i
         aend = dexp(aend)
         call dverk(dum,NumEqs,EvolveBackground,astart,y,aend,atol,ind,c,NumEqs,w)
         aVals(i+1) = aend
         grhodm_a(i+1) = y(1)
         grhode_a(i+1) = y(2)
      enddo

      call Flip(aVals)
      call Flip(grhodm_a)
      call Flip(grhode_a)

      do i=1, NumPoints+1
         aVals(i)=dlog(aVals(i))
      enddo

      call spline(aVals,grhodm_a,NumPoints+1,1.d30,1.d30,ddgrhodm_a)
      call spline(aVals,grhode_a,NumPoints+1,1.d30,1.d30,ddgrhode_a)

   end subroutine History

!This subroutine is to invert the order of the splines.
   subroutine Flip(xdat)
      real(dl) :: xdat(NumPoints),swap_x
      integer i,pos

      do i=1, NumPoints+1
         pos = (NumPoints+1)-i
         if (pos > i) then
            swap_x = xdat(pos)
            xdat(pos) = xdat(i)
            xdat(i) = swap_x
         endif
      end do
   end subroutine

!rho_dm as a function of "a".
   function grhodm(a)  !8 pi G rho_dm
      real(dl) :: grhodm, al
      real(dl), intent(IN) :: a

      al=dlog(a)
      if(al.lt.aVals(1)) then
         grhodm=grhodm_a(1)             !if a < minimum a from wa.dat
      else
         if(al.gt.aVals(NumPoints)) then
            grhodm=grhodm_a(NumPoints)        !if a > maximus a from wa.dat
         else
            call cubicsplint(aVals,grhodm_a,ddgrhodm_a,NumPoints,al,grhodm)
         endif
      endif

   end function grhodm
```

```
!rho_de as a function of "a"
   function grhode(a)  !8 pi G rho_de
      real(dl) :: grhode, al
      real(dl), intent(IN) :: a

      al=dlog(a)
      if(al.lt.aVals(1)) then
         grhode=grhode_a(1)             !if a < minimum a from wa.dat
      else
         if(al.gt.aVals(NumPoints)) then
            grhode=grhode_a(NumPoints)        !if a > maximus a from wa.dat
         else
            call cubicsplint(aVals,grhode_a,ddgrhode_a,NumPoints,al,grhode)
         endif
      endif

   end function grhode

!The adiabatic sound speed of dark energy.
   function ca2(a)
      real(dl) :: ca2, grhodeda
      real(dl), intent(IN) :: a

      grhodeda = -3._dl*(1._dl/a)*(1._dl+w_de(a))*grhode(a)-3._dl*(1._dl/a)*
           (lambda1*grhodm(a)+lambda2*grhode(a))
      ca2 = w_de(a) - wa_ppf*grhode(a)/grhodeda

   end function ca2


end module Couple
.
.
.
!Background evolution
function dtauda(a)
!get d tau / d a

!  8*pi*G*rho*a**4.

   grhoa2=grhok*a2+grhob*a+grhog+grhornomass+(grhodm(a)+grhode(a))*a2**2

dtauda=sqrt(3/grhoa2)

end function dtauda
.
.
.
!Initial values for perturbations.
if (coupled) then
    initv(1,i_clxc)=0.75_dl*initv(1,i_clxg)*(1._dl-lambda1-lambda2*
         (grhode(a)/grhodm(a)))
    initv(1,i_clxq)=0.75_dl*initv(1,i_clxg)*(1._dl+w_de(a)+lambda1*
         (grhodm(a)/grhode(a))+lambda2)
    initv(1,i_vq)=initv(1,i_qg)
else
    initv(1,i_clxc)=initv(1,i_clxb)
endif
```

```
.
.
.
   grhoc_t=grhodm(a)*a2
   grhov_t=grhode(a)*a2
   w_eff = w_de(a)

!total perturbations: matter terms first, then add massive nu, de and radiation
!  8*pi*a*a*SUM[rho_i*clx_i]
dgrho=grhob_t*clxb+grhoc_t*clxc
!  8*pi*a*a*SUM[(rho_i+p_i)*v_i]
dgq=grhob_t*vb


clxq=ay(EV%w_ix)
vq=ay(EV%w_ix+1)
dgrho=dgrho + clxq*grhov_t
dgq = dgq + vq*grhov_t*(1._dl+w_eff)
.
.
.
!Perturbed dark energy equation of motion
if (coupled) then
   ayprime(Ev%w_ix)= 3._dl*adotoa*w_eff*clxq + &
                     3._dl*adotoa*lambda1*(grhoc_t/grhov_t)*(clxq - clxc)&
                     - (1._dl+w_eff)*k*vq - 3._dl*adotoa*cs2_lam*clxq - &
                     3._dl*adotoa*(cs2_lam-ca2(a))*(3._dl*adotoa*(1._dl+w_eff) + &
                     3._dl*adotoa*(lambda1*(grhoc_t/grhov_t) + lambda2))*&
                     vq/k - (1._dl+w_eff)*k*z

   ayprime(Ev%w_ix+1)= -adotoa*(1._dl-3._dl*cs2_lam)*vq + &
                       (3._dl*adotoa/(1._dl+w_eff))*(1._dl+cs2_lam)*&
                       (lambda1*(grhoc_t/grhov_t) + lambda2)*vq + &
                       cs2_lam*k*clxq/(1._dl+w_eff)

!  CDM equation of motion
    clxcdot= -k*z + 3._dl*adotoa*lambda2*(grhov_t/grhoc_t)*(clxq - clxc)
    ayprime(3) = clxcdot
else
    clxcdot=-k*z
    ayprime(3)=clxcdot
endif
```

Appendix B

Camb Code: Lagrangian Model

```
!This appendix shows the most import steps to introduce the lagrangian
!interacting model in the CAMB code.
!We implemented the module QCouple in CAMB. Its purpose is to obtain the evolution
!of rho_dm, phi and phidot with the scale factor a for the interacting model.
!The perturbations are introduced in the GaugeInterface module of CAMB.
!We only present the most important modifications to that module.

module QCouple
  use precision
  use Errors
  use ModelParams
  use LambdaGeneral
  implicit none
  integer, parameter :: NumPoints = 2000, NumPointsEx = NumPoints+2
  real(dl) aVals(NumPointsEx), grhodm_a(NumPointsEx), phi_a(NumPointsEx),
       phidot_a(NumPointsEx)
  real(dl) ddgrhodm_a(NumPointsEx), ddphi_a(NumPointsEx), ddphidot_a(NumPointsEx)
  real(dl) initial_grhoc, initial_phi, initial_phidot, adot, y_grhoc, norm_grhoc
  real(dl), parameter :: amin = 1.d-9


  real(dl) :: lambda = 0._dl, r_int = 0._dl, rphi = -1.d0
  logical :: OK_int = .true.


contains

!This is to call the parameters lambda and r_int from the params.ini file.
!lambda is the power of the potential V(psi) and r_int is the coupling constant
!divided by the dark matter mass, respectively.
  subroutine Couple_ReadParams(Ini)
     use IniFile
     Type(TIniFile) :: Ini


     if (coupled) then
        lambda = Ini_Read_Double_File(Ini,'lambda',0.d0)
        r_int = Ini_Read_Double_File(Ini,'r_int',0.d0)
        rphi = Ini_Read_Double_File(Ini,'rphi',-1.d0)
        write(*,'("(lambda, r_int, rphi) = (", f8.5,", ", f8.5, ", ", f8.5, ")")')
        lambda, r_int, rphi
     end if
```

```
  end subroutine Couple_ReadParams


  function Vofphi(phi,deriv)
!Returns (8*Pi*G)^(1-deriv/2)*d^{deriv}V(psi)/d^{deriv}psi evaluated at psi
!times (Mpc/c)^2 to get units in 1/Mpc^2
!The input variable phi is sqrt(8*Pi*G)*psi
     use constants
     implicit none
     real(dl) phi, Vofphi
     integer deriv
     real(dl) norm


!Normalized so that lambda=0 and r_int=0 gives norm=grhov
     norm = 3._dl*CP%H0**2*(1000)**2/c**2*CP%omegav

     if (deriv==0) then
        Vofphi = norm*exp(-lambda*phi)
     else
        if (deriv==1) then
           Vofphi = -lambda*norm*exp(-lambda*phi)
        else
           if (deriv==2) then
              Vofphi = lambda**2*norm*exp(-lambda*phi)
           else
              stop 'Invalid deriv in Vofphi'
           endif
        endif
     endif

  end function Vofphi


!The system of differential equations for rho as a function of "a" is given here.
  subroutine EvolveBackground(dum,num,x,y,yprime)
     use constants
     use MassiveNu
     implicit none
     real dum
     integer num
     real(dl) x, y(num), yprime(num)
     real(dl) x2, grhodm_ev, phi, phidot, ga2T00_de, ga2T00, dphida, Q_int
     real(dl) rhonu
     integer nu_i

     OK_int = .true.

     x2 = x**2

     phi = y(1)
     phidot = y(2)/x2

     if (x == amin) then
        norm_grhoc = y_grhoc*amin**3/(1-r_int*phi)
     endif

     grhodm_ev = norm_grhoc/x**3*(1 - r_int*phi)
```

```
     y_grhoc = grhodm_ev

     if (rphi < 0) then
        if (r_int*phi < 1._dl) then
           Q_int = -r_int/(1._dl - r_int*phi)
        else
           grhodm_ev = 0._dl
           Q_int = 0
           OK_int = .false.
        endif
     else
        if (r_int*phi > 1._dl) then
           Q_int = -r_int/(1._dl - r_int*phi)
        else
           grhodm_ev = 0._dl
           Q_int = 0
           OK_int = .false.
        endif
     endif


     ga2T00_de = x2*(0.5d0*phidot**2 + x2*Vofphi(phi,0))
     ga2T00 = grhok*x2+grhob*x+grhog+grhornomass+grhodm_ev*x2**2+ga2T00_de


     if (CP%Num_Nu_massive /= 0) then
!Get massive neutrino density relative to massless
        do nu_i = 1, CP%nu_mass_eigenstates
           call Nu_rho(x*nu_masses(nu_i),rhonu)
           ga2T00 = ga2T00 +rhonu*grhormass(nu_i)
        end do
     end if

     adot = sqrt(ga2T00/3.0d0)
     dphida = phidot/adot


     yprime(1) = dphida
     yprime(2) = -x2**2*(Vofphi(phi,1) + Q_int*grhodm_ev)/adot

  end subroutine EvolveBackground


  function GetOmegaFromInitial(astart,grhoc_initial,phi,phidot,atol)
!Get CP%omegac and CP%omegav today given particular conditions grhoc, phi and
!phidot at a=astart
     implicit none
     real(dl), intent(IN) :: astart, grhoc_initial, phi, phidot, atol
     real(dl), dimension(2) :: GetOmegaFromInitial
     integer, parameter ::  NumEqs=2
     real(dl) c(24), w(NumEqs,9), y(NumEqs), ast
     integer ind, i
     real dum


     ast=astart

     ind=2
```

```
     do i=1,9
        c(i)=0._dl
     enddo

     c(4)=1d-30
     c(5)=100

     y_grhoc = grhoc_initial
     y(1) = phi
     y(2) = phidot*astart**2  !Fixed Dec 02

     call dverk(dum,NumEqs,EvolveBackground,ast,y,1._dl,atol,ind,c,NumEqs,w)
     if (OK_int) then
        call EvolveBackground(dum,NumEqs,1._dl,y,w(:,1))
        GetOmegaFromInitial(1) = y_grhoc/(3*adot**2)
        GetOmegaFromInitial(2) = (0.5d0*y(2)**2 + Vofphi(y(1),0))/(3*adot**2)
     else
        return
     endif


!Search for initial phi.
  subroutine GetInitialPhi(trial_grhoc,error_phi)
     implicit none
     real(dl) astart
     real(dl) atol
     real(dl) initial_phi2
     real(dl), dimension(2):: om
     real(dl) :: omv1, omv2, deltaphi, phi, trial_grhoc, initial_phi_inv
     real(dl) :: omv_min, initial_phi_min, omv_max, initial_phi_max, phi1, phi2
     integer, optional :: error_phi
     logical OK
     integer:: iter = 0, iter2

     iter2 = 0
     omv_min = 1000
     omv_max = -1000
     astart = amin


!These two must bracket the correct value to give CP%omegav today
!Assume that higher initial phi gives higher CP%omegav today
!Can fix initial_phi to correct value
     if (rphi < 0) then
        if (r_int > 0) then
           initial_phi = 1._dl/r_int - 1._dl/(100*r_int)
           initial_phi2 = -100/lambda
        else
           if (r_int < 0) then
              initial_phi = 100/lambda
              initial_phi2 = 1._dl/r_int - 1._dl/(100*r_int)
           else
              initial_phi = 100/lambda
              initial_phi2 = -100/lambda
           endif
        endif
     else
```

```
         if (r_int < 0) then
            initial_phi = 1._dl/r_int + 1._dl/(100*r_int)
            initial_phi2 = -100/lambda
         else
            if (r_int > 0) then
               initial_phi = 100/lambda
               initial_phi2 = 1._dl/r_int + 1._dl/(100*r_int)
            else
               initial_phi = 100/lambda
               initial_phi2 = -100/lambda
            endif
         endif
      endif


      if (CP%omegav < 0) then
         initial_phi_inv = initial_phi
         initial_phi = initial_phi2
         initial_phi2 = initial_phi_inv
      endif

      initial_phidot = 0._dl

      atol = 1d-5

!See if initial conditions are giving correct CP%omegav now
      om = GetOmegaFromInitial(astart,trial_grhoc,initial_phi,initial_phidot,atol)

      if (OK_int .and. om(2) < CP%omegav) then
         omv1 = om(2)
      else
         do while (OK_int == .false. .or. om(2) > CP%omegav)
            iter2 = iter2 + 1
            phi = initial_phi + (initial_phi2 - initial_phi)/2
            om = GetOmegaFromInitial(astart,trial_grhoc,phi,initial_phidot,atol)
            if (om(2) < CP%omegav .or. OK_int == .false.) then
               initial_phi = phi
            else
               initial_phi2 = phi
            endif

            if (om(2) < omv_min .and. OK_int) then
               omv_min = om(2)
               initial_phi_min = phi
            endif


            if (iter2 == 50 .and. omv_min > CP%omegav) then
               do iter2 = 1, 10
                  phi1 = initial_phi_min + 1
                  phi2 = initial_phi_min - 1
                  om = GetOmegaFromInitial(astart,trial_grhoc,phi1,initial_phidot,atol)
                  omv1 = om(2) - CP%omegav
                  om = GetOmegaFromInitial(astart,trial_grhoc,phi2,initial_phidot,atol)
                  omv2 = om(2) - CP%omegav
                  phi = phi2 - (phi2 - phi1)*omv2/(omv2 - omv1)
                  om = GetOmegaFromInitial(astart,trial_grhoc,phi,initial_phidot,atol)
                  if (OK_int) then
```

```
                phi1 = phi2
                phi2 = phi
             else
                phi1 = phi
             endif


             if (om(2) < omv_min .and. OK_int) then
                omv_min = om(2)
                initial_phi_min = phi
             endif

             if (om(2) <= CP%omegav .and. OK_int) then
                initial_phi = phi
                exit
             endif
             if (iter2 == 10) then
                om(2) = omv_min
                initial_phi = initial_phi_min
             endif
          enddo
          exit
       endif
    enddo
    omv1 = om(2)
 endif


 if (abs(omv1-CP%omegav) > 1d-5) then
!if not, do binary search in the interval
    OK = .false.
    iter2 = 0
    om = GetOmegaFromInitial(astart,trial_grhoc,initial_phi2,initial_phidot,atol)

    if (OK_int .and. om(2) > CP%omegav) then
       omv2 = om(2)
    else
       do while (OK_int == .false. .or. om(2) < CP%omegav)
          iter2 = iter2 + 1
          phi = initial_phi2 + (initial_phi - initial_phi2)/2
          om = GetOmegaFromInitial(astart,trial_grhoc,phi,initial_phidot,atol)
          if (om(2) > CP%omegav .or. OK_int == .false.) then
             initial_phi2 = phi
          else
             initial_phi = phi
          endif
          omv2 = om(2)

          if (om(2) > omv_max .and. OK_int) then
             omv_max = om(2)
             initial_phi_max = phi
          endif

          if (iter2 == 50 .and. omv_max < CP%omegav) then
             do iter2 = 1, 10
                phi1 = initial_phi_max + 1
                phi2 = initial_phi_max - 1
                om = GetOmegaFromInitial(astart,trial_grhoc,phi1,initial_phidot,
```

```
                    atol)
               omv1 = om(2) - CP%omegav
               om = GetOmegaFromInitial(astart,trial_grhoc,phi2,initial_phidot,atol)
               omv2 = om(2) - CP%omegav
               phi = phi1 - (phi1 - phi2)*omv1/(omv1 - omv2)
               om = GetOmegaFromInitial(astart,trial_grhoc,phi,initial_phidot,atol)
               if (OK_int) then
                  phi2 = phi1
                  phi1 = phi
               else
                  phi2 = phi
               endif

               if (om(2) > omv_max .and. OK_int) then
                  omv_max = om(2)
                  initial_phi_max = phi
               endif

               if (om(2) >= CP%omegav .and. OK_int) then
                  initial_phi2 = phi
                  exit
               endif
               if (iter2 == 10) then
                  om(2) = omv_max
                  initial_phi2 = initial_phi_max
               endif
            enddo
            exit
         endif
   enddo
   omv2 = om(2)
endif


      if (omv1 > CP%omegav .or. omv2 < CP%omegav) then
         if (error_phi == 100) then
            write (*,*) 'Initial phi values must bracket required value.'
            call GlobalError('Initial phi values must bracket required value.',
                  error_evolution)
         else
            return
         endif
      end if

      do iter = 1,100
         deltaphi = initial_phi2 - initial_phi
         phi = initial_phi + deltaphi/2
         om = GetOmegaFromInitial(astart,trial_grhoc,phi,initial_phidot,atol)

         if (OK_int) then
            if (om(2) < CP%omegav) then
               omv1 = om(2)
               initial_phi = phi
            else
               omv2 = om(2)
               initial_phi2 = phi
            end if
         else
```

```
            if (phi >= initial_phi) then
               initial_phi = phi
            else
               initial_phi2 = phi
            endif
         endif

         if (omv2 - omv1 < 1d-5) then
            OK = .true.
            initial_phi = (initial_phi2 + initial_phi)/2
            exit
         end if

      end do

      if (.not. OK .and. error_phi == 100) then !this shouldn't happen
         write (*,*) 'Search for good phi initial condition did not converge.'
         call GlobalError('Search for good phi initial condition did not converge.',
               error_evolution)
      endif

   endif

  end subroutine GetInitialPhi


!Search for initial grhoc.
  subroutine Init_background
   implicit none
   real(dl) astart
   real(dl) atol
   real(dl) initial_grhoc2
   real(dl), dimension(2):: om
   real(dl) omc1, omc2, deltagrhoc, rhoc
   logical OK
   integer:: iter = 0

   astart = amin

   atol = 1d-5

   if (lambda == 0._dl .and. r_int == 0._dl) then
!These two must bracket the correct value to give CP%omegac today
!Assume that higher initial grhoc gives higher CP%omegac today
!Can fix initial_grhoc to correct value
   initial_grhoc = 1d1*grhoc/astart**3
   initial_grhoc2 = 1d-1*grhoc/astart**3
   initial_phi = 10
   initial_phidot = 0._dl

!See if initial conditions are giving correct CP%omegac now
   om = GetOmegaFromInitial(astart,initial_grhoc,initial_phi,initial_phidot,atol)
   omc1 = om(1)

   if (abs(omc1-CP%omegac) > 1d-4) then
!if not, do binary search in the interval
      OK = .false.
      om = GetOmegaFromInitial(astart,initial_grhoc2,initial_phi,initial_phidot,atol)
```

```
        omc2 = om(1)
        if (omc1 < CP%omegac .or. omc2 > CP%omegac) then
           write (*,*) 'Initial grhoc values must bracket required value.'
           call GlobalError('Initial grhoc values must bracket required value.',
                 error_evolution)
        end if

        do iter = 1,100
           deltagrhoc = initial_grhoc2 - initial_grhoc
           rhoc = initial_grhoc + deltagrhoc/2
           om = GetOmegaFromInitial(astart,rhoc,initial_phi,initial_phidot,atol)
           if (om(1) > CP%omegac) then
              omc1 = om(1)
              initial_grhoc = rhoc
           else
              omc2 = om(1)
              initial_grhoc2 = rhoc
           end if

           if (omc1 - omc2 < 1d-5 .and. abs(om(2)-CP%omegav) < 1d-4) then
              OK = .true.
              initial_grhoc = (initial_grhoc2 + initial_grhoc)/2
              if (FeedbackLevel > 0) write(*,*) 'grhoc_initial = ', initial_grhoc
              if (FeedbackLevel > 0) write(*,*) 'phi_initial = ', initial_phi

              om = GetOmegaFromInitial(astart,initial_grhoc,initial_phi,initial_phidot,
                   atol)
              if (FeedbackLevel > 0) write(*,*) 'Omegac0, Omegac = ', om(1), CP%omegac
              if (FeedbackLevel > 0) write(*,*) 'Omegav0, Omegav = ', om(2), CP%omegav
              exit
           end if

        end do

        if (.not. OK) then !this shouldn't happen
           write (*,*) 'Search for good initial conditions did not converge.'
           call GlobalError('Search for good initial conditions did not converge.',
                 error_evolution)
        endif

     endif

     else

!These two must bracket the correct value to give CP%omegac today
!Assume that higher initial grhoc gives higher CP%omegac today
!Can fix initial_grhoc to correct value
        initial_grhoc = 1d3*grhoc/astart**3
        initial_grhoc2 = 1d-3*grhoc/astart**3

!See if initial conditions are giving correct CP%omegac now
        call GetInitialPhi(initial_grhoc,0)
        om = GetOmegaFromInitial(astart,initial_grhoc,initial_phi,initial_phidot,atol)
        if (OK_int .and. om(1) > CP%omegac) then
           omc1 = om(1)
        else
           do iter = 1,10
              initial_grhoc = initial_grhoc/2
```

```
            call GetInitialPhi(initial_grhoc,0)
            om = GetOmegaFromInitial(astart,initial_grhoc,initial_phi,initial_phidot,
                 atol)
            if (OK_int .and. om(1) > CP%omegac) then
               omc1 = om(1)
               exit
            endif
         enddo
         omc1 = om(1)
      endif


      if (abs(omc1-CP%omegac) > 1d-5) then
!if not, do binary search in the interval
         OK = .false.
         call GetInitialPhi(initial_grhoc2,0)
         om = GetOmegaFromInitial(astart,initial_grhoc2,initial_phi,initial_phidot,
              atol)
         if (OK_int .and. om(1) < CP%omegac) then
            omc2 = om(1)
         else
            do iter = 1,10
               initial_grhoc2 = 2*initial_grhoc2
               call GetInitialPhi(initial_grhoc2,0)
               om = GetOmegaFromInitial(astart,initial_grhoc2,initial_phi,
                    initial_phidot,atol)
               if (OK_int .and. om(1) < CP%omegac) then
                  omc2 = om(1)
                  exit
               endif
            enddo
            omc2 = om(1)
         endif


         if (omc1 < CP%omegac .or. omc2 > CP%omegac) then
            write (*,*) 'Initial grhoc values must bracket required value.'
            call GlobalError('Initial grhoc values must bracket required value.',
                 error_evolution)
         end if

         do iter = 1,100
            deltagrhoc = initial_grhoc2 - initial_grhoc
            rhoc = initial_grhoc + deltagrhoc/2
            call GetInitialPhi(rhoc,iter)
            om = GetOmegaFromInitial(astart,rhoc,initial_phi,initial_phidot,atol)
            if (om(1) > CP%omegac) then
               omc1 = om(1)
               initial_grhoc = rhoc
            else
               omc2 = om(1)
               initial_grhoc2 = rhoc
            end if

            if (omc1 - omc2 < 1d-5 .and. abs(om(2)-CP%omegav) < 1d-4) then
               OK = .true.
               initial_grhoc = (initial_grhoc2 + initial_grhoc)/2
               if (FeedbackLevel > 0) write(*,*) 'grhoc_initial = ', initial_grhoc
```

```
                if (FeedbackLevel > 0) write(*,*) 'phi_initial = ', initial_phi

                om = GetOmegaFromInitial(astart,initial_grhoc,initial_phi,
                     initial_phidot,atol)
                if (FeedbackLevel > 0) write(*,*) 'Omegac0, Omegac =',om(1),CP%omegac
                if (FeedbackLevel > 0) write(*,*) 'Omegav0, Omegav =',om(2),CP%omegav

                exit
             end if
          end do


          if (.not. OK) then !this shouldn't happen
             write (*,*) 'Search for good initial conditions did not converge.'
             call GlobalError('Search for good initial conditions did not converge.',
                   error_evolution)
          endif

       endif
    endif

  end subroutine Init_background


!Here we make interpolation tables.
  subroutine History
     implicit none
     real(dl) :: astart, afrom, aend
     integer, parameter :: NumEqs=2
     real(dl) c(24), w(NumEqs,9), y(NumEqs), atol, splZero
     integer ind, i
     real dum

     ind = 1
     atol = 1.d-5

     astart = amin
     afrom = astart

     call Init_background

     y_grhoc = initial_grhoc
     y(1) = initial_phi
     y(2) = initial_phidot

     aVals(1) = astart
     grhodm_a(1) = y_grhoc
     phi_a(1) = y(1)
     phidot_a(1) = y(2)


!For better interpolation I go a little into the future (a > 1).
     do i=1, NumPointsEx-1
        aend = dlog(astart)-(dlog(astart)/(NumPoints-1))*i
        aend = dexp(aend)
        call dverk(dum,NumEqs,EvolveBackground,afrom,y,aend,atol,ind,c,NumEqs,w)
        call EvolveBackground(dum,NumEqs,aend,y,w(:,1))
        aVals(i+1) = aend
```

```
        grhodm_a(i+1) = y_grhoc
        phi_a(i+1) = y(1)
        phidot_a(i+1) = y(2)
        if (i==NumPoints-1) then
           if (FeedbackLevel > 0) then
              write(*,*) 'Omega_Q_0=',real((0.5d0*phidot_a(i+1)**2 +
              Vofphi(phi_a(i+1),0))/(3*adot**2)), &
              '  w_0=',real((0.5d0*phidot_a(i+1)**2 - Vofphi(phi_a(i+1),0))/
                   (0.5d0*phidot_a(i+1)**2 + Vofphi(phi_a(i+1),0)))
            end if
        end if
     enddo

     splZero = 0
     call spline(aVals,grhodm_a,NumPointsEx,splZero,splZero,ddgrhodm_a)
     call spline(aVals,phi_a,NumPointsEx,splZero,splZero,ddphi_a)
     call spline(aVals,phidot_a,NumPointsEx,splZero,splZero,ddphidot_a)


  end subroutine History


!rho_dm as a function of "a".
  function grhodm(a)  !8 pi G rho_dm
     real(dl) :: grhodm
     real(dl), intent(IN) :: a


     if(a.lt.aVals(1)) then
        grhodm=grhodm_a(1)                    !if a < minimum
     else
        if(a.gt.aVals(NumPointsEx)) then
           grhodm=grhodm_a(NumPointsEx)              !if a > maximus
        else
           call cubicsplint(aVals,grhodm_a,ddgrhodm_a,NumPointsEx,a,grhodm)
        endif
     endif

  end function grhodm


!phi as a function of "a"
  function fphi(a)  !sqrt(8*pi*G)*psi
     real(dl) :: fphi
     real(dl), intent(IN) :: a


     if(a.lt.aVals(1)) then
        fphi=phi_a(1)                    !if a < minimum
     else
        if(a.gt.aVals(NumPointsEx)) then
           fphi=phi_a(NumPointsEx)              !if a > maximus
        else
           call cubicsplint(aVals,phi_a,ddphi_a,NumPointsEx,a,fphi)
        endif
     endif

  end function fphi
```

```
!phidot as a function of "a"
  function fphidot(a)  !sqrt(8*pi*G)*psidot
     real(dl) :: fphidot
     real(dl), intent(IN) :: a


     if(a.lt.aVals(1)) then
        fphidot=phidot_a(1)                !if a < minimum
     else
        if(a.gt.aVals(NumPointsEx)) then
           fphidot=phidot_a(NumPointsEx)          !if a > maximus
        else
           call cubicsplint(aVals,phidot_a,ddphidot_a,NumPointsEx,a,fphidot)
        endif
     endif

  end function fphidot

end module QCouple
.
.
.
!Background evolution
function dtauda(a)
!get d tau / d a

!  8*pi*G*rho*a**4.

  phi = fphi(a)
  grhoa2=grhok*a2+grhob*a+grhog+grhornomass+grhodm(a)*a2**2+
        (0.5d0*fphidot(a)**2 + a2*Vofphi(phi,0))*a2

dtauda=sqrt(3/grhoa2)

end function dtauda
.
.
.
!Initial values for perturbations.
if (coupled) then
    initv(1,i_clxc)=0.75_dl*initv(1,i_clxg)
    i_phi = fphi(a)
    i_phidot = fphidot(a)
    i_Vofphi = Vofphi(i_phi,0)

    if (lambda /= 0) then
       initv(1,i_clxq)=(2._dl*initv(1,i_clxc)*i_phidot**2*i_Vofphi)/
            ((i_phidot**2 + 2._dl*a2*i_Vofphi)*Vofphi(i_phi,1))
    else
       initv(1,i_clxq)=0._dl
    endif
    initv(1,i_vq)=(initv(1,i_clxc)*i_phidot**3)/(i_phidot**2 + 2._dl*a2*i_Vofphi)
    initv(1,i_vc)=0._dl
else
    initv(1,i_clxc)=initv(1,i_clxb)
endif
```

```
.
.
.
   grhoc_t=grhodm(a)*a2
   phia=fphi(a)
   phidota=fphidot(a)
   Vofphia=Vofphi(phia,0)
   grhov_t=0.5d0*phidota**2 + a2*Vofphia
   w_eff = (0.5d0*phidota**2 - Vofphia)/(0.5d0*phidota**2 + Vofphia)

!total perturbations: matter terms first, then add massive nu, de and radiation
!  8*pi*a*a*SUM[rho_i*clx_i]
dgrho=grhob_t*clxb+grhoc_t*clxc
!  8*pi*a*a*SUM[(rho_i+p_i)*v_i]
dgq=grhob_t*vb+grhoc_t*vc

clxq=ay(EV%w_ix)
vq=ay(EV%w_ix+1)
dgrho=dgrho + phidota*vq + a2*Vofphi(phia,1)*clxq
dgq = dgq + k*phidota*clxq
.
.
.
!Perturbed dark energy equation of motion
if (coupled) then
   Q_inter = -r_int/(1._dl - r_int*phia)
   Q_phiphi = r_int**2/(1._dl - r_int*phia)**2

   ayprime(Ev%w_ix)= vq

   ayprime(Ev%w_ix+1)= -2._dl*adotoa*vq - k2*clxq - a2*Vofphi(phia,2)*clxq &
                       - k*z*phidota - a2*(Q_phiphi)&
                       *clxq*grhoc_t/a2 - a2*(Q_inter)&
                       *(grhoc_t/a2)*clxc

!  CDM equation of motion
   clxcdot= -k*z - k*vc + (Q_inter)*vq + &
                 (Q_phiphi)*phidota*clxq
   ayprime(3) = clxcdot

   ayprime(Ev%w_ix+2)= -adotoa*vc - (Q_inter)*phidota*vc&
                            + k*(Q_inter)*clxq
else
   clxcdot=-k*z
   ayprime(3)=clxcdot
endif
```

Appendix C

CosmoMC Code: Lookback Time

```
!This appendix shows the most import steps to introduce the lookback time
!likelihood in the CosmoMC code.

    module LBT
    use cmbtypes
    use CAMB, only: Hofz, DeltaPhysicalTimeGyr
    use constants
    use Precision
    use likelihood
    implicit none

    real(dl) Age_universe_theory, Age_universe_obs, Age_universe_err

    type, extends(CosmologyLikelihood) :: LBTLikelihood
        integer :: num_lbt !total number of points used
        real(dl), allocatable, dimension(:) :: lbt_z, lbt_age, lbt_err
        real(dl), allocatable, dimension(:,:) :: lbt_invcov

    contains

    procedure :: LogLike => LBT_LnLike
    end type LBTLikelihood


    contains

!This is to add the Lookback Time Likelihood
    subroutine LBTLikelihood_Add(LikeList, Ini)
    use IniFile
    use settings
    class(LikelihoodList) :: LikeList
    Type(TIniFile) :: ini
    Type(LBTLikelihood), pointer :: like

    integer numlbtsets, i

    if (Ini_Read_Logical_File(Ini, 'use_LBT',.false.)) then

        Age_universe_obs = Ini_Read_Double_File(Ini,'Age_universe_obs',0.d0)
        Age_universe_err = Ini_Read_Double_File(Ini,'Age_universe_err',0.d0)

        numlbtsets = Ini_Read_Int_File(Ini,'lbt_numdatasets',0)
        if (numlbtsets<1) call MpiStop('Use_LBT but numlbtsets = 0')
```

```
        do i= 1, numlbtsets
           allocate(like)
           call ReadLBTDataset(like, ReadIniFileName(Ini,numcat('lbt_dataset',i)) )
           like%LikelihoodType = 'LBT'
           like%needs_background_functions = .true.
           call like%loadParamNames(trim(DataDir)//'LBT.paramnames')
           call LikeList%Add(like)
        end do
        if (Feedback>1) write(*,*) 'read lookback time datasets'
    end if

    end subroutine LBTLikelihood_Add

!This is to read the Lookback Time data
    subroutine ReadLBTDataset(bset, gname)
    use MatrixUtils
    type (LBTLikelihood) bset
    character(LEN=*), intent(IN) :: gname
    character(LEN=Ini_max_string_len) :: lbt_measurements_file, lbt_invcov_file
    integer i,iopb
    logical bad
    Type(TIniFile) :: Ini
    integer file_unit


    file_unit = new_file_unit()
    call Ini_Open_File(Ini, gname, file_unit, bad, .false.)
    if (bad) then
        write (*,*)  'Error opening data set file '//trim(gname)
        stop
    end if

    bset%name = Ini_Read_String_File(Ini,'name')

    Ini_fail_on_not_found = .false.
    if (Feedback > 0) write (*,*) 'reading lookback time data set: '//trim(bset%name)
    bset%num_lbt = Ini_Read_Int_File(Ini,'num_lbt',0)
    if (bset%num_lbt.eq.0) write(*,*) ' ERROR: parameter num_lbt not set'

    allocate(bset%lbt_z(bset%num_lbt))
    allocate(bset%lbt_age(bset%num_lbt))
    allocate(bset%lbt_err(bset%num_lbt))

    lbt_measurements_file = ReadIniFileName(Ini,'lbt_measurements_file')
    call OpenTxtFile(lbt_measurements_file, tmp_file_unit)
    do i=1,bset%num_lbt
      read (tmp_file_unit,*, iostat=iopb) bset%lbt_z(i),bset%lbt_age(i),bset%lbt_err(i)
    end do
    close(tmp_file_unit)


    allocate(bset%lbt_invcov(bset%num_lbt,bset%num_lbt))
    bset%lbt_invcov = 0

    if(Ini_HasKey_File(Ini,lbt_invcov_file)) then
       lbt_invcov_file = ReadIniFileName(Ini, 'lbt_invcov_file')
       call OpenTxtFile(lbt_invcov_file, tmp_file_unit)
       do i=1, bset%num_lbt
```

```
          read (tmp_file_unit,*,iostat=iopb) bset%lbt_invcov(i,:)
       end do
       close(tmp_file_unit)

       if (iopb.ne.0) then
          call MpiStop('Error reading lookback time file '//trim(lbt_invcov_file))
       endif
    else
       do i=1,bset%num_lbt
           bset%lbt_invcov(i,i) = 1._dl/(bset%lbt_err(i)**2 + Age_universe_err**2)
       end do
    endif


    call Ini_Close_File(Ini)
    call ClearFileUnit(file_unit)

    end subroutine ReadLBTDataset

!Lookback Time integrand
    function f_lbt(z)
!    Type(CMBParams) CMB
    real(dl), intent(in) :: z
    real(dl) f_lbt

    f_lbt = 1._dl/((1._dl + z)*Hofz(z))

    end function f_lbt

!Lookback Time integral
    function lookbacktime(z)
!    Type(CMBParams) CMB
    real(dl), intent(in) :: z
    real(dl) rombint, lookbacktime, atol
    external rombint

    atol = 1d-5

    lookbacktime = rombint(f_lbt,0.,z,atol)*Mpc/c/Gyr

    end function lookbacktime

!Here we calculate the Lookback Time Likelihood
    function LBT_LnLike(like, CMB, Theory, DataParams)
!    use ModelParams
    Class(LBTLikelihood) :: like
    Class(CMBParams) CMB
    Class(TheoryPredictions) Theory
    real(mcp) :: DataParams(:)
    integer j,k
    real(mcp) LBT_LnLike
    real(dl), allocatable :: LBT_theory(:), LBT_obs(:)
    real(dl) sigma_lbt

    LBT_LnLike=0
    allocate(LBT_theory(like%num_lbt))
    allocate(LBT_obs(like%num_lbt))
```

```
Age_universe_theory = DeltaPhysicalTimeGyr(0._dl,1._dl)
sigma_lbt = DataParams(1)

do j=1, like%num_lbt
    LBT_theory(j) = lookbacktime(like%lbt_z(j))
    LBT_obs(j) = Age_universe_obs - like%lbt_age(j) - sigma_lbt
end do


do j=1, like%num_lbt
    do k=1, like%num_lbt
        LBT_LnLike = LBT_LnLike +&
                     (LBT_theory(j)-LBT_obs(j))*like%lbt_invcov(j,k)*&
                     (LBT_theory(k)-LBT_obs(k))
    end do
end do

LBT_LnLike = LBT_LnLike + (Age_universe_theory - Age_universe_obs)**2/&
     Age_universe_err**2

LBT_LnLike = LBT_LnLike/2.d0
deallocate(LBT_theory)
deallocate(LBT_obs)


end function LBT_LnLike


end module LBT
```

References

[1] S. Weinberg, Rev.Mod.Phys. **61**, 1 (1989).

[2] L. P. Chimento, A. S. Jakubi, D. Pavon, and W. Zimdahl, Phys.Rev. **D67**, 083513 (2003), arXiv:astro-ph/0303145 [astro-ph] .

[3] L. Amendola, Phys.Rev. **D62**, 043511 (2000), arXiv:astro-ph/9908023 [astro-ph] .

[4] L. Amendola and C. Quercellini, Phys.Rev. **D68**, 023514 (2003), arXiv:astro-ph/0303228 [astro-ph] .

[5] L. Amendola, S. Tsujikawa, and M. Sami, Phys.Lett. **B632**, 155 (2006), arXiv:astro-ph/0506222 [astro-ph] .

[6] D. Pavon and W. Zimdahl, Phys.Lett. **B628**, 206 (2005), arXiv:gr-qc/0505020 [gr-qc] .

[7] S. del Campo, R. Herrera, and D. Pavon, Phys.Rev. **D78**, 021302 (2008), arXiv:0806.2116 [astro-ph] .

[8] C. G. Boehmer, G. Caldera-Cabral, R. Lazkoz, and R. Maartens, Phys.Rev. **D78**, 023505 (2008), arXiv:0801.1565 [gr-qc] .

[9] S. Chen, B. Wang, and J. Jing, Phys.Rev. **D78**, 123503 (2008), arXiv:0808.3482 [gr-qc] .

[10] G. Olivares, F. Atrio-Barandela, and D. Pavon, Phys.Rev. **D71**, 063523 (2005), arXiv:astro-ph/0503242 [astro-ph] .

[11] G. Olivares, F. Atrio-Barandela, and D. Pavon, Phys.Rev. **D77**, 063513 (2008), arXiv:0706.3860 [astro-ph] .

[12] J. Valiviita, E. Majerotto, and R. Maartens, JCAP **0807**, 020 (2008), arXiv:0804.0232 [astro-ph] .

[13] J.-H. He, B. Wang, and E. Abdalla, Phys.Lett. **B671**, 139 (2009), arXiv:0807.3471 [gr-qc] .

[14] P. S. Corasaniti, Phys.Rev. **D78**, 083538 (2008), arXiv:0808.1646 [astro-ph] .

[15] B. M. Jackson, A. Taylor, and A. Berera, Phys.Rev. **D79**, 043526 (2009), arXiv:0901.3272 [astro-ph.CO] .

[16] D. Pavon and B. Wang, Gen.Rel.Grav. **41**, 1 (2009), arXiv:0712.0565 [gr-qc] .

[17] B. Wang, C.-Y. Lin, D. Pavon, and E. Abdalla, Phys.Lett. **B662**, 1 (2008), arXiv:0711.2214 [hep-th] .

[18] B. Wang, J. Zang, C.-Y. Lin, E. Abdalla, and S. Micheletti, Nucl.Phys. **B778**, 69 (2007), arXiv:astro-ph/0607126 [astro-ph] .

[19] F. Simpson, B. M. Jackson, and J. A. Peacock, **MNRAS**, 411 (2): 1053 (2011), arXiv:1004.1920 [astro-ph.CO] .

[20] W. Zimdahl, Int.J.Mod.Phys. **D14**, 2319 (2005), arXiv:gr-qc/0505056 [gr-qc] .

[21] Z.-K. Guo, N. Ohta, and S. Tsujikawa, Phys.Rev. **D76**, 023508 (2007), arXiv:astro-ph/0702015 [ASTRO-PH] .

[22] C. Feng, B. Wang, E. Abdalla, and R.-K. Su, Phys.Lett. **B665**, 111 (2008), arXiv:0804.0110 [astro-ph] .

[23] J. Valiviita, R. Maartens, and E. Majerotto, Mon.Not.Roy.Astron.Soc. **402**, 2355 (2010), arXiv:0907.4987 [astro-ph.CO] .

[24] J.-Q. Xia, Phys.Rev. **D80**, 103514 (2009), arXiv:0911.4820 [astro-ph.CO] .

[25] J.-H. He, B. Wang, and P. Zhang, Phys.Rev. **D80**, 063530 (2009), arXiv:0906.0677 [gr-qc] .

[26] M. Martinelli, L. Lopez Honorez, A. Melchiorri, and O. Mena, Phys.Rev. **D81**, 103534 (2010), arXiv:1004.2410 [astro-ph.CO] .

[27] L. L. Honorez, B. A. Reid, O. Mena, L. Verde, and R. Jimenez, JCAP **1009**, 029 (2010), arXiv:1006.0877 [astro-ph.CO] .

[28] J.-H. He and B. Wang, JCAP **0806**, 010 (2008), arXiv:0801.4233 [astro-ph] .

[29] J.-H. He, B. Wang, and Y. Jing, JCAP **0907**, 030 (2009), arXiv:0902.0660 [gr-qc] .

[30] G. Caldera-Cabral, R. Maartens, and B. M. Schaefer, JCAP **0907**, 027 (2009), arXiv:0905.0492 [astro-ph.CO] .

[31] J.-H. He, B. Wang, E. Abdalla, and D. Pavon, JCAP **1012**, 022 (2010), arXiv:1001.0079 [gr-qc] .

[32] O. Bertolami, F. Gil Pedro, and M. Le Delliou, Phys.Lett. **B654**, 165 (2007), arXiv:astro-ph/0703462 [ASTRO-PH] .

[33] O. Bertolami, F. G. Pedro, and M. Le Delliou, Gen.Rel.Grav. **41**, 2839 (2009), arXiv:0705.3118 [astro-ph] .

[34] E. Abdalla, L. R. W. Abramo, J. Sodre, L., and B. Wang, Phys.Lett. **B673**, 107 (2009), arXiv:0710.1198 [astro-ph] .

[35] E. Abdalla, L. R. Abramo, and J. C. C. de Souza, Phys.Rev. **D82**, 023508 (2010), arXiv:0910.5236 [gr-qc] .

[36] C. Pellicer, E. G. Ferreira, D. C. Guariento, A. A. Costa, L. L. Graef, *et al.*, Mod.Phys.Lett. **A27**, 1250144 (2012), arXiv:1102.5113 [astro-ph.CO] .

[37] A. B. Pavan, E. G. M. Ferreira, S. M. R. Micheletti, J. C. C. de Souza, and E. Abdalla, Phys.Rev. **D86**, 103521 (2012), arXiv:1111.6526 [gr-qc] .

[38] S. Micheletti, E. Abdalla, and B. Wang, Phys.Rev. **D79**, 123506 (2009), arXiv:0902.0318 [gr-qc] .

[39] S. M. Micheletti, JCAP **1005**, 009 (2010), arXiv:0912.3992 [gr-qc] .

[40] K. Koyama, R. Maartens, and Y.-S. Song, JCAP **0910**, 017 (2009), arXiv:0907.2126 [astro-ph.CO] .

[41] J. Zhou, B. Wang, D. Pavon, and E. Abdalla, Mod.Phys.Lett. **A24**, 1689 (2009), arXiv:0807.3128 [gr-qc] .

[42] B. Wang, C.-Y. Lin, and E. Abdalla, Phys.Lett. **B637**, 357 (2006), arXiv:hep-th/0509107 [hep-th] .

[43] B. Wang, Y.-g. Gong, and E. Abdalla, Phys.Lett. **B624**, 141 (2005), arXiv:hep-th/0506069 [hep-th] .

[44] J.-H. He, B. Wang, and E. Abdalla, Phys.Rev. **D83**, 063515 (2011), arXiv:1012.3904 [astro-ph.CO] .

[45] V. Salvatelli, A. Marchini, L. Lopez-Honorez, and O. Mena, Phys.Rev. **D88**, 023531 (2013), arXiv:1304.7119 [astro-ph.CO] .

[46] X.-D. Xu, B. Wang, P. Zhang, and F. Atrio-Barandela, (2013), arXiv:1308.1475 [astro-ph.CO] .

[47] P. Ade *et al.* (Planck Collaboration), (2013), arXiv:1303.5062 [astro-ph.CO] .

[48] P. Ade *et al.* (Planck Collaboration), (2013), arXiv:1303.5076 [astro-ph.CO] .

[49] P. Ade *et al.* (Planck collaboration), (2013), arXiv:1303.5075 [astro-ph.CO] .

[50] F. Beutler, C. Blake, M. Colless, D. H. Jones, L. Staveley-Smith, *et al.*, Mon.Not.Roy.Astron.Soc. **416**, 3017 (2011), arXiv:1106.3366 [astro-ph.CO] .

[51] N. Padmanabhan, X. Xu, D. J. Eisenstein, R. Scalzo, A. J. Cuesta, *et al.*, Mon.Not.Roy.Astron.Soc. **427**, 2132 (2012), arXiv:1202.0090 [astro-ph.CO] .

[52] L. Anderson, E. Aubourg, S. Bailey, D. Bizyaev, M. Blanton, *et al.*, Mon.Not.Roy.Astron.Soc. **427**, 3435 (2013), arXiv:1203.6594 [astro-ph.CO] .

[53] N. Suzuki, D. Rubin, C. Lidman, G. Aldering, R. Amanullah, *et al.*, Astrophys.J. **746**, 85 (2012), arXiv:1105.3470 [astro-ph.CO] .

[54] A. G. Riess, L. Macri, S. Casertano, H. Lampeitl, H. C. Ferguson, *et al.*, Astrophys.J. **730**, 119 (2011), arXiv:1103.2976 [astro-ph.CO] .

[55] S. Capozziello, V. F. Cardone, M. Funaro, and S. Andreon, Phys.Rev. **D70**, 123501 (2004), arXiv:astro-ph/0410268 [astro-ph] .

[56] L. Samushia, A. Dev, D. Jain, and B. Ratra, Phys.Lett. **B693**, 509 (2010), arXiv:0906.2734 [astro-ph.CO] .

[57] S. Weinberg, *Gravitation and Cosmology: Principles and Applications of the General Theory of Relativity* (Wiley and Sons, New York, 1972).

[58] W. Hu and S. Dodelson, Ann.Rev.Astron.Astrophys. **40**, 171 (2002), arXiv:astro-ph/0110414 [astro-ph] .

[59] J. Yadav, S. Bharadwaj, B. Pandey, and T. Seshadri, Mon.Not.Roy.Astron.Soc. **364**, 601 (2005), arXiv:astro-ph/0504315 [astro-ph] .

[60] S. Dodelson, *Modern cosmology* (Academic Press, 2003).

[61] L. Amendola and S. Tsujikawa, *Dark Energy: Theory and Observations* (Cambridge University Press, New York, 2010).

[62] E. W. Kolb and M. S. Turner, *The Early universe*, Vol. 69 (1990) pp. 1–547.

[63] J. C. Mather, D. Fixsen, R. Shafer, C. Mosier, and D. Wilkinson, Astrophys.J. **512**, 511 (1999), arXiv:astro-ph/9810373 [astro-ph] .

[64] D. Fixsen, E. Cheng, J. Gales, J. C. Mather, R. Shafer, *et al.*, Astrophys.J. **473**, 576 (1996), arXiv:astro-ph/9605054 [astro-ph] .

[65] W. Freedman *et al.* (HST Collaboration), Astrophys.J. **553**, 47 (2001), arXiv:astro-ph/0012376 [astro-ph] .

[66] M. Fukugita, C. Hogan, and P. Peebles, Astrophys.J. **503**, 518 (1998), arXiv:astro-ph/9712020 [astro-ph] .

[67] M. Rauch, J. Miralda-Escude, W. L. Sargent, T. A. Barlow, D. H. Weinberg, *et al.*, Astrophys.J. **489**, 7 (1997), arXiv:astro-ph/9612245 [astro-ph] .

[68] G. Hinshaw *et al.* (WMAP Collaboration), Astrophys.J.Suppl. **180**, 225 (2009), arXiv:0803.0732 [astro-ph] .

[69] J. M. O'Meara, D. Tytler, D. Kirkman, N. Suzuki, J. X. Prochaska, *et al.*, Astrophys.J. **552**, 718 (2001), arXiv:astro-ph/0011179 [astro-ph] .

[70] J. N. Bahcall, *NEUTRINO ASTROPHYSICS* (Cambridge University Press, Cambridge, 1989).

[71] Y. Fukuda *et al.* (Super-Kamiokande Collaboration), Phys.Rev.Lett. **81**, 1562 (1998), arXiv:hep-ex/9807003 [hep-ex] .

[72] M. Kamionkowski, (1998), arXiv:astro-ph/9809214 [astro-ph] .

[73] K. Begeman, A. Broeils, and R. Sanders, Mon.Not.Roy.Astron.Soc. **249**, 523 (1991).

[74] F. Zwicky, Helv.Phys.Acta **6**, 110 (1933).

[75] N. A. Bahcall and X.-h. Fan, Astrophys.J. **504**, 1 (1998), arXiv:astro-ph/9803277 [astro-ph] .

[76] A. Kashlinsky, Phys.Rept. **307**, 67 (1998), arXiv:astro-ph/9806236 [astro-ph] .

[77] R. G. Carlberg *et al.*, Astrophys. J. **516**, 552 (1999).

[78] C. Weinheimer, , 335 (2003), arXiv:hep-ex/0306057 [hep-ex] .

[79] A. Miller, R. Caldwell, M. Devlin, W. Dorwart, T. Herbig, *et al.*, Astrophys.J. **524**, L1 (1999), arXiv:astro-ph/9906421 [astro-ph] .

[80] P. de Bernardis *et al.* (Boomerang Collaboration), Nature **404**, 955 (2000), arXiv:astro-ph/0004404 [astro-ph] .

[81] S. Hanany, P. Ade, A. Balbi, J. Bock, J. Borrill, *et al.*, Astrophys.J. **545**, L5 (2000), arXiv:astro-ph/0005123 [astro-ph] .

[82] E. Leitch, C. Pryke, N. Halverson, J. Kovac, G. Davidson, *et al.*, Astrophys.J. **568**, 28 (2002), arXiv:astro-ph/0104488 [astro-ph] .

[83] A. G. Riess *et al.* (Supernova Search Team), Astron.J. **116**, 1009 (1998), arXiv:astro-ph/9805201 [astro-ph] .

[84] S. Perlmutter *et al.* (Supernova Cosmology Project), Astrophys.J. **517**, 565 (1999), arXiv:astro-ph/9812133 [astro-ph] .

[85] S. M. Carrol, Living Rev. Relativity **4**, 1 (2001).

[86] V. Mukhanov, *Physical foundations of cosmology* (Cambridge University Press, New York, 2005).

[87] M. E. Peskin and D. V. Schroeder, *An Introduction to quantum field theory* (Perseus Books, Massachusetts, 1995).

[88] C.-P. Ma and E. Bertschinger, Astrophys.J. **455**, 7 (1995), arXiv:astro-ph/9506072 [astro-ph] .

[89] G. Olivares, F. Atrio-Barandela, and D. Pavon, AIP Conf.Proc. **841**, 550 (2006), arXiv:astro-ph/0511474 [astro-ph] .

[90] G. Olivares, F. Atrio-Barandela, and D. Pavon, Phys.Rev. **D74**, 043521 (2006), arXiv:astro-ph/0607604 [astro-ph] .

[91] L. Amendola, G. Camargo Campos, and R. Rosenfeld, Phys.Rev. **D75**, 083506 (2007), arXiv:astro-ph/0610806 [astro-ph] .

[92] R. Rosenfeld, Phys.Rev. **D75**, 083509 (2007), arXiv:astro-ph/0701213 [astro-ph] .

[93] C. Feng, B. Wang, Y. Gong, and R.-K. Su, JCAP **0709**, 005 (2007), arXiv:0706.4033 [astro-ph] .

[94] R. Bean, E. E. Flanagan, I. Laszlo, and M. Trodden, Phys.Rev. **D78**, 123514 (2008), arXiv:0808.1105 [astro-ph] .

[95] A. Lewis, A. Challinor, and A. Lasenby, Astrophys.J. **538**, 473 (2000), arXiv:astro-ph/9911177 [astro-ph] .

[96] S. Weinberg, *Cosmology* (Oxford University Press, New York, 2008).

[97] S. M. R. Micheletti, *Vínculos Observacionais em Modelos de Energia Escura Interagente*, Ph.D. thesis, Universidade de São Paulo (2009).

[98] A. A. Costa, X.-D. Xu, B. Wang, E. G. M. Ferreira, and E. Abdalla, Phys.Rev. **D89**, 103531 (2014), arXiv:1311.7380 [astro-ph.CO] .

[99] A. A. Costa, L. C. Olivari, and E. Abdalla, (2014), arXiv:1411.3660 [astro-ph.CO] .

[100] A. A. Costa, L. C. Olivari, R. Rhavia, and E. Abdalla, (2014), to be published .

[101] D. S. Sivia and J. Skilling, *Data Analysis: A Bayesian Tutorial* (Oxford University Press, New York, 2006).

[102] L. Verde, (2007), arXiv:0712.3028 [astro-ph] .

[103] C. Bennett *et al.* (WMAP), Astrophys.J.Suppl. **208**, 20 (2013), arXiv:1212.5225 [astro-ph.CO] .

[104] J. Guy *et al.* (SNLS Collaboration), Astron.Astrophys. **466**, 11 (2007), arXiv:astro-ph/0701828 [ASTRO-PH] .

[105] A. Lewis and S. Bridle, Phys.Rev. **D66**, 103511 (2002), arXiv:astro-ph/0205436 [astro-ph] .

[106] A. Lewis, Phys.Rev. **D87**, 103529 (2013), arXiv:1304.4473 [astro-ph.CO] .

[107] O. Pisanti, A. Cirillo, S. Esposito, F. Iocco, G. Mangano, *et al.*, Comput.Phys.Commun. **178**, 956 (2008), arXiv:0705.0290 [astro-ph] .

[108] J. Hamann, S. Hannestad, G. G. Raffelt, and Y. Y. Wong, JCAP **1109**, 034 (2011), arXiv:1108.4136 [astro-ph.CO] .